



5th Annual Meeting of the Bulgarian Section of SIAM
December 20-21, 2010
Sofia

BGSIAM'10

PROCEEDINGS

HOSTED BY THE INSTITUTE OF MATHEMATICS AND INFORMATICS
BULGARIAN ACADEMY OF SCIENCES

5th Annual Meeting of the Bulgarian Section of SIAM
December 20-21, 2010, Sofia
BGSIAM'10 Proceedings

©2011 by Demetra

ISSN: 1313-3357

Printed in Sofia, Bulgaria
Cover design: Boris Staikov
Printing and binding: Demetra Ltd.

PREFACE

The Bulgarian Section of SIAM (BGSIAM) was founded on January 18, 2007 and the accepted Rules of Procedure were officially approved by the SIAM Board of Trustees on July 15, 2007. The activities of BGSIAM follow the general objectives of SIAM, as established in its Certificate of Incorporation.

Being aware of the importance of interdisciplinary collaboration and the role the applied mathematics plays in advancing science and technology in industry, we appreciate the support of SIAM as the major international organization for Industrial and Applied Mathematics in order to promote the application of mathematics to science, engineering and technology in the Republic of Bulgaria.

The 5th Annual Meeting of BGSIAM (BGSIAM'10) was hosted by the Institute of Mathematics and Informatics, Bulgarian Academy of Sciences, Sofia. It took part on December 20 and 21, 2010. The conference support provided by SIAM is very highly appreciated.

Following the established tradition, a wide range of problems concerning recent achievements in the field of industrial and applied mathematics were presented and discussed during BGSIAM'10 conference. The meeting provided a forum for exchange of ideas between scientists, who develop and study mathematical methods and algorithms, and researchers, who apply them for solving real life problems.

More than 50 participants from seven universities, five institutes of the Bulgarian Academy of Sciences and also from outside the traditional academic departments took part in BGSIAM'10. They represent most of the strongest Bulgarian research groups in the field of industrial and applied mathematics. The involvement of younger researchers was especially encouraged and we are glad to report that 9 from the presented 22 talks were given by students or young researchers.

LIST OF INVITED LECTURES:

- PETAR POPIVANOV
Institute of Mathematics and Informatics, Bulgarian Academy of Sciences
PDE ARISING IN FLUID MECHANICS: SINGULARITIES, CREATION
AND PROPAGATION
- GEORGI POPOV
University of Nantes, France
EFFECTIVE STABILITY OF HAMILTONIAN SYSTEMS
- LYUDMIL ZIKATANOV
Penn State, University Park, PA, USA
ENERGY MINIMIZING COARSE SPACES WITH FUNCTIONAL
CONSTRAINT

- ZAHARI ZLATEV
National Environmental Research Institute, Roskilde, Denmark
RICHARDSON EXTRAPOLATION: ACCURACY, STEPSIZE CONTROL
AND STABILITY

The present volume contains extended abstracts of the conference talks (Part A) and list of participants (Part B).

Svetozar Margenov
Chair of BGSIAM Section

Stefka Dimova
Vice-Chair of BGSIAM Section

Angela Slavova
Secretary of BGSIAM Section

Sofia, January 2011

Table of Contents

Part A: Extended abstracts	1
<i>Andrey Andreev, Milena Racheva, Georgi Tsanev</i>	
A Nonconforming Finite Element with Integral Type Bubble Function	3
<i>R. Anguelov, Y. Dumont, J. M.-S. Lubuma</i>	
Monotone Dynamical Systems: Application to population dynamics	7
<i>Christo I. Christov, Natalia Kolkovska, Daniela Vasileva</i>	
Numerical Investigation of Unsteady Solutions for the 2D Boussinesq Paradigm Equation	11
<i>Ivan Dimov, Rayna Georgieva</i>	
Monte Carlo Approaches for Model Sensitivity Studies	17
<i>Ivan Dimov and Zahari Zlatev</i>	
Richardson Extrapolation: Accuracy, Stepsize Control and Stability	23
<i>Stefka Fidanova, Pencho Marinov</i>	
Ant Colony Optimization Start Strategies: Two Case Studies	29
<i>Ivan Georgiev, Johannes Kraus, Maria Lymbery, Svetozar Margenov</i>	
On Two-Level Splittings for Quadratic FEM Anisotropic Elliptic Problems	35
<i>Krassimir Georgiev, Zahari Zlatev</i>	
Some Notes on the Implementation of Sparse Matrix Techniques in an Advection-Diffusion Module	41
<i>Vladimir S. Gerdjikov, Georgi G. Grahovski, Rossen I. Ivanov</i>	
On the (Non)-Integrability of the Perturbed KdV Hierarchy with Generic Self-consistent Sources	45
<i>Ivan Hristov</i>	
Fluxon States in Linear Josephson Stacks	51
<i>Svetoslav Markov</i>	
On the Computation with Approximate Numbers	55
<i>Petar Popivanov</i>	
PDE Arising in Fluid Mechanics: Singularities, Creation and Propagation	61
<i>Tsviatko Rangelov, Yonko Stoynov, Petia Dineva</i>	
Dynamic crack problems in functionally graded magnetoelastic solids	65

<i>Angela Slavova, Maya Markova, Pietro Zecca</i> Modeling tsunami waves via Cellular Nonlinear Networks	71
<i>Angela Slavova, Victoria Rashkova</i> Cellular Nonlinear Network Model for Image Denoising	77
<i>Antoaneta Tsokova</i> Vibrational Recursive Geometry	82
Part B: List of participants	86

Part A
Extended abstracts¹

¹Arranged alphabetically according to the family name of the first author.

A Nonconforming Finite Element with Integral Type Bubble Function

Andrey Andreev, Milena Racheva, Georgi Tsanev

1 Introduction

The nonconforming finite element methods play a significant role in the numerical approximation of elliptic PDEs when conforming methods and others are too costly or unstable. Integral type nonconforming elements use integral values on their edges or/and on the element itself as degrees of freedom. Thus, the obtained finite element space is integrally continuous at the common edges between any two neighboring elements. This feature enables us to construct smoothing and convergence accelerating a posteriori procedures [1, 2, 6]. On the other hand, a key role of some postprocessing methods play by certain locally supported, nonnegative functions that are commonly referred to as a bubble functions [3]. We consider triangular Crouzeix-Raviart elements extended by the interior bubble function which is presented by integral value of this function on a single element and study some approximation properties of this incomplete quadratic nonconforming finite element.

Let Ω be a bounded polygonal domain in \mathbf{R}^2 with boundary $\partial\Omega$, $H^m(\Omega)$ be the usual m -th order Sobolev space on Ω with a norm $\|\cdot\|_{m,\Omega}$ and seminorm $|\cdot|_{m,\Omega}$ and (\cdot, \cdot) denotes the $L_2(\Omega)$ -inner product.

Consider the following second-order model problem for $f \in L_2(\Omega)$:

$$\begin{aligned} -\Delta u + a_0 u &= f && \text{in } \Omega, \\ u &= 0 && \text{on } \partial\Omega, \end{aligned} \tag{1}$$

where $a_0(x)$ is a nonnegative bounded function in Ω .

The weak formulation of the problem (1) is: find $u \in H_0^1(\Omega)$ such that:

$$a(u, v) = (f, v), \quad \forall v \in V \equiv H_0^1(\Omega), \tag{2}$$

$$a(u, v) = \int_{\Omega} (\nabla u \cdot \nabla v + a_0 uv) \, dx \, dy \quad \forall u, v \in H_0^1(\Omega).$$

By analogy of (2), the variational elliptic eigenvalue problem is: find $(\lambda, u) \in \mathbf{R} \times H_0^1(\Omega)$ such that:

$$a(u, v) = \lambda(u, v), \quad \forall v \in V. \tag{3}$$

Since the bilinear form $a(\cdot, \cdot)$ is symmetric and coercive on $H_0^1(\Omega)$, the solution of (3) is given by a sequence of pairs (λ_j, u_j) , with positive eigenvalues λ_j diverging to $+\infty$. Then we can assume that $0 < \lambda_1 \leq \lambda_2 \leq \dots$. The associated eigenfunctions u_j can be chosen to be orthonormal in $L_2(\Omega)$ and they constitute a Hilbert basis for V .

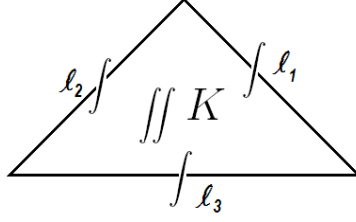


Figure 1: The considered incomplete quadratic nonconforming FE

2 Nonconforming Finite Element Method

Let τ_h be family of regular finite element partitions of Ω which fulfill the usual shape regularity conditions [5]. We assume that any two triangles in τ_h share at most a vertex or an edge. Denote by h_K the diameter of the triangle K and $h = \max_{K \in \tau_h} h_K$ is mesh parameter. The edges of any $K \in \tau_h$ are denoted by l_j , $j = 1, 2, 3$. We define nonconforming piecewise incomplete quadratic finite element space with integral type degrees of freedom (Fig. 1): $V_h = \{v \in V_K \in \mathcal{P}_K \text{ is integrally continuous on the edges of } K, \text{ for all } K \in \tau_h \text{ and } \int_l v \, dl = 0\}$ for every l being a side of the FE triangle that lies on the boundary $\partial\Omega$. Here, $\mathcal{P}_1 \subseteq \mathcal{P}_K \subseteq \mathcal{P}_2$, where \mathcal{P}_s is the set of polynomials of degree less than or equal to s . Obviously, any two adjacent triangles of τ_h have the same integral value $\int_l v_h \, dl$, $v_h \in V_h$ on their common edge l .

Let $T = \{(t_1, t_2) : t_1, t_2 \geq 0, t_1 + t_2 \leq 1\}$ be the reference element. Then, the shape functions of introduced extended C-R element on T φ_j , $j = 1, 2, 3, 4$ are obtained under conditions:

$$\int_{l_i} \varphi_j \, dl = \delta_{ij}; \quad \int \int_T \varphi_j \, dt_1 \, dt_2 = \delta_{4j}, \quad i = 1, 2, 3; \quad j = 1, 2, 3, 4.$$

We define the following bilinear form on $V_h + H_0^1(\Omega)$:

$$a_h(u, v) = \sum_{K \in \tau_h} \int_K (\nabla u \cdot \nabla v + a_0 uv) \, dx.$$

The linear form (f, \cdot) needs not be approximated since the inclusion $V_h \subset L_2(\Omega)$ holds. So, the nonconforming approximation of (2) is: find $u_h \in V_h$ such that:

$$a_h(u_h, v_h) = (f, v_h), \quad \forall v_h \in V_h. \quad (4)$$

Thus, it is easy to prove the following proposition:

Proposition 1 (see [5]) *The set of degrees of freedom is \mathcal{P}_K -unisolvent.*

We also consider the nonconforming FE approximation to the associated elliptic variational EVP: find $(\lambda_h, u_h) \in \mathcal{R} \times V_h$ with $\|u_h\|_{1,\Omega}$, such that

$$a_h(u_h, v_h) = \lambda_h(u_h, v_h), \quad \forall v_h \in V_h. \quad (5)$$

This problem reduces to a generalized EVP involving positive definite symmetric matrices. It attains a finite number of eigenpairs $(\lambda_{h,j}, u_{h,j}), j = 1, \dots, N_h$; $N_h = \dim V_h$ with positive eigenvalues: $\lambda_{h,1} \leq \dots \leq \lambda_{h,N_h}$.

For any $v \in L_2(\Omega)$ with $v|_K \in H^m(K)$, for all $K \in \tau_h$ we define the mesh-dependent norm and seminorm [4]:

$$\|v\|_{m,h} = \left\{ \sum_{K \in \tau_h} \|v\|_{m,K}^2 \right\}^{1/2}, \quad |v|_{m,h} = \left\{ \sum_{K \in \tau_h} |v|_{m,K}^2 \right\}^{1/2}, \quad m = 0, 1.$$

Observe that for any $v_h \in V_h$, $\|v_h\|_{0,h} = \|v_h\|_{0,\Omega}$.

3 Some Approximation Properties

The finite element considered here could be referred to the C-R linear extended case. As we mentioned above, the FE space consists of piecewise incomplete quadratic polynomials.

Let us introduce the interpolation operator i_h associated with the considered nonconforming element. The operator $i_h : L_2(\Omega) \rightarrow V_h$ is defined under the following conditions: for any $v \in L_2(\Omega)$ and for all $K \in \tau_h$,

$$\int_{l_j} i_h v \, dl = \int_{l_j} v \, dl, \quad j = 1, 2, 3 \quad \text{and} \quad \int_K i_h v \, dx = \int_K v \, dx.$$

Obviously, $i_h v \in V_h$, for all $v \in L_2(\Omega)$ and $i_h v \equiv v$, for all $v \in V_h$.

The next theorem contains the essential result (henceforth, C represents generic and positive constant):

Theorem 1 *Let u and u_h be the solution of (2) and (4), respectively. If $u \in H^2(\Omega) \cap V$, then $\|u - u_h\|_{s,h} \leq Ch^{2-s}\|u\|_{2,\Omega}$, $s = 0, 1$.*

We also derive a superclose property of the interpolation operator i_h with respect to the elliptic a_h -form:

Lemma 1 *Let $v \in H^2(\Omega) \cap V$ and $i_h v$ be its interpolant constructed by means of extended C-R integral type nonconforming finite element. Then*

$$|a_h(v - i_h v, v_h)| \leq Ch^2|v|_{2,\Omega} \quad \forall v_h \in V_h.$$

If in addition $a_0(x) \equiv 0$, then $a_h(v - i_h v, v_h) = 0 \quad \forall v_h \in V_h$.

4 Lower Bounds for Eigenvalues

We analyze the approximation for the eigenvalues of the Laplace operator by the nonconforming extended C-R integral type finite element. So, the bilinear form is

$$a_h(u, v) = \sum_{K \in \tau_h} \int_K \nabla u \cdot \nabla v \, dx, \quad \forall u, v \in V. \quad (6)$$

In the next theorem asymptotically lower bounds of the exact second order eigenvalues by using defined above nonconforming finite element are proved.

Theorem 2 *Let (λ_k, u_k) and $(\lambda_{h,k}, u_{h,k})$ be the solutions of (3) and (5), respectively, for any positive integer k and let also a_h be determined by (6). Assume that the eigenfunctions are normalized $\|u_k\|_{0,\Omega} = \|u_{h,k}\|_{0,\Omega} = 1$. Then, for small enough h :*

$$\lambda_{h,k} \leq \lambda_k.$$

If in addition $u_k \in H^2(\Omega)$, then $\lambda_k - \lambda_{h,k} \leq Ch^2 \|u_k\|_{2,\Omega}^2$.

Acknowledgement This work is partially supported by the Bulgarian Ministry of Science (grant D 002-147/2008) and by the Technical University of Gabrovo (grant C1001/2010).

References

- [1] Andreev, A.B., Racheva, M.R.: Lower Bounds for Eigenvalues and Postprocessing by an Integral Type Nonconforming FEM, SibJNM (to appear).
- [2] Andreev, A.B., Racheva, M.R.: Superconvergence of the interpolated quadratic finite elements on triangular meshes. Math. Balkanica, New Series. Vol.19 (2005) Fasc. 3-4 385-404
- [3] Ainsworth M., J.T. Oden: A Posteriori Error Estimation in Finite Element Analysis. Wiley Interscience, New York, 2000.
- [4] Brenner, S., Scott, L.R.: The Mathematical Theory for Finite Element Methods, Springer-Verlag, New York, 1992.
- [5] Ciarlet, P.: Basic Error Estimates for the FEM, Elsevier, Vol. 2 Amsterdam, 17-351 (1991).
- [6] Lin, Q., Yan, N., Zhou, A.: A rectangle test for interpolated finite elements. In: Proceedings of Systems Science & Systems Engineering, Culture Publish Co. (1991) 217-229.

Monotone Dynamical Systems: Application to population dynamics

R. Anguelov, Y. Dumont, J. M.-S. Lubuma

1 Introduction

Mathematical models of biosystems, in general, and in population studies, in particular, are often represented by continuous dynamical systems. The qualitative analysis of such systems regarding the long term behavior of their solutions is one of the main mathematics involvements in such studies. Our main concern in this paper is properties of global nature like basins of attraction and global asymptotic stability of equilibria. We should note that in high dimensions the Lyapunov function is about the only general method for establishing such properties and deriving it commonly relies on specific constructions for any particular system. The theory of monotone dynamical systems offers an alternative monotonicity-based approach which is to a large extent independent of the dimensionality of the system. Here we state some basic theorems and demonstrate their application to a model for controlling a mosquito population via Sterile Insect Technique (SIT).

2 Elements of the theory of monotone systems

Let $\Omega \subseteq \mathbb{R}^d$, $d \geq 1$ be a given domain and let us assume that the system of ODEs

$$\frac{dy}{dt} = g(t, y) \tag{1}$$

where the $g : [0, +\infty) \times \Omega \rightarrow \mathbb{R}^n$, define a (positive) dynamical system on $D \subset \Omega$. This means that, for every $x \in D$, equation (1) has a unique solution $y = y(x, t) \in D$ for all $t \in [0, \infty)$ and satisfying $y(x, 0) = x$. The system (1) is called *monotone* or *cooperative* if for every $i, j \in \{1, 2, \dots, n\}$ such that $i \neq j$ the function $g_i(t, y_1, \dots, y_n)$ is monotone increasing with respect to y_j . The following theorem is often referred to as Kamke's theorem, e.g see [1]. A proof can be found in [4].

Theorem 1 *If the system (1) is monotone then for every $a, b \in D$*
$$a \leq b \implies y(a, t) \leq y(b, t), \quad t > 0.$$

While the above theorem holds for all monotone systems most of the theory is actually developed for autonomous systems

$$\frac{dy}{dt} = f(y) \tag{2}$$

The main results are collected in [3]. The following theorem, which is also an easy consequence of Theorem 1, is used in the sequel.

Theorem 2 *Let (2) be monotone. If $a \in D$ is such that $f(a) \geq \mathbf{0}$ ($f(a) \leq \mathbf{0}$) then the solution $y(a, t)$ is monotone increasing (decreasing) function of $t \in [0, +\infty)$.*

The combined application of the monotonicity with respect to initial value given in Theorem 1 and the monotonicity of the solutions given in Theorem 2 provides a new approach for studying dynamical systems. As usual we call an equilibrium asymptotically stable if it is both stable and attractive. An asymptotically stable equilibrium is called globally asymptotically stable (GAS) if the basin of attraction is the whole domain D . Naturally, any asymptotically stable equilibrium is globally asymptotically stable on any positively invariant subset of its basin of attraction.

Theorem 3 *Let (2) be monotone and let $a, b \in D$ be such that $a < b$, $[a, b] \subseteq D$ and $f(b) \leq \mathbf{0} \leq f(a)$. Then (2) defines a (positive) dynamical system on $[a, b]$. Moreover, if $[a, b]$ contains a unique equilibrium p , then p is GAS on $[a, b]$.*

3 Model of SIT control of a mosquito population

SIT is a nonpolluting method of insect control that relies on the release of sterile insects. Mating of released sterile males with wild females leads to non hatching eggs. Thus, if males are released in sufficient numbers or over a sufficient period of time, it can lead to the local elimination or suppression of the wild population.

The life cycle of a mosquito consists of two main stages: aquatic (egg, larva, pupa) and adult. After emergence from pupa a female mosquito needs to mate (only once) and to take a blood meal, and then it can deposit eggs. Along its life, the female will take blood meals and will deposit eggs in different breeding sites. For mathematical description we divide the population into the following compartments

A - the size of the population in aquatic stage (eggs, larvae, pupae)

Y - number of young females, not yet laying eggs

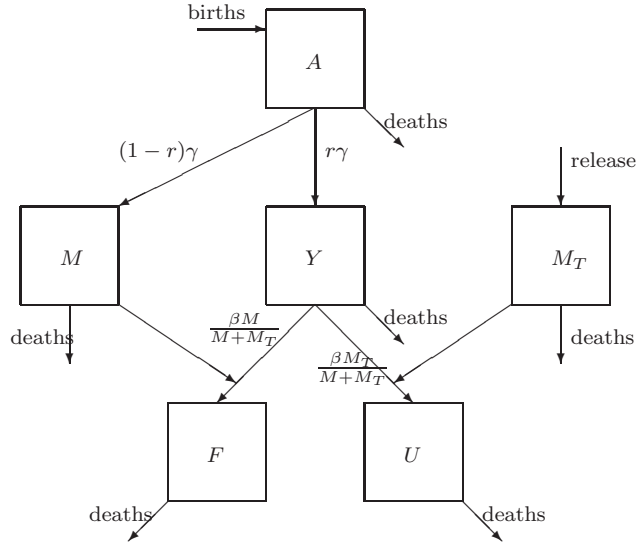
F - number of eggs laying females fertilized by wild mosquito

M - number of wild males

M_T - number of the released treated males

U - number of eggs laying females fertilized by treated mosquito

Flow diagram giving the transfers between compartments is given on the next page. Note that the compartment U can be decoupled from the diagram.



Further, the size of M_T is controlled by human intervention and independent from the rest of the population. Hence, we assume that $M_T = M_T(t)$ can be derived. The mathematical model is a system of four differential equations as follows:

$$\frac{dA}{dt} = \phi F - (\gamma + \mu_1 + \mu_2 A)A \quad (3)$$

$$\frac{dY}{dt} = r\gamma A - (\beta + \mu_Y)Y \quad (4)$$

$$\frac{dF}{dt} = \frac{\beta M}{M + M_T(t)}Y - \mu_F F \quad (5)$$

$$\frac{dM}{dt} = (1-r)\gamma A - \mu_M M \quad (6)$$

where ϕ is the reproduction rate, μ with all subscripts refers to respective mortality rates and the meaning of rest of the parameters is evident from the flow diagram. In equation (3), we have considered a non constant density mortality rate, a common assumption for *Anopheles* mosquitoes, responsible of Malaria's transmission. The system (3)–(6) is of the form (1) where $y = (A, Y, F, M)'$ and the right hand side g depends directly on t via $M_T(t)$, i.e. it can be written as $g(t, y) = \psi(M_T(t), y)$. It is also easy to see that this system is monotone. In the absence of treated mosquito, that is, when $M_T(t) = 0$, the system is of the form (2) with $f(y) = \psi(0, y)$, which is monotone as well. Let $m > 0$ and let A_m be so large that the inequalities

$$A_m \geq \max \left\{ m, \frac{1}{\mu_2} \left(\frac{4r\gamma\beta\phi}{(\beta + \mu_Y)\mu_F} - \gamma - \mu_1 \right) \right\}$$

$$F_m := \frac{(\gamma + \mu_1 + \mu_2 A_m)A_m}{2\phi} \geq m$$

$$Y_m := \frac{\mu_F}{2\beta} F_m \geq m, \quad M_m := \frac{2(1-r)\gamma A_m}{\mu_M} \geq m$$

all hold. Then $f(b_m) < \mathbf{0}$, where $b_m = (A_m, Y_m, F_m, M_m)'$. Using that $a = \mathbf{0}$ is an equilibrium, it follows from Theorem 3 that when $M_T = 0$ equations (3)–(6) define a dynamical system on $[\mathbf{0}, b_m]$. Furthermore, since $g(t, y) = \psi(M_T(t), y) \leq \psi(0, y) = f(y)$, (3)–(6) defines a dynamical system on $[\mathbf{0}, b_m]$ for any nonnegative function $M_T = M_T(t)$. The vector b_m can be selected larger than any $y \in \mathbb{R}_+^4$. Therefore, (3)–(6) defines a dynamical system on $D = \mathbb{R}_+^4$.

Let us assume that $\lim_{t \rightarrow \infty} M_T(t) = M_T^*$. Then following the LaSalle Invariance Principle the dynamics of the system (3)–(6) are reduced to the case when $M_T(t) = M_T^*$, that is, one needs to analyze an autonomous monotone system of the form (2) with $f(y) = \psi(M_T^*, y)$. Solving the equation $\psi(M_T^*, y) = \mathbf{0}$, we obtain that there exist a threshold value ξ of M_T^* such that the dynamical system has zero, one or two positive equilibria according as $M_T^* > \xi$, $M_T^* = \xi$ or $M_T^* < \xi$.

Theorem 4 *Let $\lim_{t \rightarrow \infty} M_T(t) = M_T^*$ and let ξ be the threshold value above.*

- (a) *If $M_T^* > \xi$ then $\mathbf{0}$ is GAS equilibrium of (3)–(6) on $D = \mathbb{R}_+^4$.*
- (b) *If $M_T^* = \xi$ the system (3)–(6) has one positive equilibrium y^* . The set $[\mathbf{0}, y^*]$ is in the basin of attraction of $\mathbf{0}$ while $\{y \in \mathbb{R}_+^4; y \geq y^*\}$ is in the basin of attraction of y^* .*
- (c) *If $M_T^* < \xi$ the system (3)–(6) has two positive equilibria y^* and y^{**} , $y^* < y^{**}$. The set $[\mathbf{0}, y^*]$ is in the basin of attraction of $\mathbf{0}$, while $\{y \in \mathbb{R}_+^4 : y > y^*\}$ is in the basin of attraction of y^{**} .*

The proof of (a) follows directly from Theorem 3. The proofs of (b) and (c) are obtained also from Theorem 3 by constructing suitable points similarly to b_m .

4 Conclusion

While the importance of local stability properties of equilibria is not in doubt, the fact that they characterize the behavior of the solutions only in a sufficiently small neighborhood of the equilibria is an essential limitation in practical applications. In this paper we discussed a method of establishing global properties, namely global asymptotic stability and basins of attraction of equilibria, by using the theory of monotone dynamical systems.

References

- [1] M.W. Hirsch, Systems of differential equations which are competitive or cooperative II: convergence almost everywhere. SIAM J. Math. Anal. 16(1985), 423–439.
- [2] A Maiti, B Patra, GP Samanta, Sterile insect release method as a control measure of insect pests: a mathematical model, Journal of Applied Mathematics and Computing **22**(3) (2006) 71–86
- [3] H L Smith, Monotone Dynamical Systems, AMS, 1995.
- [4] W. Walter, Differential and Integral Inequalities, Springer-Verlag, Berlin - Heidelberg - New york, 1970

Numerical Investigation of Unsteady Solutions for the 2D Boussinesq Paradigm Equation

Christo I. Christov, Natalia Kolkovska, Daniela Vasileva

An implicit, energy conserving and unconditionally stable difference scheme with second order truncation error in space and time is presented for the solution of the 2D Boussinesq Paradigm Equation (BPE) [1]:

$$u_{tt} = \Delta [u - F(u) + \beta_1 u_{tt} - \beta_2 \Delta u], \quad F(u) := \alpha u^2, \quad (1)$$

where u is the surface elevation of the wave, $\beta_1, \beta_2 > 0$ are two dispersion coefficients, and $\alpha > 0$ is an amplitude parameter. The main difference of (1) from the original Boussinesq Equation is the presence of a term proportional to $\beta_1 \neq 0$ called “rotational inertia”.

It has been recently shown that the 2D BPE admits stationary translating localized solutions [2, 3, 4], which can be obtained approximately using finite differences, perturbation technique, or Galerkin spectral method. First results about their time behaviour and structural stability are presented in [5] and [6], and here we continue their investigation, designing an energy conserving numerical method.

Numerical method for solving BPE. We introduce the following new dependent function

$$v(x, y, t) := u - \beta_1 \Delta u \quad (2a)$$

and substituting it in Eq. (1) we get the following equation for v

$$v_{tt} = \frac{\beta_2}{\beta_1} \Delta v + \frac{\beta_1 - \beta_2}{\beta_1^2} (u - v) - \Delta F(u). \quad (2b)$$

Thus we obtain a system consisting of an elliptic equation for u , Eq. (2a), and a hyperbolic equation for v : Eq. (2b).

The following implicit time stepping can be designed for the system (2)

$$\begin{aligned} \frac{v_{ij}^{n+1} - 2v_{ij}^n + v_{ij}^{n-1}}{\tau^2} &= \frac{\beta_2}{2\beta_1} \Lambda [v_{ij}^{n+1} + v_{ij}^{n-1}] + \frac{\beta_1 - \beta_2}{2\beta_1^2} [u_{ij}^{n+1} - v_{ij}^{n+1} + u_{ij}^{n-1} - v_{ij}^{n-1}] \\ &\quad - \Lambda G(u_{ij}^{n+1}, u_{ij}^{n-1}), \end{aligned} \quad (3a)$$

$$u_{ij}^{n+1} - \beta_1 \Lambda u_{ij}^{n+1} = v_{ij}^{n+1}, \quad i = 0, \dots, N_x + 1, \quad j = 0, \dots, N_y + 1. \quad (3b)$$

Here τ is the time increment, $G(u_{ij}^{n+1}, u_{ij}^{n-1}) = [(u_{ij}^{n+1})^2 + u_{ij}^{n+1} u_{ij}^{n-1} + (u_{ij}^{n-1})^2] / 3$, and $\Lambda = \Lambda^{xx} + \Lambda^{yy}$ stands for the difference approximation of the Laplace operator Δ on a non-uniform grid, for example

$$\Lambda^{xx} \phi_{ij} = \frac{2\phi_{i-1j}}{h_{i-1}^x (h_i^x + h_{i-1}^x)} - \frac{2\phi_{ij}}{h_i^x h_{i-1}^x} + \frac{2\phi_{i+1j}}{h_i^x (h_i^x + h_{i-1}^x)} = \frac{\partial^2 \phi}{\partial x^2} \Big|_{ij} + O(|h_i^x - h_{i-1}^x|).$$

For a smooth distribution of the nonuniform grid (as the one considered here) one has

$$O(|h_i^x - h_{i-1}^x|) \approx \frac{\partial h^x}{\partial x} O(|h_{i-1}|^2) = O(|h_{i-1}|^2).$$

The values of the sought functions at the $(n-1)$ -st and n -th time stages are considered as known when computing the $(n+1)$ -st stage. The nonlinear term G is linearized using Picard method, i.e., we perform successive iterations for u and v on the $(n+1)$ -st stage, starting with initial conditions from the already computed n -th stage.

The unconditional stability of the scheme and the conservation of the energy are shown in [7, 8]. The convergence is investigated in [8].

The following non-uniform grid is used in the x -direction

$$x_i = \sinh[\hat{h}_x(i - n_x)], \quad x_{N_x+1-i} = -x_i, \quad i = n_x + 1, \dots, N_x + 1, \quad x_{n_x} = 0,$$

where N_x is an odd number, $n_x = (N_x + 1)/2$, $\hat{h}_x = D_x/N_x$, and D_x is selected in a manner to have large enough computational region. The grid in the y -direction is defined in the same way.

Because of the localization of the wave profile, the boundary conditions can be set equal to zero, when the size of the computational domain is large enough. The initial conditions are created using the best-fit approximation provided in [4]. The coupled system of equations (3) is solved by the Bi-Conjugate Gradient Stabilized Method with ILU preconditioner [9].

Numerical experiments. Denote by $u^s(x, y; c)$ the best-fit approximation of the stationary translating (with speed c) localized solutions, obtained in [4]

$$\begin{aligned} u^s(x, y; c) &= f(x, y) + c^2 [(1 - \beta_1)g_a(x, y) + \beta_1 g_b(x, y)] \\ &+ c^2 [(1 - \beta_1)h_1(x, y) + \beta_1 h_2(x, y)] \cos[2 \arctan(y/x)], \end{aligned}$$

where the formulas for the functions f , g_a , g_b may be found in [4]. For $t = 0$, the first initial condition is obvious: $u(x, y, 0) = u^s(x, y; c)$, and the second initial condition may be chosen as

$$u(x, y, -\tau) = u^s(x, y + c\tau; c). \quad (4)$$

The solutions for $\beta_1 = 3$, $\beta_2 = 1$, $\alpha = 1$ are computed on three different grids in the region $x, y \in [-50, 50]$ (with 161×161 , 321×321 and 641×641 grid points), and with at least three different time increments ($\tau = 0.2, 0.1$ and 0.05). The results for $c = 0, 0.25$ and 0.3 are in good agreement with those in [6], where the nonlinear term was approximated on the already computed n -th time stage, but the corresponding scheme is not energy conserving. That is why here we will present some results for different values of c .

Example 1. We present the evolution of the solution for the case $c = 0.27$ in Fig. 1. The values of the maximum of the solution u_{\max} and its y -coordinate y_{\max} as functions of time are also shown in Fig. 1. The behaviour of the solution is the same on all grids and for all times steps. For $t \leq 10$, the solution not only moves with a speed,

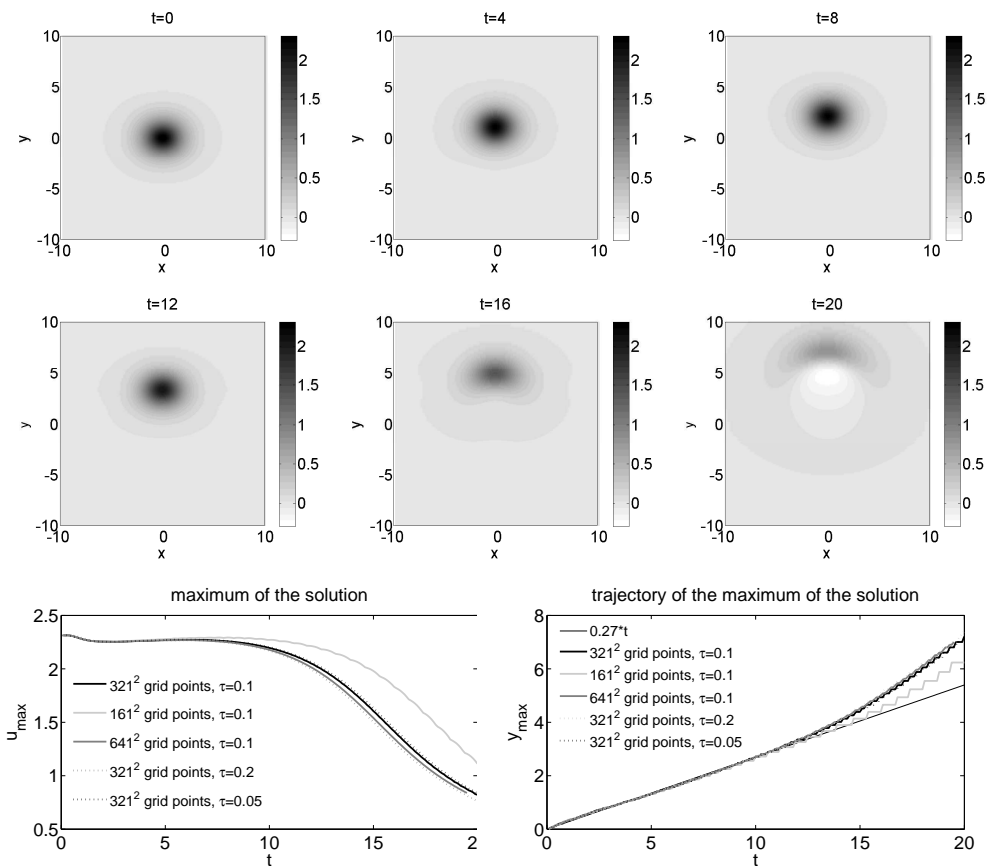


Figure 1: Evolution of the solution for $c = 0.27$, the maximum $u(0, y_{\max})$, and the trajectory of the maximum.

close to $c = 0.27$, but also behaves like a soliton, i.e., preserves its shape, albeit its maximum decreases slightly. For larger times, the solution transforms into a diverging propagating wave. The phase speed of the wave increases and reaches the limit for the small linear waves, $c = 1$.

For $t = 4, 8, 12$ the computed maximum of the solution u_{\max} , the difference $\Delta u_{\max} := u_{\max}^{\text{prev}} - u_{\max}$ (subscript 'prev' denotes the previous row in the table), and the rate of convergence $l = \log_2(|u_{\max}^{\text{prev}} - u_{\max}^{\text{prev,prev}}|/|u_{\max} - u_{\max}^{\text{prev}}|)$, are shown in Table 1. It is seen that the method has second order numerical accuracy in space and time. The last column in the table is for the energy of the numerical solution, as defined in [8]. The energy is really conserved during the computations and the presented values are for each $t \in [0, 30]$.

Table 1: The maximum of the solution, convergence in space and time, $c = 0.27$

		$t = 4$			$t = 8$			$t = 12$			$t \in [0, 30]$
τ	$N_x + 1$	u_{\max}	Δu_{\max}	l	u_{\max}	Δu_{\max}	l	u_{\max}	Δu_{\max}	l	energy
0.1	160	2.2683			2.2929			2.2108			9.153520
0.1	320	2.2631	5.23e-3		2.2553	3.76e-2		2.0426	1.68e-1		9.151786
0.1	640	2.2615	1.60e-3	1.7	2.2473	8.06e-3	2.2	2.0047	3.78e-2	2.2	9.151368
0.2	320	2.2627			2.2400			1.9701			9.151562
0.1	320	2.2631	-3.84e-4		2.2553	-1.53e-2		2.0426	-7.25e-2		9.151786
0.05	320	2.2632	-1.15e-4	1.7	2.2597	-4.38e-3	1.8	2.0602	-1.77e-2	2.0	9.151861
0.025	320	2.2633	-3.00e-5	1.9	2.2608	-1.12e-3	2.0	2.0650	-4.79e-3	1.9	9.151877

Table 2: The maximum of the solution, convergence in space and time, $c = 0.28$

		$t = 4$			$t = 8$			$t = 12$			$t \in [0, 30]$
τ	$N_x + 1$	u_{\max}	Δu_{\max}	l	u_{\max}	Δu_{\max}	l	u_{\max}	Δu_{\max}	l	energy
0.1	160	2.2767			2.3555			2.6126			9.266297
0.1	320	2.2698	6.97e-3		2.3213	3.42e-2		2.4007	2.11e-1		9.264460
0.1	640	2.2680	1.79e-3	2.0	2.3125	8.80e-3	2.0	2.3510	4.97e-2	2.1	9.264001
0.2	320	2.2700			2.3058			2.3116			9.264181
0.1	320	2.2698	2.34e-4		2.3213	-1.54e-2		2.4007	-8.90e-2		9.264460
0.05	320	2.2697	5.50e-5	2.1	2.3247	-3.40e-3	2.2	2.4220	-2.13e-2	2.1	9.264524

Here is to be mentioned that the evolution of the solution for phase speeds $c \leq 0.27$ is qualitatively the same. Quantitatively, the time needed the solution to set on the dispersive track is usually smaller for a smaller phase speed, because of the reduced self-focusing role of the nonlinearity.

Example 2. In Fig. 2, results for $c = 0.28$ are presented. For $t < 10$ the behavior of the solution is similar to that in the previous example, but for larger times and when the time step τ is less than 0.2, it turns to grow and blows-up for $t \approx 20$. The blow-up is connected with the fact that the energy functional is not positive definite for BPE with quadratic nonlinearity (see [10] and the literature cited therein). Even when the amplitude is increasing, the energy is kept constant. A threshold value $c = 0.3$ was the last one for which a non-blowing-up evolution was found in [5] on the coarsest grid, while blow-up was encountered on the finest grid. Here we observe a non-blow-up for large time steps ($\tau = 0.2$) and a smaller value of c , which is probably due to the different numerical method used, namely the different scheme dispersion. Let us also note that when the energy non-conserving method from [6] is used, the solution blows-up for $\tau = 0.2$, as well.

As can be seen from Table 2 the method has second order numerical accuracy in space and time.

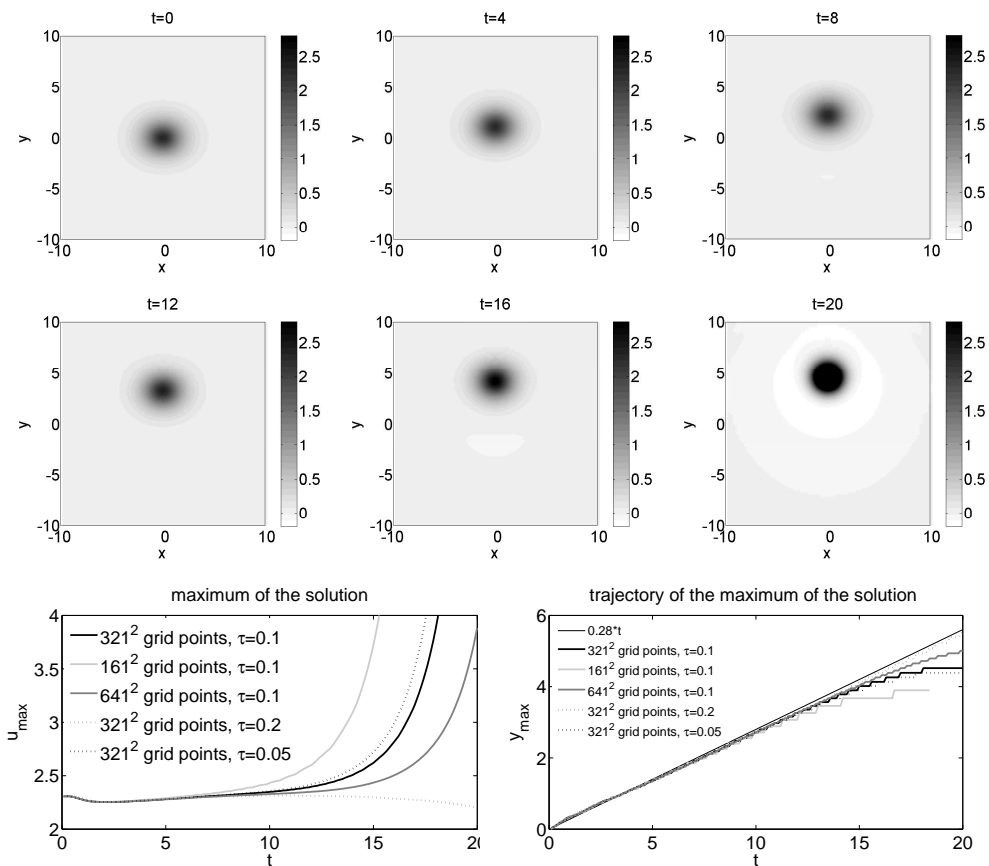


Figure 2: Evolution of the solution for $c = 0.28$, the maximum $u(0, y_{\max})$, and the trajectory of the maximum.

Conclusion. An energy conserving difference scheme for the investigation of the time evolution of the localized solutions of the Boussinesq Paradigm Equation (BPE) in two spatial dimensions is devised. The grid is non-uniform and the truncation error is second order in space and time. The results obtained for the time evolution of supposedly stationary propagating waves for different phase speeds are very similar to those in [6]. We have found that for phase speeds $0 \neq c \leq 0.27$, the initially localized wave disperses in the form of ring-wave expanding to infinity. Respectively, for $c \geq 0.29$ the initial evolution resembles a stationary propagation, but after some period of time a blow-up of the solution takes place. When $c = 0.28$, the asymptotic behavior of the solution depends on the numerical dispersion of the scheme, which is contingent on the value of time increment. Our results are in good agreement with [5], where a similar ($c = 0.3$) threshold is established for the appearance of the blow-up.

The fact that for $c \approx 0.28$, an time interval exists in which the solution is virtually reserving its shape while steadily translating means that 2D solitons could be found for the class of BPEs. This means that the nonlinearity is strong enough to balance the dispersion which is now much stronger than in the 1D case. In order to firmly establish this fact, our future plans are to consider also equations with different nonlinearities for which the blow-up is not possible.

Acknowledgment. This work has been partially supported by Grant DDVU02/71 from the National Science Fund by Ministry of Education, Youth, and Science of Republic of Bulgaria.

References

- [1] Christov, C.I.: An energy-consistent Galilean-invariant dispersive shallow-water model. *Wave Motion*, **34** (2001) 161–174
- [2] Christou, M.A., Christov, C.I.: Fourier-Galerkin method for 2D solitons of Boussinesq equation. *Math. Comput. Simul.*, **74** (2007) 82–92
- [3] Christov, C.I.: Numerical implementation of the asymptotic boundary conditions for steadily propagating 2D solitons of Boussinesq type equations, *Math. Comp. Simul.*, Appeared online August 10, 2010 Doi:10.1016/j.matcom.2010.07.030
- [4] Christov, C.I., Choudhury, J.: Perturbation solution for the 2D Boussinesq Equation. *Mech. Res. Commun.* (accepted)
- [5] Chertock, A., Christov, C.I., Kurganov, A.: Central-upwind schemes for the Boussinesq paradigm equation. *Proc. 4th Russian-German Advanced Research Workshop on Comp. Science and High Performance Computing*, 2010 (accepted)
- [6] Christov, C.I., Kolkovska, N., Vasileva, D.: On the Numerical Simulation of Unsteady Solutions for the 2D Boussinesq Paradigm Equation, *Lecture Notes Computer Science*, **6046** (2011) 386–394
- [7] Kolkovska, N.: Two Families of Finite Difference Schemes for Multidimensional Boussinesq Equation. *AIP Conference Proceedings*, **1301** (2010) 395–403
- [8] Kolkovska, N.: Convergence of Finite Difference Schemes for a Multidimensional Boussinesq Equation. *Lecture Notes Computer Science*, **6046** (2011) 469–476
- [9] van der Vorst, H.: Iterative Krylov methods for large linear systems. *Cambridge Monographs on Appl. and Comp. Math.*, **13** (2009)
- [10] Christov, C.I., Velarde, M.G.: Inelastic interaction of Boussinesq solitons. *I. J. Bifurcation & Chaos*, **4** (1994), 1095–1112

Monte Carlo Approaches for Model Sensitivity Studies

Ivan Dimov, Rayna Georgieva

1 Introduction

Simulation models are used (for diagnostic or prognostic purposes) in many fields to understand complex phenomena (natural or social) and therefore as tools to support decisions and policy. That is why it is very important to develop tools for estimation of uncertainties in model inputs, assumptions, and models structures in order to study how they affect inferences used for policy decisions. The significance of sensitivity analysis is illustrated on Figure 1 where the Rosen's view of modeling [6] is presented. Following the diagram, sensitivity analysis could be considered a mapping of the uncertainty in the inference (decoding) back onto the uncertainty in the assumptions (encoding) [8]. Sensitivity analysis (SA) decomposes the uncertainty in inference (policy conclusions) to uncertainty in inputs to identify which inputs are relevant for the prediction and then investigate how their uncertainty can be reduced in order to improve the accuracy of the prediction. Global SA explores uncertain inputs over a range, emphasizes interactions among input parameters and it is applicable to any kind of model.

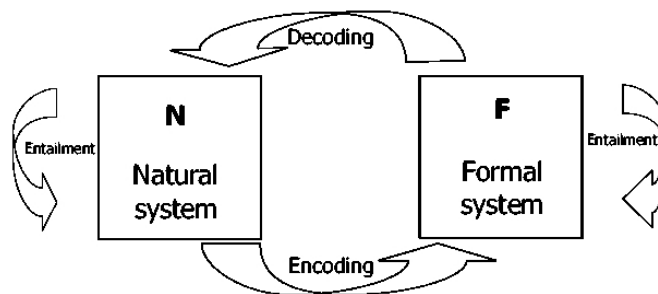


Figure 1: Modelling after Rosen.

The aim of the present work is to study the sensitivity of the ozone concentration levels due to variation of chemical rates applying variance-based techniques for global sensitivity analysis and Monte Carlo approaches (MCA) for numerical integration. The input data for sensitivity analysis has been obtained during runs of a large-scale mathematical model for remote transport of air pollutants (**Unified Danish Eulerian Model**, UNI-DEM¹, [12]).

¹UNI-DEM has been developed at the Danish National Environmental Research Institute (<http://www2.dmu.dk/AtmosphericEnvironment/DEM/>).

2 Background

There are three important issues during the process of sensitivity analysis applied to a given mathematical model. Firstly, it is crucial to choose an appropriate and an efficient sensitivity analysis technique with respect to the model features and purposes: local approach (one-at-a-time experiments), screening methods [1], variance-based methods [8, 9, 11], derivative-based global sensitivity approach [10]. The general concept is sampling-based and one need reliable sampling techniques (Latin hypercube sampling, importance sampling, stratified sampling, low-discrepancy sequences) and pseudo/quasi-random number generators. And finally, advanced efficient Monte Carlo methods for sensitivity measures estimation are required [2].

2.1 Sensitivity Analysis Method

Consider a scalar model output $u = f(x)$ corresponding to a number of non-correlated model parameters $x = (x_1, x_2, \dots, x_d)$ with a joint probability density function $p(x) = p(x_1, \dots, x_d)$. In Sobol' approach [9] the parameter importance is studied via numerical integration in the terms of **analysis of variance** (ANOVA) model representation [8, 9]:

$$f(x) = f_0 + \sum_{\nu=1}^d \sum_{l_1 < \dots < l_\nu} f_{l_1 \dots l_\nu}(x_{l_1}, x_{l_2}, \dots, x_{l_\nu}), \quad \text{where } f_0 = \text{const},$$

$f(x)$ is a square integrable model function, and $\int_0^1 f_{l_1 \dots l_\nu}(x_{l_1}, \dots, x_{l_\nu}) dx_{l_k} = 0, \quad 1 \leq k \leq \nu, \quad \nu = 1, \dots, d.$

An approach for evaluating *small* sensitivity indices (to avoid loss of accuracy because the analyzed database comes under this case) has been applied. It is a combined approach between approach of reducing of the mean value and correlated sampling suggested in [11]. Its idea is to replace the original model function with the function $\varphi(x) = f(x) - c$ where the constant $c \sim f_0$. Thus the partial and total variance estimations are presented in such a way:

$$D_y = \int \varphi(x) [\varphi(y, z') dx dz' - \varphi(x')] dx dx',$$

$$D = \int \varphi(x) [\varphi(x) - \varphi(x')] dx dx'.$$

2.2 Random Number Generators

A very fast 128-bit pseudorandom number generator of period $2^{19937} - 1$ has been used during the calculations:

- Mersenne Twister generator:
<http://www.math.sci.hiroshima-u.ac.jp/~m-mat/MT/emt.html>;

- SIMD-oriented Fast Mersenne Twister (SFMT) generator [7]:
<http://www.math.sci.hiroshima-u.ac.jp/~m-mat/MT/SFMT/index.html>.

In this work an algorithm with Gray code implementation and sets of direction numbers proposed by Joe and Kuo [5] for generating Sobol's quasirandom sequences are used.

2.3 Monte Carlo Algorithms

The *adaptive Monte Carlo algorithm* applied here uses a posteriori information about the variance [3]: the domain of integration is separated initially into subdomains with identical volume and the subdomain with the largest standard deviation is chosen for the next division.

The second *Monte Carlo algorithm is based on modified Sobol's $\Lambda\Pi_\tau$ sequences* (MCA-MSS). A Sobol's vector of dimension d ($\Lambda\Pi_\tau$ point) is considered as a centrum of a sphere with a radius ρ . Then a random point uniformly distributed on the sphere is taken and a random variable is defined as a value of the integrand at that random point (see [4]).

The values of the radius ρ are presented according to the number of samples N used in our experiments. Obviously, the possible radius ρ depends on the density of $\Lambda\Pi_\tau$ points. The higher the density is the smaller the radius should be. We also introduce a fixed coefficient, *radius coefficient* $\kappa = \rho/\delta$, where δ is the minimal distance between Sobol's points. To fulfill the assumption that the new random point $\xi^{(i)}(\rho)$, $i = 1, \dots, N$, belongs to the same elementary d -interval \mathbf{E}_i^d as the corresponding quasirandom point $\mathbf{x}^{(i)}$, the radius of spheres should satisfy the following condition:

$$\rho \leq \frac{\sigma}{2} \sqrt{\frac{d}{N}},$$

where σ is the side length of the d -dimensional cube (the integration domain) and N is the number of subdomains. Following the theory of low-discrepancy sequences each quasirandom point belongs to only one subdomain. It means that N is also the number of quasirandom points.

3 Discussion of Numerical Results

Our main aim here is to study the sensitivity of the ozone concentration according to the rate variation of some chemical reactions. On the other hand, we would like to compare efficiency (in terms of relative error) of the *plain Monte Carlo approach* [2], an *adaptive Monte Carlo algorithm*, a *Sobol' quasi-Monte Carlo algorithm*, and *MCA-MSS* to compute Sobol' global sensitivity measures.

Relative error (in absolute value) and total computational time for estimation of g_0 , total variance \mathbf{D} and main and total effects of input parameters using plain MCA,

Table 1: Relative error (in absolute value) and computational time for estimation of sensitivity indices of input parameters using various Monte Carlo approaches ($N = 7200$, $c \approx 0.51365$, $\delta \approx 0.08$).

Estimated quantity	Plain MCA	Adaptive MCA	Sobol' quasi-MCA	MCA-MSS	
				ρ	Rel. error
g_0	0.0005	-	0.0001	0.0007	4.6e-05
				0.002	7.9e-05
D	0.0131	0.0333	3.7e-05	0.0007	0.0015
				0.002	0.0010
S_1	0.0047	0.0031	0.0032	0.0007	0.0023
				0.002	0.0023
S_2	0.0103	0.0065	0.0034	0.0007	0.0021
				0.002	0.0027
S_3	0.5351	0.3493	0.0269	0.0007	0.0194
				0.002	0.0230
$S_{x_1}^{tot}$	0.0059	0.0061	0.0030	0.0007	0.0019
				0.002	0.0023
$S_{x_2}^{tot}$	0.0079	0.0035	0.0037	0.0007	0.0026
				0.002	0.0029
$S_{x_3}^{tot}$	0.7489	0.0893	0.0119	0.0007	0.0026
				0.002	0.0258
Time (s)	0.188	0.232	1.881	2.318	

adaptive MCA, Sobol' quasi-MCA and MCA-MSS are presented in Table 1. The quantity g_0 is the integral over the integration domain. Calculations have been carried out on a PC with Intel(R) Pentium(R) 4 Processor. Each estimated value applying plain MCA, adaptive MCA, and MCA-MSS is obtained after 10 algorithm runs. The total computational time for algorithms under consideration is of the same order. That is why the values of relative error could be considered as a measure of algorithm efficiency.

In our case the model function obtained after approximation is smooth and has a single peak at one of the domain corners. Adaptive procedures have been established as suitable techniques for numerical integration of functions with local computational difficulties. The latter fact gives a reason to apply an adaptive Monte Carlo algorithm for computing Sobol' global sensitivity indices. As we can expect, relative errors for adaptive algorithm are smaller than relative errors obtained applying plain MCA. A detailed discussion of numerical results for these two algorithms is given in [3].

Quasi-Monte Carlo algorithm and MCA-MSS lead to smaller relative errors especially for smaller quantities in absolute value - total variance, S_3 and $S_{x_3}^{tot}$ (see the results presented on Table 1). Two values of the *radius coefficient* κ have been chosen - $\kappa = 0.009$ and $\kappa = 0.02$. The results also show that additional effort is needed to

achieve estimates with satisfying accuracy for small sensitivity indices besides applying the combined approach. It should be noted that in this case the integrand is a smooth function. Although the Sobol's algorithm is known to be very good for smooth functions, the latter one has advantages against Sobol' quasi-Monte Carlo (smaller relative errors) for most cases. It is inspired by an increased dimension of integration domain in comparison with previous studies of this algorithm (see [4]).

The main conclusion (derived from current and preliminary studies) about extent of sensitivity of the mathematical model under consideration according the inputs is that the main effect of input parameters dominates over higher-order interactions. The following conclusion can be done on the base of preliminary and current studies - ozone concentrations are influenced in the highest extent by variability of rates of these three chemical reactions:

- $O_3 + NO \implies NO_2$
- $HO_2 + NO \implies OH + NO_2$
- $OH + CO \implies HO_2$

Note that the ozone does not necessarily participate in all these reactions. Important precursors of ozone participate instead.

4 Concluding remarks

The analysis of Monte Carlo algorithms under consideration show that:

- for *smooth* output relatively simple algorithms like plain Monte Carlo or quasi-Monte Carlo are efficient enough;
- for *non-smooth* output with *computational difficulties* more complicated algorithms like adaptive Monte Carlo or MCA-MSS should be applied;
- for relatively small sensitivity indices and non-regular output MCA-MSS is the most accurate approach.

Acknowledgment

This work is partly supported by the Bulgarian NSF Grants DTK 02/44/2009, DCVP 02/1 and DO 02-215/2008.

References

- [1] F. Campolongo, J. Cariboni, A. Saltelli. An Effective Screening Design for Sensitivity Analysis of Large Models. *Environmental Modelling and Software* **20** (10) (2007), 1509–1518. Elsevier Science Publishers B. V. Amsterdam, The Netherlands. ISSN: 1364-8152.

- [2] I.T. Dimov. *Monte Carlo Methods for Applied Scientists*. World Scientific, Singapore (2008).
- [3] I.T. Dimov, R. Georgieva. Monte Carlo Adaptive Technique for Sensitivity Analysis of a Large-scale Air Pollution Model. - In: Proceeding of LSSC'09. LNCS **5910** (2010), 387–394. Springer. ISSN: 978-3-642-12534-8.
- [4] I.T. Dimov, R. Georgieva. Monte Carlo Method for Numerical Integration based on Sobol's Sequences. - In: Proceeding of NMA'10. LNCS **6046** (2011), 50–59. Springer. ISSN: 0302-9743.
- [5] S. Joe, F.Y. Kuo. Constructing Sobol Sequences with Better Two-dimensional Projections. *SIAM J. Sci. Comput.* **30** (2008), 2635–2654.
- [6] R. Rosen. *Life Itself - a Comprehensive Inquiry into Nature, Origin, and Fabrication of Life*. Columbia University Press (1991).
- [7] M. Saito, M. Matsumoto. SIMD-oriented Fast Mersenne Twister: a 128-bit Pseudorandom Number Generator. - In: Proceeding of MCQMCM'06. Springer, 607–622 (2008).
- [8] A. Saltelli, M. Ratto, T. Andres, F. Campolongo, J. Cariboni, D. Gatelli, M. Saisana, S. Tarantola. *Global Sensitivity Analysis. The Primer*. John Wiley & Sons Ltd. (2008). ISBN: 978-0-470-05997-5.
- [9] I. M. Sobol'. Global Sensitivity Indices for Nonlinear Mathematical Models and Their Monte Carlo Estimates. *Mathematics and Computers in Simulation* **55 (1-3)** (2001), 271–280.
- [10] I. M. Sobol', S. Kucherenko. A New Derivative Based Importance Criterion for Groups of Variables and Its Link with the Global Sensitivity Indices. *Computer Physics Communications* **181 (7)** (2010), 1212–1217.
- [11] I. Sobol', E. Myshetskaya. Monte Carlo Estimators for Small Sensitivity Indices. *Monte Carlo Methods and Applications* **13 (5-6)** (2007), 455–465.
- [12] Z. Zlatev, I.T. Dimov. *Computational and Numerical Challenges in Environmental Modelling*. Elsevier, Amsterdam (2006).

Richardson Extrapolation: Accuracy, Stepsize Control and Stability

Ivan Dimov and Zahari Zlatev

1. Introduction of the Richardson Extrapolation. Consider the classical initial value problem for systems of ordinary differential equations (ODEs):

$$\frac{dy}{dt} = f(t, y), \quad t \in [a, b], \quad b > a, \quad y \in \mathfrak{R}^s, \quad f \in \mathfrak{R}^s, \quad s \geq 1, \quad (1)$$

with a given initial value $y(a) = y_0$.

Assume that $N \geq 1$ is a given integer and that $h = (b - a)/N$ is a real constant. It is convenient to consider the equidistant grid defined by

$$T_N = \{t_n, n = 0, 1, \dots, N \mid t_0 = a, t_n = t_{n-1} + h (n = 1, 2, \dots, N), t_N = b\}, \quad (2)$$

but the results could easily be extended for the case of non-equidistant grids.

Assume that an approximation $y_{n-1} \approx y(t_{n-1})$ has been calculated and used to obtain two approximations z_n and w_n of $y(t_n)$ by using a numerical method of order p and a large stepsize h and two small stepsizes $0.5h$ respectively. Then the Richardson Extrapolation, [9], can be defined by the following equality:

$$y_n = \frac{2^p w_n - z_n}{2^p - 1}. \quad (3)$$

2. Improvement of accuracy by using the Richardson Extrapolation. The following two relationships can be written (it is assumed that the numerical method used is of order p):

$$y(t_n) = z_n + h^p K + O(h^{p+1}), \quad (4)$$

$$y(t_n) = w_n + (0.5h)^p K + O(h^{p+1}). \quad (5)$$

Multiply (5) by 2^p and subtract (4) from (5). The result is:

$$y(t_n) = \frac{2^p w_n - z_n}{2^p - 1} + O(h^{p+1}). \quad (6)$$

The first term in the right-hand-side of (6) is the the approximation y_n from (3). This means that the Richardson Extrapolation results in a numerical method of order $p + 1$ and y_n will in general be more accurate than both z_n and w_n (at least when function f is smooth and the stepsize h is small). Thus, the Richardson extrapolation can be used in the efforts to improve the accuracy of the approximate solution.

3. Stepsize control. Neglect the last two terms in (4) and (5) and eliminate $y(n)$. The result is:

$$K = \frac{2^p(w_n - z_n)}{h^p(2^p - 1)}. \quad (7)$$

Substitute this value of K in (5) to obtain:

$$y(t_n) = w_n + \frac{w_n - z_n}{2^p - 1} + O(h^{p+1}). \quad (8)$$

Introduce the notation:

$$ERROR_n = \frac{w_n - z_n}{2^p - 1}. \quad (9)$$

Then a new, hopefully better, stepsize can be calculated by using the following relationship:

$$h_{new} = \omega \sqrt[p]{\frac{ERROR_n}{TOL}} h, \quad (10)$$

where TOL is the tolerance and ω is some constant ($\omega = 0.8$ is used in many codes for automatic control of the stepsize, see, for example, [10]).

4. Stability definitions. Three definitions related to the stability of the numerical methods for solving systems of ODEs will be introduced in this section and used further on. These definitions can be found, for example, in [2], [3], [5], [6], [7], [12] and are based on the fact that if a one-step method for solving systems of ODEs is applied to solve numerically the scalar equation $y' = \lambda y$ (where λ is a complex constant), then the computations can be carried out by using the formula $y_n = R(\mu) y_{n-1}$ with $\mu = \lambda h$ and $R(\mu) = P(\mu)/Q(\mu)$, $P(\mu)$ and $Q(\mu)$ being polynomials.

Definition 1. A one-step method for solving systems of ODEs is A-stable if $R(\mu) \leq 1$ for all $\mu = \alpha + i\beta$ with $\alpha \leq 0$.

Definition 2. An A-stable one-step method for solving systems of ODEs is strongly A-stable if $\lim_{\mu \rightarrow \infty} (R(\mu)) = \sigma < 1$.

Definition 3. An A-stable one-step method for solving systems of ODEs is strongly A-stable if $\lim_{\mu \rightarrow \infty} (R(\mu)) = 0$.

5. Some stability results. Consider the following seven numerical methods for solving systems of ODEs:

- **BDF**, the Backward Differentiation Formula of order one ([5], [6], [7]),
- **TRA**, the Trapezoidal Rule ([5], [6], [7]),

- **θ -M**, the θ -method ([5], [6], [7]),
- **IMP**, the Implicit Mid-Point Rule ([5], [6], [7]),
- **RK2**, the Modified Diagonally Implicit Runge-Kutta Method of order two ([12]),
- **RK5**, the Fully Implicit Three-stage Runge-Kutta Method of order five ([5], [6], [7]),
- **ROS**, the two-stage Rosenbrock Method of order two ([6]).

Consider also two splitting procedures:

- the sequential splitting (it was introduced, by an example, in [1]) and
- the Marchuk-Strang splitting (introduced simultaneously in 1968 by Marchuk, [8] and Strang, [11]).

More details about these two splittings and their use in large-scale scientific models can be found in [13] and [14].

Stability results were obtained when each of the seven numerical methods listed above is used:

- directly,
- in combination with the Richardson Extrapolation,
- in combination with the sequential splitting procedure and the Richardson Extrapolation and
- in combination with the Marchuk-Strang splitting procedure and the Richardson Extrapolation

These stability results are presented in a systematic manner in Table 1. It was convenient to apply the following abbreviations in this table:

- **AS**: means that the method is A-stable,
- **SAS**: means that the method is strongly A-stable,
- **LS**: means that the method is L-stable,
- **NS**: means that the method is **not** A-stable,
- **?**: means that the stability properties of the method are not investigated yet.

Table 1: Stability results obtained when seven numerical methods for systems of ODEs are used directly and in combination with the Richardson Extrapolation and two splitting procedures.

Numerical method	Direct Implementation	Richardson Extrapolation	Seq. Spl. + Richardson	M-S Spl. + Richardson
BDF	LS	LS	LS	?
TRA	AS	NS	NS	NS
θ -M	SAS, $0.5 < \theta < 1$	SAS, $2/3 < \theta < 1$	SAS, $0.64 < \theta < 1$?
IMP	AS	NS	NS	NS
RK2	LS	?	?	?
RK5	LS	?	?	?
ROS	LS	?	?	?

Roughly speaking, the statement of a theorem is given in each cell of Table 1 (excluding the cells with question marks). Two examples are given below: the first of them is for the cell in the fourth row and the third column, and the second one is for the cell in the third row and the fifth column.

Theorem 1. The combination of the θ -method and the Richardson Extrapolation is strongly A-stable for $2/3 < \theta < 1$.

Theorem 2. The combination of the Trapezoidal Rule, the Marchuk-Strang splitting procedure and the Richardson Extrapolation is not A-stable.

The results presented in the second column of Table 1 (stability properties of numerical methods for solving systems of ODEs implemented directly) are well known; see, for example, [5], [6], [7]. The results presented in the other columns (excluding the cells with question marks) are proven in [4] and [16].

6. Numerical experiments. An atmospheric chemical scheme containing 56 species ([13] and [14]) has been used in the numerical experiments. The problem is computationally very hard (badly-scaled, very stiff and extremely ill-conditioned Jacobian matrix). More details about the organization of the computations in connection with this chemical scheme are given in [4].

Numerical results obtained when the θ -method with $\theta = 0.75$ is used directly and in combination with the Richardson Extrapolation are given in Table 2. Eleven runs were performed. After each run the stepsize was reduced by a factor of two (which means that the number of steps is increased by a factor of two).

It is clearly seen that while the direct implementation of the θ -method with $\theta = 0.75$ performs as a first-order method (as it should). The accuracy of the combined

Table 2: Numerical results obtained when θ -method with $\theta = 0.75$ is run directly and in combination with the Richardson Extrapolation

Job No.	Time-steps	Direct use of the θ -method		Richardson Extrapolation	
		Accuracy	Rate	Accuracy	Rate
1	168	1.439E-00	-	3.988E-01	-
2	336	6.701E-01	2.147	5.252E-02	7.593
3	672	3.194E-01	2.098	1.503E-02	3.495
4	1344	1.550E-01	2.060	3.787E-03	3.968
5	2688	7.625E-02	2.033	9.502E-04	3.985
6	5376	3.779E-02	2.018	2.384E-04	3.986
7	10752	1.881E-02	2.009	5.980E-05	3.986
8	21504	9.385E-03	2.005	1.499E-05	3.989
9	43008	4.687E-03	2.002	3.754E-06	3.993
10	86016	2.342E-03	2.001	9.394E-07	3.996
11	172032	1.171E-03	2.001	2.353E-07	3.993

method (the θ -method with $\theta = 0.75$ plus the Richardson Extrapolation) is a second order method. The latter fact illustrates clearly that the accuracy can be improved considerably when the Richardson Extrapolation is used.

7. Conclusions and plans for future research. Some properties of the Richardson extrapolation applied when systems of ODEs are to be solved numerically were studied in this paper. Several results concerning stability were obtained. It is necessary to continue this work by

- proving stability results for some other numerical methods (first and foremost, for the methods where there are question marks in Table 1) and
- developing Richardson extrapolation for partial differential equations (some preliminary results are reported in [15]).

Acknowledgment. This work is partly supported by the Bulgarian NSF Grants DTK 02/44/2009 and DCVP 02/1.

References

- [1] Bagrinovskii, K. A. and Godunov, S. K.: Difference schemes for multi-dimensional problems. Dokl. Akad. Nauk USSR, 115, 431-433, 1957.
- [2] Dahlquist, G.: A special stability problem for linear multistep methods. BIT 3, 27-43 (1963).

- [3] Ehle, B. L.: On Padé approximations to the exponential function and A-stable methods for the numerical solution of initial value problems. Research Report CSRR 2010, Dept. AACS, University of Waterloo, Ontario, Canada (1969).
- [4] Faragó, I., Havasi, Á. and Zlatev, Z: Efficient implementation of stable Richardson Extrapolation algorithms. *Computers and Mathematics with Applications*, 60, 2309-2325, (2010).
- [5] Hairer, E. and Wanner, G., *Solving Ordinary Differential Equations: II Stiff and Differential-Algebraic Problems*. Springer-Verlag, Berlin (1991).
- [6] Hundsdorfer, W. and Verwer, J. G.: *Numerical Solution of Time-Dependent Advection-Diffusion-Reaction Equations*. Springer-Verlag, Berlin (2003).
- [7] Lambert, J. D.: *Numerical Methods for Ordinary Differential Equations*. Wiley, New York (1991).
- [8] Marchuk, G. I.: Some application of splitting-up methods in the solution of mathematical physics problems. *Applications of Mathematics (Applikace Matematiky)*, Vol. 13, No. 2, 103.132 (1968).
- [9] Richardson, L. F.: The deferred approach to the limit. *Phil. Trans. R. Soc. Lond. Ser. A*, 226,299-341 (1927).
- [10] Shampine, L. and Watts, H.: Global error estimation for ordinary differential equations. *ACM Trans. Math. Softw.* 2, 172-186 (1976)
- [11] Strang, G.: On the construction and comparison of numerical schemes. *SIAM Journal on Numerical Analysis*, 5, 505-517, 1968.
- [12] Zlatev, Z.: Modified diagonally implicit Runge-Kutta methods. *SIAM Journal on Scientific and Statistical Computing* 2, 321-334 (1981).
- [13] Zlatev, Z.: *Computer treatment of large air pollution models*. Kluwer Academic Publishers, Dordrecht-Boston-London (1995).
- [14] Zlatev, Z., Dimov, I.: *Computational and Numerical Challenges in Environmental Modelling*. Elsevier, Amsterdam-Boston-Heidelberg-London-New York-Oxford-Paris- San Diego-San Francisco-Singapore-Sidney-Tokyo (2006).
- [15] Zlatev, Z., Dimov, I. Faragó, I., Georgiev, K., Havasi, Á. and Ostromsky, Tz.: *Richardson Extrapolated Numerical Methods for Treatment of One-Dimensional Advection Equations*, Springer-Verlag, LNCS 6046, Berlin, Heidelberg, 7th International Conference, NMA 2010 Borovets, Bulgaria, August 20-24, 2010, Revised Papers, 198–206 (2011).
- [16] Zlatev, Z., Faragó, I., Havasi, Á.: Stability of Richardson Extrapolation and the θ -method. *Journal of Computational and Applied Mathematics*, 235, 507-517 (2010).

Ant Colony Optimization Start Strategies: Two Case Studies

Stefka Fidanova, Pencho Marinov

1 Introduction

The ability of ant colonies to form paths for carrying food is rather fascinating. The problem is solved collectively by the whole colony. This ability is explained by the fact that ants communicate in an indirect way by laying trails of pheromone. The higher the pheromone trail within a particular direction, the higher the probability of choosing this direction. The collective problem solving mechanism has given rise to a metaheuristic referred to as Ant Colony Optimization (ACO).

The ACO algorithm uses a colony of artificial ants that behave as cooperative agents in a mathematical space where they are allowed to search and reinforce pathways (solutions) in order to find the optimal ones. The problem is represented by graph and the ants walk on the graph to construct solutions. The solutions are represented by paths in the graph. After the initialization of the pheromone trails, the ants construct feasible solutions, starting from random nodes, and then the pheromone trails are updated. At each step the ants compute a set of feasible moves and select the best one (according to some probabilistic rules) to continue the rest of the tour. The structure of the ACO algorithm is shown by the pseudo-code below. The transition probability $p_{i,j}$, to choose the node j when the current node is i , is based on the heuristic information $\eta_{i,j}$ and the pheromone trail level $\tau_{i,j}$ of the move, where $i, j = 1, \dots, n$.

$$p_{i,j} = \frac{\tau_{i,j}^a \eta_{i,j}^b}{\sum_{k \in Unused} \tau_{i,k}^a \eta_{i,k}^b},$$

where *Unused* is the set of unused nodes of the graph. The higher the value of the pheromone and the heuristic information, the more profitable it is to select this move and resume the search. In the beginning, the initial pheromone level is set to a small positive constant value τ_0 ; later, the ants update this value after completing the construction stage. ACO algorithms adopt different criteria to update the pheromone level.

The pheromone trail update rule is given by:

$$\tau_{i,j} \leftarrow \rho \tau_{i,j} + \Delta \tau_{i,j},$$

where ρ models evaporation in the nature and $\Delta \tau_{i,j}$ is the new added pheromone which is proportional to the quality of the solution.

As other metaheuristics, ACO algorithm is applied on hard combinatorial optimization problems coming from real life and industry. It is unpractical to apply exact

```

Ant Colony Optimization
Initialize number of ants;
Initialize the ACO parameters;
while not end-condition do
    for k=0 to number of ants
        ant k choses start node;
        while solution is not constructed do
            ant k selects higher probability node;
        end while
    end for
    Update-pheromone-trails;
end while

```

Figure 1: Pseudocode for ACO

methods or traditional numerical methods on this kind of problems, because they need huge amount of computational resources, time and memory. Examples of optimization problems are Traveling Salesman Problem [6], Vehicle Routing [7], Minimum Spanning Tree [5], Multiple Knapsack Problem [4], etc.

In this paper we propose two kind of estimation of start nodes with respect to the quality of the solutions and thus to better manage the search process. We offer various start strategies and their combinations.

2 Subset Estimations

The essential part of ACO algorithm is starting from random node when ants create solutions. It is a kind of diversification of the search and leads to using small number of ants, which means less computational resources. But for some problems, especially subset problems, it is important from which node the search process starts. For example if an ant starts from node which does not belong to the optimal solution, probability to construct it is zero. Therefore we offer several start strategies.

Let the graph of the problem has m nodes. We divide the set of nodes on N subsets. There are different ways for dividing. Normally, the nodes of the graph are randomly enumerated. An example for creating of the nodes subsets, without loss of generality, is: the node number one is in the first subset, the node number two is in the second subset, etc. the node number N is in the N -th subset, the node number $N + 1$ is in the first subset, etc. Thus the number of the nodes in the subsets are almost equal. We introduce estimations $D_j(i)$ and $E_j(i)$ of the node subsets, where $i \geq 2$ is the number of the current iteration. $D_j(i)$ shows how good is the j -th subset and $E_j(i)$ shows how bad is the j -th subset. $D_j(i)$ and $E_j(i)$ are weight coefficients of j -th node subset ($1 \leq j \leq N$). We propose two ways to estimate the nodes subsets:

Estimation 1

$$D_j(i) = \frac{i \cdot D_j(i-1) + E_j(i)}{i},$$

$$E_j(i) = \frac{i.E_j(i-1) + G_j(i)}{i},$$

Estimation 2

$$D_j(i) = \varphi.D_j(i-1) + (1-\varphi).F_j(i), \quad (1)$$

$$E_j(i) = \varphi.E_j(i-1) + (1-\varphi).G_j(i), \quad (2)$$

where $i \geq 1$ is the current process iteration and for each j ($1 \leq j \leq N$):

$$F_j(i) = \begin{cases} \frac{f_{j,A}}{n_j} & \text{if } n_j \neq 0 \\ F_j(i-1) & \text{otherwise} \end{cases}, \quad (3)$$

$$G_j(i) = \begin{cases} \frac{g_{j,B}}{n_j} & \text{if } n_j \neq 0 \\ G_j(i-1) & \text{otherwise} \end{cases}, \quad (4)$$

$f_{j,A}$ is the number of the solutions among the best $A\%$, $g_{j,B}$ is the number of the solutions among the worst $B\%$, where $A + B \leq 100$, $i \geq 2$ and

$$\sum_{j=1}^N n_j = n, \quad (5)$$

where n_j ($1 \leq j \leq N$) is the number of solutions obtained by ants starting from nodes subset j , n is the number of ants. Initial values of the weight coefficients are: $D_j(1) = 1$ and $E_j(1) = 0$. The parameter φ , $0 \leq \varphi \leq 1$, shows the weight of the information from the previous iterations and from the last iteration. When $\varphi = 0$ only the information from the last iteration is taken in to account. If $\varphi = 0.5$ the influence of the previous iterations versus the last is equal. When $\varphi = 1$ only the information from the previous iterations is taken in to account. When $\varphi = 0.25$ the weight of the information from the previous iterations is three times less than this one of the last iteration. When $\varphi = 0.75$ the weight of the previous iterations is three times higher than this one of the last iteration. The balance between the weights of the previous iterations and the last is important. At the beginning when the current best solution is far from the optimal one, some of the node subsets can be estimated as good. Therefore, if the value of the parameter φ is too high the estimation can be distorted. If the weight of the last iteration is too high then information for good and bad solutions from previous iterations is ignored, which can distort estimation too.

We try to use the experience of the ants from previous iteration to choose the better starting node. Other authors use this experience only by the pheromone, when the ants construct the solutions [3]. Let us fix threshold E for $E_j(i)$ and D for $D_j(i)$, than we construct several strategies to choose start node for every ant, the threshold E increases every iteration with $1/i$ where i is the number of the current iteration:

- (1) If $E_j(i)/D_j(i) > E$ then the subset j is forbidden for current iteration and we choose the starting node randomly from $\{j \mid j \text{ is not forbidden}\}$;

- (2) If $E_j(i)/D_j(i) > E$ then the subset j is forbidden for current simulation and we choose the starting node randomly from $\{j \mid j \text{ is not forbidden}\}$;
- (3) If $E_j(i)/D_j(i) > E$ then the subset j is forbidden for K_1 consecutive iterations and we choose the starting node randomly from $\{j \mid j \text{ is not forbidden}\}$;
- (4) Let $r_1 \in [0.5, 1)$ is a random number. Let $r_2 \in [0, 1]$ is a random number. If $r_2 > r_1$ we randomly choose node from subset $\{j \mid D_j(i) > D\}$, otherwise we randomly chose a node from the not forbidden subsets, r_1 is chosen and fixed at the beginning.
- (5) Let $r_1 \in [0.5, 1)$ is a random number. Let $r_2 \in [0, 1]$ is a random number. If $r_2 > r_1$ we randomly choose node from subset $\{j \mid D_j(i) > D\}$, otherwise we randomly chose a node from the not forbidden subsets, r_1 is chosen at the beginning and increase with r_3 every iteration.

Where $0 \leq K_1 \leq$ "number of iterations" is a parameter. If $K_1 = 0$, than strategy 3 is equal to the random choose of the start node. If $K_1 = 1$, than strategy 3 is equal to the strategy 1. If $K_1 =$ "maximal number of iterations", than strategy 3 is equal to the strategy 2.

We can use more than one strategy for choosing the start node, but there are strategies which can not be combined. We distribute the strategies into two sets: $St1 = \{strategy1, strategy2, strategy3\}$ and $St2 = \{strategy4, strategy5\}$. The strategies from same set can not be used at once. Thus we can use strategy from one set or combine it with strategies from the other set. Exemplary combinations are $(strategy1)$, $(strategy2; strategy5)$, $(strategy3; strategy4)$. When we combine strategies from $St1$ and $St2$, first we apply the strategy from $St1$ and according it some of the regions (node subsets) become forbidden, and after that we choose the starting node from not forbidden subsets according the strategy from $St2$.

3 Computational Results

We test the ideas for controlled start on MKP. MKP is a real world problem and is a representative of the class of subset problems. The MKP has numerous applications in theory as well as in practice. It also arises as a subproblem in several algorithms for more complex problems and these algorithms will benefit from any improvement in the field of MKP. The following major applications can be mentioned: problems in cargo loading, cutting stock, bin-packing, budget control and financial management. The computational experience of the ACO algorithm is shown using 10 MKP instances from "OR-Library" available within WWW access at <http://people.brunel.ac.uk/mastjjb/jeb/orlib/>, with 100 objects and 10 constraints. The parameters are fixed as follows: $\rho = 0.5$, $a = 1$, $b = 1$, number of used ants is 20, $A = 30$, $B = 30$, $D = 1.5$, $E = 0.5$, $K_1 = 5$, $r_3 = 0.01$. The values of ACO parameters (ρ, a, b) are from [4] and experimentally is found that they are best for MKP. The tests are run with 1, 2, 4, 5 and 10 nodes within the nodes subsets and values for φ are 0, 0.25, 0.5 and 0.75. For

Table 1: Estimation 1 and Estimation 2

number nodes	10	5	4	2	1	number nodes	10	5	4	2	1
random	32	32	32	32	32	random	32	32	32	32	32
strat. 1	83	90	86	86	94	strat. 1	64	86	83	90	93
strat. 2	35	31	38	61	83	strat. 2	63	87	83	91	91
strat. 3	65	86	86	86	94	strat. 3	62	89	83	90	88
strat. 4	84	84	84	84	84	strat. 4	84	82	84	87	92
strat. 5	84	84	84	84	84	strat. 5	85	85	86	90	87
strat. 1-4	85	92	87	87	96	strat. 1-4	68	89	85	93	95
strat. 1-5	85	92	87	87	96	strat. 1-5	62	90	81	92	92
strat. 2-4	35	37	37	62	84	strat. 2-4	65	89	86	90	93
strat. 2-5	35	37	37	62	84	strat. 2-5	59	88	84	92	93
strat. 3-4	71	85	86	93	94	strat. 3-4	66	90	84	94	93
strat. 3-5	71	85	86	93	94	strat. 3-5	61	86	81	94	92

every experiment, the results are obtained by performing 30 independent runs, then averaging the fitness values. The computational time which takes start strategies is negligible with respect to the computational time which takes solution construction. The problem which arises is how to compare the achieved solutions by different strategies and different node-devisions. Therefore the difference (interval) d between the worst and best average result for every problem is divided to 10. If the average result for some strategy, node deviation and φ is in the first interval with borders the worst average result and worst average plus $d/10$ it is appreciated with 1. If it is in the second interval with borders the worst average plus $d/10$ and worst average plus $2d/10$ it is appreciated with 2 and so on. If it is in the 10th interval with borders the best average minus $d/10$ and the best average result, it is appreciated with 10. Thus for a test problem the achieved results for every strategy, every nodes deviation and every φ is appreciated from 1 to 10. After that is summed the rate of all test problems for every strategy, every nodes deviation and φ . So the rate of the strategies/node-devision/ φ becomes between 10 and 100, because the benchmark problems are 10. It is mode of result classification.

For all values of the parameter φ the best rate according node deviation is when there is only one node in node-subsets. So we put in tables the rate of the start strategies when the node subsets consist one node, with bold is the best rate. We compare the achieved results by the estimation method 2 with results by the estimation method 1 when $\varphi = 0.5$ because it is the best value for φ .

Comparing the tables me observe that rates of the estimation method 1 are higher than rates of estimation method 2 in most of the cases with exeption of strategy 2 and its combinations with strategies 4 and 5. The best rate with estimation 1 is 96 while the best rate estimation 2 is 95. The both are achieved wen strategy 1 is combined with strategy 4. We can conclude that the estimation method 1 achieves better results than estimation method 2.

4 Conclusion

In this paper we address the modeling of the process of ant colony optimization method by using two kind of nodes estimations, combining 5 start strategies. So, the start node of each ant depends of the goodness of the respective region. In a future we will focus on parameter settings which manage the starting procedure. We will investigate on influence of the parameters to algorithm performance.

Acknowledgments: This work has been partially supported by the Bulgarian National Scientific Fund under the grants DID 02/29-”Modeling Processes with fixed development rules” and DTK 02/44-”Effective Monte Carlo Methods for large-scale scientific problems”.

References

- [1] Bonabeau E., Dorigo M., Theraulaz G., *Swarm Intelligence: From Natural to Artificial Systems*, New York, Oxford University Press, 1999.
- [2] Dorigo M., Gambardella L.M., *Ant Colony System: A Cooperative Learning Approach to the Traveling Salesman Problem*. *IEEE Transactions on Evolutionary Computation* 1, 53-66, 1997.
- [3] Dorigo M., Stutzle T., *Ant Colony Optimization*, MIT Press, 2004.
- [4] Fidanova S., *Evolutionary Algorithm for Multiple Knapsack Problem*, *Int. Conference Parallel Problems Solving from Nature, Real World Optimization Using Evolutionary Computing*, ISBN No 0-9543481-0-9, Granada, Spain, 2002.
- [5] Reiman M., Laumanns M., *A Hybrid ACO algorithm for the Capacitated Minimum Spanning Tree Problem*, In *proc. of First Int. Workshop on Hybrid Metaheuristics*, Valencia, Spain, 2004, 1-10.
- [6] Stutzle T. Dorigo M., *ACO Algorithm for the Traveling Salesman Problem*, In K. Miettinen, M. Makela, P. Neittaanmaki, J. Periaux eds., *Evolutionary Algorithms in Engineering and Computer Science*, Wiley, 163-183, 1999.
- [7] Zhang T., Wang S., Tian W., Zhang Y., *ACO-VRPTWRV: A New Algorithm for the Vehicle Routing Problems with Time Windows and Re-used Vehicles based on Ant Colony Optimization*, *Sixth International Conference on Intelligent Systems Design and Applications*, IEEE press, 2006, 390-395.

On Two-Level Splittings for Quadratic FEM Anisotropic Elliptic Problems

Ivan Georgiev, Johannes Kraus, Maria Lymbery,
Svetozar Margenov

1 Introduction

This note deals with the construction of subspaces for quadratic FEM anisotropic elliptic problems with a focus on the robustness with respect to mesh and coefficient anisotropy. It is known that standard hierarchical basis (HB) techniques do not result in splittings in which the angle between the coarse space and its (hierarchical) complement is uniformly bounded with respect to the ratio of anisotropy.

The presented numerical experiments give a comparison between the HB approach and an alternative construction that makes use of a particular Schur complement approximation, which avoids an HB representation of the stiffness matrix.

Let us consider the linear system of equations

$$A_h \mathbf{u}_h = F_h, \quad (1)$$

which has been obtained after finite element discretization of the elliptic boundary value problem

$$-\nabla \cdot (a(x) \nabla u(x)) = f(x) \quad \text{in } \Omega, \quad (2)$$

$$u = 0 \quad \text{on } \Gamma_D, \quad (3)$$

$$(a(x) \nabla u(x)) \cdot \mathbf{n} = 0 \quad \text{on } \Gamma_N. \quad (4)$$

The notations used in the above equations are as follows: Ω - a polygonal convex domain in R^2 ; $f(x)$ - a given function in $L_2(\Omega)$; $a(x)$ - a symmetric positive definite 2×2 coefficient matrix, uniformly bounded in Ω ; \mathbf{n} - the outward unit vector normal to the boundary $\Gamma = \partial\Omega$, $\Gamma = \Gamma_D \cup \Gamma_N$; A_h - the corresponding global stiffness matrix; F_h - the global right hand side; h - the mesh parameter of the underlying partition \mathcal{T}_h of Ω .

We assume that conforming quadratic finite elements have been used in the process of discretization of (2)–(4) and also that the partition of the domain Ω has been performed in such a way that over each element $e \in \mathcal{T}_h$ the functions $a_{i,j}(x)$ are constant. Due to the partitioning of the domain Ω into finite elements, the stiffness matrix A_h can be written in the form

$$A_h = \sum_{e \in \mathcal{T}_h} R_e^T A_e R_e, \quad (5)$$

where A_e is the element stiffness matrix and R_e is the mapping that restricts a global vector to a given element $e \in \mathcal{T}_h$.

It can be proved that it is equivalent to analyze an arbitrary anisotropic symmetric positive definite coefficient matrix $a(e)$ on the reference triangle \tilde{e} with coordinates $(0, 0)$, $(1, 0)$, $(0, 1)$, or, alternatively, the isotropic Laplace operator, i.e., $a(e) = I$, on a triangle of arbitrary shape. In the present paper we use the second approach for which the element stiffness matrix A_e can be written in the form

$$A_e = \begin{bmatrix} \frac{b+c}{2} & -\frac{2c}{3} & \frac{c}{6} & 0 & \frac{b}{6} & -\frac{2b}{3} \\ -\frac{2c}{3} & \frac{4(a+b+c)}{3} & -\frac{2c}{3} & -\frac{4b}{3} & 0 & -\frac{4a}{3} \\ \frac{c}{6} & -\frac{2c}{3} & \frac{a+c}{2} & -\frac{2a}{3} & \frac{a}{6} & 0 \\ 0 & -\frac{4b}{3} & -\frac{2a}{3} & \frac{4(a+b+c)}{3} & -\frac{2a}{3} & -\frac{4c}{3} \\ \frac{b}{6} & 0 & \frac{a}{6} & -\frac{2a}{3} & \frac{a+b}{2} & -\frac{2b}{3} \\ -\frac{2b}{3} & -\frac{4a}{3} & 0 & -\frac{4c}{3} & -\frac{2b}{3} & \frac{4(a+b+c)}{3} \end{bmatrix},$$

where a , b and c equal the cotangents of the angles in $e \in \mathcal{T}_h$.

One of the most popular iterative methods for solving systems of linear algebraic equations with large sparse symmetric and positive definite matrices is the Preconditioned Conjugate Gradient (PCG) method whose convergence rate crucially depends on the quality of the used preconditioner. The general strategy for efficient preconditioning requires that the spectral condition number $\kappa(C^{-1}A_h)$ of the preconditioned matrix is much less than the condition number of the original matrix and that the computational complexity $\mathcal{N}(C^{-1}\mathbf{v})$ of applying the preconditioner is much smaller than the complexity of solving the original problem. The symmetric and positive definite matrix C is referred to as an optimal preconditioner for the system (1) if $\kappa(C^{-1}A_h) = O(1)$ and $\mathcal{N}(C^{-1}\mathbf{v}) = O(N)$, where N is the total number of unknowns.

2 Two-level Preconditioners

Let us consider two consecutive meshes obtained from a uniform refinement procedure and let us split the unknowns of the corresponding system into two groups where the first one consists of the nodes which do not belong to the coarse mesh and the second one contains all nodes that belong to the coarse mesh. Due to this two-level splitting we present the matrix $A = A_h$, and for convenience we skip the subscript h with the matrix A from now on, in the factorized form

$$A = \begin{bmatrix} A_{11} & A_{12} \\ A_{21} & A_{22} \end{bmatrix} = \begin{bmatrix} I & \\ A_{21}A_{11}^{-1} & I \end{bmatrix} \begin{bmatrix} A_{11} & A_{12} \\ S & \end{bmatrix}, \quad (6)$$

where the Schur complement is given by $S = A_{22} - A_{21}A_{11}^{-1}A_{12}$. Then we consider the following multiplicative two-level preconditioner

$$B = \begin{bmatrix} I & \\ A_{21}A_{11}^{-1} & I \end{bmatrix} \begin{bmatrix} A_{11} & A_{12} \\ & Q \end{bmatrix} = \begin{bmatrix} A_{11} & A_{12} \\ A_{21} & Q + A_{21}B_{11}^{-1}A_{12} \end{bmatrix} \quad (7)$$

where Q is an approximation to the exact Schur complement S . It can easily be seen that the spectral condition number

$$\kappa(B^{-1}A) = \frac{\lambda_{max}(B^{-1}A)}{\lambda_{min}(B^{-1}A)} \quad (8)$$

measuring the quality of the two-level preconditioner B defined via (7) depends on the extremal eigenvalues of $Q^{-1}S$, in other words, it involves the bounds

$$\check{\alpha}v_2^T S v_2 \leq v_2^T Q v_2 \leq \hat{\alpha}v_2^T S v_2 \quad \forall v_2$$

where $\check{\alpha}$ and $\hat{\alpha}$ denote positive constants, which (without loss of generality) satisfy $0 < \check{\alpha} \leq 1$, and $1 \leq \hat{\alpha} < \infty$. More precisely, we have that

$$\kappa(B^{-1}A) \leq \frac{\hat{\alpha}}{\check{\alpha}}. \quad (9)$$

Two level preconditioners like (7) are the basis for constructing multilevel preconditioners, which can be obtained by applying recursively a two-level method to the coarse-level matrix (Schur complement approximation). Optimal multilevel methods, however, additionally exploit certain stabilization techniques. For example, the so-called Algebraic Multi-Level Iteration (AMLI) algorithm stabilizes the condition number via certain matrix polynomials, cf. [7, 8]. The AMLI preconditioner can be proven to be optimal if the degree ν of the polynomial satisfies the condition

$$(1 - \gamma^2)^{-1/2} < \nu < \rho, \quad (10)$$

where γ is the constant in the strengthened Cauchy-Bunyakowski-Schwarz (CBS) inequality and ρ is the reduction factor of the number of degrees of freedom. For 2D problems and regular mesh refinement typically $\rho = 4$.

2.1 Hierarchical Basis Approximation

A commonly used approach for constructing two-level preconditioners involves the hierarchical basis, see e.g. [4, 7, 8]. Let \mathcal{T}_H and \mathcal{T}_h be two successive mesh refinements of the domain Ω and let $\{\phi_H^{(k)}, k = 1, 2, \dots, N_H\}$ and $\{\phi_h^{(k)}, k = 1, 2, \dots, N_h\}$ denote the corresponding standard finite element nodal basis functions. Then we split the mesh points of \mathcal{T}_h into two groups - coarse grid nodes, i.e. points from \mathcal{T}_H , and the rest, i.e. points from $\mathcal{T}_h \setminus \mathcal{T}_H$. Now we define the hierarchical two-level basis as follows:

$$\{\tilde{\phi}_h^{(i)}\}_{i=1}^{N_h} = \{\phi_h^{(m)} \text{ on } \mathcal{T}_h \setminus \mathcal{T}_H\} \cup \{\phi_H^{(l)} \text{ on } \mathcal{T}_H\}.$$

Obviously, the nodal basis matrix A and the hierarchical basis matrix \tilde{A} are related to each other via

$$\tilde{A} = \begin{bmatrix} \tilde{A}_{11} & \tilde{A}_{12} \\ \tilde{A}_{21} & \tilde{A}_{22} \end{bmatrix} = JAJ^T$$

where the transformation matrix J has the form

$$J = \begin{bmatrix} I & \\ J_{21} & I \end{bmatrix}.$$

The hierarchical basis two-level (multiplicative) two-level preconditioner is defined by

$$C = \begin{bmatrix} I & \\ \tilde{A}_{21}\tilde{A}_{11}^{-1} & I \end{bmatrix} \begin{bmatrix} \tilde{A}_{11} & \tilde{A}_{12} \\ & \tilde{A}_{22} \end{bmatrix}. \quad (11)$$

The pivot block and the Schur complement are invariant with respect to the above basis transformation, i.e.,

$$\tilde{A}_{11} = A_{11}, \quad \tilde{S} = S.$$

For the second diagonal block, which is related to the unknowns from the coarse mesh, we have

$$\tilde{A}_{22} = A_H.$$

Then the relative condition number with respect to the multiplicative two-level preconditioner C can be estimated by

$$\kappa(C^{-1}\tilde{A}) \leq \kappa(A_H^{-1}S) = \kappa(A_H^{-1}\tilde{S}) \leq \frac{1}{1-\gamma^2} \quad (12)$$

where γ is the CBS constant related to the considered hierarchical two-level splitting. In [9] is shown numerically that for highly anisotropic elliptic problems $\gamma \rightarrow 1$ and thus the preconditioner (11) is not robust with respect to anisotropy.

2.2 Schur Complement Approximation

An alternative approach to construct a two-level preconditioner is to approximate the exact Schur complement S in (6) by a proper sparse matrix Q without changing the basis. The technique for computing such an approximation Q we are studying here has been introduced in [1]. The idea is first to compute all local macroelement Schur complements

$$S_E = A_{E,22} - A_{E,21}A_{E,11}^{-1}A_{E,12}, \quad \forall E \in \mathcal{T}_H,$$

associated with a partition of the mesh into macro elements E and then to assemble the small-sized local Schur complement matrices S_E in order to obtain the global Schur complement approximation Q . That is, we define

$$Q := \sum_E R_E^T S_E R_E \quad (13)$$

where R_E is the mapping that restricts a global vector to a macro element $E \in \mathcal{T}_H$. Note that when replacing A_H with Q in (12) the estimate still holds true, i.e.,

$$\kappa(B^{-1}A) \leq \kappa(Q^{-1}S) \leq \frac{1}{1-\gamma^2} \quad (14)$$

see [6] for details.

3 Numerical Tests

Without loss of generality we may assume that the angles of the element e satisfy the inequalities $\theta_1 \geq \theta_2 \geq \theta_3$. If a , b , and c equal their cotangents, then we have $c = (1-ab)/(b+a)$ and $|a| \leq b \leq c$. Further, by setting $\alpha = a/c$, and $\beta = b/c$, we can estimate the relative condition number with respect to the presented preconditioners in the domain $D = \{(\alpha, \beta) \in \mathcal{R}^2 : -1/2 < \alpha \leq 1, \max\{-\alpha/(\alpha+1), |\alpha|\} \leq \beta \leq 1\}$. The subdomains of D where the condition number estimate $\kappa(Q^{-1}S) < 4$ is valid are shown in Fig. 1. Here $\hat{\kappa}$ denotes the condition number obtained by using the Schur complement approximation while $\tilde{\kappa}$ denotes the condition number corresponding to the ‘‘First Reduce’’ variant of the hierarchical basis approximation, cf. [3]. According to the AMLI optimality condition (10), this case corresponds to a stabilization polynomial of degree $\nu = 2$. Similarly, Fig. 2 shows the subdomains of the same parameters $\{\alpha, \beta\}$ for which $\kappa(Q^{-1}S) < 9$, i.e. a stabilization polynomial of degree three can be used to obtain an optimal order method, see (10). What we can ob-

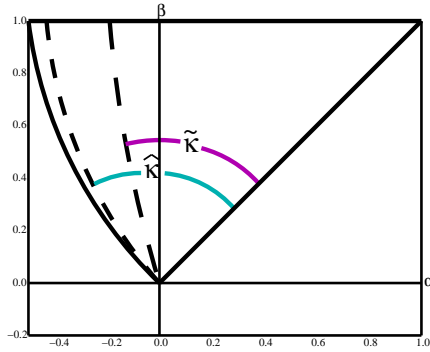


Figure 1: $\{\alpha, \beta\} : \kappa(Q^{-1}S) < 4$

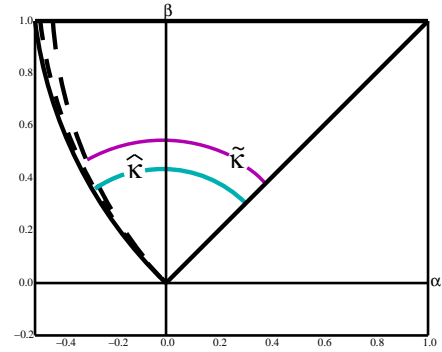


Figure 2: $\{\alpha, \beta\} : \kappa(Q^{-1}S) < 9$

serve is that the region subtended by the condition number of the Schur complement approximation in both cases is bigger than the region subtended by the hierarchical basis approximation.

On the basis of the obtained computational results, we conclude that it is sufficient to fix the minimal angle θ_3 to be $\geq 20^\circ$ for the Schur complement approximation and $\geq 30^\circ$ for the hierarchical basis approximation in order to meet the optimality

condition (10) for $\nu = 2$. The AMLI method with $\nu = 3$ will satisfy the condition (10) if $\theta_3 \geq 10^\circ$ in case of the Schur complement approximation (13), and if $\theta_3 \geq 20^\circ$ in case of the hierarchical basis approximation. Let us remark that the restriction $\theta_3 \geq 27^\circ$ can be controlled for example by the mesh generator TRIANGLE.

Remark: We should also note that the estimates for $\tilde{\kappa}$ have been obtained using general assumptions for \mathcal{T}_0 while the numerical results for $\hat{\kappa}$ are only for uniform initial triangulations.

Acknowledgment: The partial support of the Bulgarian NSF Grants DCVP 02/1 and DO 02-338/08 and Austrian FWF grant P22989-N18 is highly appreciated.

References

- [1] Kraus, J.: Algebraic multilevel preconditioning of finite element matrices using local Schur complements, *Numer. Linear Algebra Appl.* 13(2006),pp. 49-70.
- [2] Axelsson, O.: Stabilization of Algebraic Multilevel Iteration method; additive methods, *Numerical Algorithms*, (1999), 23-47.
- [3] Blaheta, R., Margenov, S., Neytcheva, M.: Uniform Estimate of the Constant in the Strengthened CBS inequality for Anisotropic Non-conforming FEM systems, *Numerical Linear Algebra and Applications*, Vol.11 (4)(2004), 309-326.
- [4] Kraus, J., Margenov, S.: Robust Algebraic Multilevel Methods and Algorithms. De Gruyter, Germany (2009)
- [5] Maitre, J.F., Musy, S.: The Contraction Number of a Class of Two-level Methods; An Exact Evaluation for Some Finite Element Subspaces and Model Problems, *Lect. Notes Math.* 960 (1982), 535-544.
- [6] Axelsson, O., Blaheta, R., Neytcheva, M.: Preconditioning of Boundary Value Problems Using Elementwise Schur Complements, *SIAM J. Matrix Anal. Appl.* 31 (2009), 767-789.
- [7] Axelsson, O., Vassilevski, P.: Algebraic Multilevel Preconditioning Methods I, *Numer. Math.* 56 (1989), 157-177.
- [8] Axelsson, O. Vassilevski, P.: Algebraic Multilevel Preconditioning Methods II, *SIAM J. Numer. Anal.* 27 (1990), 1569-1590.
- [9] Georgiev, I., Lymbery, M., Margenov, S.: Analysis of the CBS Constant for Quadratic Finite Elements, Springer LNCS

Some Notes on the Implementation of Sparse Matrix Techniques in an Advection-Diffusion Module

Krassimir Georgiev, Zahari Zlatev

1 The 2D version of the Danish Eulerian model and rotational test

Our study is based on the Danish Eulerian model for long transport of air pollutants over the territory of Europe (UNI-DEM)([8]). In fact, the model computational domain covers Europe and parts of Asia, Africa and the Atlantic Ocean. The long-range transport of air pollution is studied by the following system of partial differential equations (PDEs):

$$\begin{aligned} \frac{\partial c_s}{\partial t} = & -\frac{\partial(uc_s)}{\partial x} - \frac{\partial(vc_s)}{\partial y} \\ & + \frac{\partial}{\partial x} \left(K_x \frac{\partial c_s}{\partial x} \right) + \frac{\partial}{\partial y} \left(K_y \frac{\partial c_s}{\partial y} \right) \\ & + E_s + Q_s(c_1, c_2, \dots, c_q) - (k_{1s} + k_{2s})c_s, \quad s = 1, 2, \dots, q, \end{aligned} \quad (1)$$

where:

- (i) $c_s(t, x, y)$ are the concentrations of the chemical species;
- (ii) $u(t, x, y)$, $v(t, x, y)$ are the wind components along the coordinate axes;
- (iii) $K_x(t, x, y)$, $K_y(t, x, y)$ are the diffusion coefficients;
- (iv) $E_s(t, x, y)$ present the emission sources;
- (v) $k_{1s}(t, x, y)$, $k_{2s}(t, x, y)$ are correspondingly the dry and wet deposition coefficients, and finally,
- (vi) $Q_s(t, x, y, c_1, c_2, \dots, c_q)$ are non-linear functions which describe the chemical reactions between species under consideration.

Very often during the process of developing and testing new numerical methods and/or algorithms the following two-dimensional module is used:

$$\begin{aligned} \frac{\partial c_s}{\partial t} = & -\mu(y - y_0) \frac{\partial c_s}{\partial x} - \mu(x_0 - x) \frac{\partial c_s}{\partial y} + K \left(\frac{\partial c_s}{\partial x^2} + \frac{\partial c_s}{\partial y^2} \right) \\ & + E_s(t, x, y) + Q_s(t, x, y, c_1, c_2, \dots, c_q), \quad s = 1, 2, \dots, q, \end{aligned} \quad (2)$$

where $x \in [a_1, b_1]$, $y \in [a_2, b_2]$, $t \in [a, b]$ $x_0 = \frac{b_1 - a_1}{2}$, $y_0 = \frac{b_2 - a_2}{2}$, $\mu = \frac{2\pi}{b - a}$. In most of the cases the space domain is square, i.e. $a_1 = a_2$, $b_1 = b_2$ and the length of the time interval is 86 400 s. i.e. 24 hours. The problem (2) is considered with a given initial value vector $c(c, y, a)$ and some boundary conditions. We will consider Dirichlet boundary conditions which is not a restriction. The most essential difference in (2) according to (1) is the special definition of the wind velocity field. The trajectories of the wind in (2) are concentric circles with center (x_0, y_0) and particles are rotated along these trajectories with a constant angular velocity. Such wind velocity field was first defined in [2, 6]. There, the test in which only the first two terms in the right-hand-side of (2) are kept (the pure advection test) was introduced. Chemical reactions were included to the Crowley-Molenkamp test by Hov et al (see [4]). Here, we will concentrate only on advection diffusion part. By setting some of the coefficients to zero or keeping all of them different

2 Sequential splitting procedure

A splitting procedure proposed in [5] is used in UNI-DEM. Such a simple sequential splitting is used in this paper. Applying this kind of splitting to (2) leads to the following two sub-problems:

$$\frac{\partial g_s}{\partial t} = -\mu(y - y_0)\frac{\partial g_s}{\partial x} - \mu(x_0 - x)\frac{\partial g_s}{\partial y} + K\left(\frac{\partial^2 g_s}{\partial x^2} + \frac{\partial^2 g_s}{\partial y^2}\right), \quad (3)$$

$$\frac{\partial h_s}{\partial t} = E_s(t, x, y) + Q_s(t, x, y, g_1, g_2, \dots, g_q) \quad (4)$$

Assume that the time-integration is carried out by using a constant stepsize Δt and that some approximation $\bar{c}_i(t_n, x, y)$ to the exact solution $c_i(t_n, x, y)$ of (3) at $t_n = a + n\Delta t$ has been calculated. Then $\bar{g}_i(t_n, x, y)$ is set equal to $\bar{c}_i(t_n, x, y)$ and an approximation $\bar{g}_i(t_{n+1}, x, y)$ to the exact solution $g_i(t_{n+1}, x, y)$ of (4) at $t_{n+1} = a + (n + 1)\Delta t$ is computed by using an appropriate numerical method. The second sub-problem is handled in a similar way: $\bar{h}_i(t_n, x, y)$ is set equal to $\bar{g}_i(t_{n+1}, x, y)$ and an approximation $\bar{h}_i(t_{n+1}, x, y)$ to the exact solution $h_i(t_{n+1}, x, y)$ of (4) at $t_{n+1} = a + (n + 1)\Delta t$ is computed by using an appropriate numerical method. Finally, $\bar{c}_i(t_{n+1}, x, y)$ is set equal to $\bar{h}_i(t_{n+1}, x, y)$, which completes the computations at an arbitrary time-step $n = 1$. The computations start with the initial vector $c(t_0, x, y) = c(a, x, y)$ which is given in advance.

It is worthwhile to emphasize here that the sequential splitting procedure allows different numerical methods to be used in the treatment of the two sub-problems. This is a very useful feature, because the two sub-problems have different properties. The first sub-problem, the advection-diffusion module is a non-stiff problem, while the second sub-problem, the chemistry module is a stiff sub-problem. Moreover, the system (3) consists of q independent PDEs. If the computational space domain is discretized into $N_x \times N_y$ grid-points, then (4) will be decoupled into $N_x \times N_y$ independent systems of ordinary differential equations (ODEs) each of which contains

q equations. This observation indicates that in general efficient parallel computations can be achieved in a natural way.

3 Numerical treatment of the advection–diffusion module

As stated in the second remark in the previous section, the advection diffusion-module consists of independent PDEs. Therefore, for the discussion of the numerical method it is sufficient to select only one of this PDEs. Consider now

$$\frac{\partial g}{\partial t} = -\mu(y - y_0)\frac{\partial g}{\partial x} - \mu(x_0 - x)\frac{\partial g}{\partial y} + K\left(\frac{\partial^2 g}{\partial x^2} + \frac{\partial^2 g}{\partial y^2}\right), \quad (5)$$

which is obtained from (3) for any value of index s . The discretization of the space derivatives in (5) by central differences followed by Crank-Nicolson time-stepping leads to the solution of a system of linear differential equations:

$$(I - A)\hat{g}_{n+1} = (I + A)\hat{g}_n + \omega_n, \quad (6)$$

where \hat{g}_n and \hat{g}_{n+1} are vectors of length $(N_x+1)(N_y+1)$ containing values of function g at all spatial grid-points and at time-points t_n and t_{n+1} respectively and ω_n is a vector of length $(N_x + 1)(N_y + 1)$ induced by the boundary conditions (in fact $N_x = N_y$ is always assumed in this paper, but this restriction can easily be removed). The transition from (5) to (6) is described in many text books (see, for example, [7] and it is not necessary to discuss this transition in detail. In the context of this paper, it is much more important to concentrate our attention to the solution of (6). The matrices $I - A$ and $I + A$ involved in (6) are five-diagonal banded matrices with bandwidth $N_x + 1$.

The main conclusion is that q independent systems of linear algebraic equations of type (6), each of them containing $(N_x + 1)(N_y + 1)$ equations, have to be solved at each time-step when the advection-diffusion module is handled.

4 Numerical methods for treatment of the matrices arising in the advection–diffusion module

The matrices, which appear in (6) after the discretization of the advection-diffusion module, are banded matrices. The system (6) is solved either by a direct method (by calling subroutines DGBTRF and DGBTRS from LAPACK, see [1]) or by using the Jacobi iterative method (see [3]). If the matrices are not very large, then the LAPACK subroutines are normally faster, but for large matrices the Jacobi method becomes better. The storage requirements are another reason to prefer iterative methods when the matrices are large. A two-dimensional array with $3N_x$ rows and $(N_x + 1)(N_y + 1)$ columns is needed when the LAPACK subroutines are called, while the corresponding

array contains *five* rows and $(N_x + 1)(N_y + 1)$ columns when the Jacobi iterative method is used. On the other hand, the Jacobi iterative method may converge very slowly or even may not converge (when this happens, the time-stepsize can gradually be reduced, however very small time-stepsizes will cause an increase of the computing time). It is clear that the choice is not very easy and will depend on the particular problem which has to be solved.

The matrices in (6) do not vary in time, but no attempt was made to exploit this property, because in the general case the velocity field will be time-dependent.

Acknowledgments

The research of K. Georgiev was partly supported by the Bulgarian National Science Fond (Grants DCVP 02/1 and DO 02-147/08)

The research of Z. Zlatev was partly supported by the NATO Scientific Programme (Collaborative Linkage Grants: No. 980505 "Impact of Climate Changes on Pollution Levels in Europe" and No. 98624 "Monte Carlo Sensitivity Studies of Environmental Security").

References

- [1] E. Anderson, Z. Bai, C. Bischof, J. Demmel, J. Dongarra, J. Du Croz, A. Greenbaum, S. Hammarling, A. McKenney, S. Ostrouchov and D. Sorensen: *LAPACK: Users' Guide*, SIAM, Philadelphia, 1992.
- [2] W. P. Crowley: *Numerical advection experiments*, Monthly Weather Review, **Vol. 96** (1968), pp. 1-11.
- [3] G. H. Golub, J. M. Ortega: *Scientific computing and differential equations*, Academic Press, (1992)
- [4] Ø. Hov, Z. Zlatev, R. Berkowicz, A. Eliassen and L. P. Prahm: *Comparison of numerical techniques for use in air pollution models with non-linear chemical reactions*, Atmospheric Environment **23** (1988), pp. 967-983.
- [5] G. I. Marchuk: *Mathematical modelling for the problem of the environment*, North-Holland, Amsterdam, 1985
- [6] C. R. Molenkamp: *Accuracy of finite-difference methods applied to the advection equation*, Journal of Applied Meteorology, **Vol. 7** (1968), 160-167.
- [7] C. Strikwerda: *Finite difference schemes and partial differential equations*, SIAM, Philadelphia, 2004
- [8] Z. Zlatev: *Computer treatment of large air pollution models*, Kluwer (1995).

On the (Non)-Integrability of the Perturbed KdV Hierarchy with Generic Self-consistent Sources

Vladimir S. Gerdjikov, Georgi G. Grahovski, Rossen I. Ivanov

1. Introduction Nonholonomic deformations of integrable equations attracted the attention of the scientific community in the last few years. In [6], based on the Painlevé test, applied to a class of sixth-order nonlinear wave equations, a list of four equations that pass the test was obtained. Among the three known ones, there was a new equation in the list (later known as sixth-order KdV equation, or just KdV6):

$$\left(-\frac{1}{4}\partial_x^3 + v_x\partial_x + \frac{1}{2}v_{xx}\right)(v_t + v_{xxx} - 3v_x^2) = 0. \quad (1)$$

One can convert (1) into a “potential” form:

$$u_t + u_{xxx} - 6uu_x - w_x = 0, \quad (2)$$

$$-\frac{1}{4}w_{xxx} + uw_x + \frac{1}{2}w u_x = 0, \quad (3)$$

or equivalently

$$\left(-\frac{1}{4}\partial_x^2 + u + \frac{1}{2}u_x\partial^{-1}\right)(u_t + u_{xxx} - 6uu_x) = 0. \quad (4)$$

Here ∂_x^{-1} is a notation for the left-inverse of ∂_x and

$$\Lambda = -\frac{1}{4}\partial_x^2 + u + \frac{1}{2}u_x\partial^{-1} \quad (5)$$

is the recursion operator for the KdV hierarchy. In [7] B. Kupershmidt described (2) and (3) as a nonholonomic deformation of the KdV equation, written in a bi-Hamiltonian form. Later on, it was shown in [9] that the KdV6 equation is equivalent to a Rosochatius deformation of the KdV equation with self-consistent sources.

Here we are dealing with the potential form of the KdV6 equation (2), we study the class of inhomogeneous equations of KdV type

$$u_t + u_{xxx} - 6uu_x = W_x[u](x), \quad (6)$$

with an inhomogeneity/perturbation that presumably belongs to the same class of functions as the field $u(x)$ (i.e. decreasing fast enough, when $|x| \rightarrow \infty$).

Generally speaking, the perturbation, as a rule destroys the integrability of the considered nonlinear evolution equation (NLEE). The idea of perturbation through nonholonomic deformation, however, is to perturb an integrable NLEE with a driving force (deforming function), such that under suitable differential constraints on the

perturbing function(s) the integrability of the entire system is preserved. In the case of local NLEE's, having a constraint given through differential relations (not by evolutionary equations) is equivalent to a nonholonomic constraint.

To the best of our knowledge, the most natural and efficient way for studying inhomogeneities/perturbations of NLEE integrable by the inverse scattering method is by using the expansions over the so-called ‘‘squared solutions’’ (squared eigenfunctions) or the so-called symplectic basis. The squared eigenfunctions of the spectral problem associated to an integrable equation represent a complete basis of functions, which helps to describe the Inverse Scattering Transform (IST) for the corresponding hierarchy as a Generalised Fourier transform (GFT). The Fourier modes for the GFT are the Scattering data. The expansion coefficients of the potential over the symplectic basis are the corresponding action-angle variables.

2. Generalised Fourier Transform for KdV Hierarchy The spectral problem for the KdV hierarchy is given by the Sturm-Liouville equation [8, 5]

$$-\Psi_{xx} + u(x)\Psi = k^2\Psi, \quad (7)$$

where $u(x)$ is a real-valued (Schwartz-class) potential on the whole axis and $k \in \mathbb{C}$ is spectral parameter. The continuous spectrum under these conditions corresponds to real k . We assume that the discrete spectrum consists of finitely many points $k_n = i\kappa_n$, $n = 1, \dots, N$ where κ_n is real.

The direct scattering problem for (7) is based on the so-called ‘‘Jost solutions’’ $f^\pm(x, k)$ and $\bar{f}^\pm(x, \bar{k})$, given by their asymptotics: $x \rightarrow \infty$ for all real $k \neq 0$ [8]:

$$\lim_{x \rightarrow \pm\infty} e^{-ikx} f^\pm(x, k) = 1, \quad k \in \mathbb{R} \setminus \{0\}. \quad (8)$$

From the reality condition for $u(x)$ it follows that $\bar{f}^\pm(x, \bar{k}) = f^\pm(x, -k)$.

A key role in the interpretation of the inverse scattering method as a generalized Fourier transform plays the so-called ‘generating’ (recursion) operator: for the KdV hierarchy it has the form [1]:

$$L_\pm = -\frac{1}{4}\partial^2 + u(x) - \frac{1}{2} \int_{\pm\infty}^x d\tilde{x} u'(\tilde{x}) \cdot \quad (9)$$

The eigenfunctions of the recursion operator are the squared eigenfunctions of the spectral problem (7):

$$F^\pm(x, k) \equiv (f^\pm(x, k))^2, \quad F_n^\pm(x) \equiv F(x, i\kappa_n), \quad (10)$$

For our purposes, it is more convenient to adopt a special set of ‘‘squared solutions’’, called symplectic basis [2, 5]. It has the property that the expansion coefficients of the potential $u(x)$ over the symplectic basis are the so-called action-angle variables for the corresponding NLEE.

For the KdV hierarchy, the symplectic basis is given by:

$$\mathcal{P}(x, k) = \mp (\mathcal{R}^\pm(k)F^\pm(x, k) - \mathcal{R}^\pm(-k)F^\pm(x, -k)), \quad (11)$$

$$\mathcal{Q}(x, k) = \mathcal{R}^-(k)F^-(x, k) + \mathcal{R}^+(k)F^+(x, k), \quad (12)$$

$$P_n(x) = -R_n^\pm F_n^\pm(x), \quad Q_n(x) = -\frac{1}{2k_n} (R_n^+ \dot{F}_n^-(x) - R_n^- \dot{F}_n^+(x)). \quad (13)$$

Its elements satisfy the following canonical relations:

$$\begin{aligned} [[\mathcal{P}(k_1), \mathcal{Q}(k_2)]] &= \delta(k_1 - k_2), & [[\mathcal{P}(k_1), \mathcal{P}(k_2)]] &= [[\mathcal{Q}(k_1), \mathcal{Q}(k_2)]] = 0, \\ [[P_m, Q_n]] &= \delta_{mn}, & [[P_m, P_n]] &= [[Q_m, Q_n]] = 0, \end{aligned} \quad (14)$$

($k_1 > 0, k_2 > 0$) with respect to the skew-symmetric product

$$[[f, g]] \equiv \frac{1}{2} \int_{-\infty}^{\infty} (f(x)g_x(x) - g(x)f_x(x))dx = \int_{-\infty}^{\infty} f(x)g_x(x)dx, \quad (15)$$

The symplectic basis satisfies the completeness relation [5]:

$$\begin{aligned} \frac{\theta(x-y) - \theta(y-x)}{2} &= \frac{1}{2\pi} \int_0^{\infty} (\mathcal{P}(x, k)\mathcal{Q}(y, k) - \mathcal{Q}(x, k)\mathcal{P}(y, k)) \frac{dk}{\beta(k)} \\ &\quad - \sum_{n=1}^N (P_n(x)Q_n(y) - Q_n(x)P_n(y)), \end{aligned} \quad (16)$$

where $\beta(k) = 2ikb(k)b(-k)$. Notice that the integration over k is from 0 to ∞ . It follows that every function $X(x)$ from the same class as the potential $u(x)$ (i.e. smooth and vanishing fast enough when $x \rightarrow \pm\infty$) can be expanded over the symplectic basis:

$$\begin{aligned} X(x) &= \frac{1}{2\pi} \int_0^{\infty} \frac{dk}{\beta(k)} (\mathcal{P}(x, k)\phi_X(k) - \mathcal{Q}(x, k)\rho_X(k)) \\ &\quad - \sum_{n=1}^N (P_n(x)\phi_{n,X} - Q_n(x)\rho_{n,X}). \end{aligned} \quad (17)$$

The expansion coefficients can be recovered from the so-called inversion formulas:

$$\begin{aligned} \phi_X(k) &= [[\mathcal{Q}(y, k), X(y)]], & \rho_X(k) &= [[\mathcal{P}(y, k), X(y)]], \\ \phi_{n,X} &= [[Q_n(y), X(y)]], & \rho_{n,X} &= [[P_n(y), X(y)]]. \end{aligned} \quad (18)$$

In particular, if $X(x) = u(x)$ is a solution of the spectral problem, one can compute [5]:

$$[[\mathcal{P}(y, k), u(y)]] = 0, \quad [[\mathcal{Q}(y, k), u(y)]] = -4ik\beta(k), \quad (19)$$

$$[[P_n(y), u(y)]] = 0, \quad [[Q_n(y), u(y)]] = 4ik_n. \quad (20)$$

Thus, from (19) one gets:

$$u(x) = \frac{2}{\pi i} \int_0^{\infty} \mathcal{P}(x, k)dk - \sum_{n=1}^N 4ik_n P_n(x). \quad (21)$$

The expression for the variation of the potential is

$$\begin{aligned} \delta u(x) &= \frac{1}{2\pi} \int_0^{\infty} \frac{dk}{\beta(k)} (\mathcal{P}_x(x, k)\delta\phi(k) - \mathcal{Q}_x(x, k)\delta\rho(k)) \\ &\quad - \sum_{n=1}^N (P_{n,x}\delta\phi_n - Q_{n,x}\delta\rho_n) \end{aligned} \quad (22)$$

with expansion coefficients

$$\rho(k) \equiv -2ik \ln |a(k)| = -2ik \ln(1 - \mathcal{R}^-(k)\mathcal{R}^-(-k)), \quad k > 0, \quad (23)$$

$$\phi(k) \equiv 2i\beta(k) \arg b(k) = \beta(k) \ln \frac{\mathcal{R}^-(k)}{\mathcal{R}^+(k)}, \quad (24)$$

$$\rho_n = -\lambda_n = -k_n^2, \quad \phi_n = 2 \ln b_n = \ln \frac{R_n^-}{R_n^+}. \quad (25)$$

These are known as action ($\rho(k)$) - angle ($\phi(k)$) variables for KdV equation [10, 8]. Due to the time-evolution of u , $\delta u(x, t) = u_t \delta t + Q((\delta t)^2)$, etc. the equations of the KdV hierarchy

$$u_t + \partial_x \Omega(\Lambda)u(x, t) = 0, \quad (26)$$

with (21) and (22) are equivalent to a system of trivial linear ordinary differential equations for the canonical variables (which can be considered as scattering data):

$$\begin{aligned} \phi_t &= 4i\beta(k)\Omega(k^2), & \rho_t(k) &= 0, \\ \phi_{n,t} &= 4ik_n\Omega(k_n^2), & \rho_{n,t} &= 0. \end{aligned} \quad (27)$$

3. Perturbations to the equations of the KdV hierarchy Let us consider a general perturbation $W_x[u]$ to an equation from the KdV hierarchy:

$$u_t + \partial_x \Omega(\Lambda)u(x, t) = W_x[u]. \quad (28)$$

The function $W_x[u]$ is assumed to belong to the class of admissible potentials for the associated spectral problem (7) (Schwartz class functions, in our case). The expansion of the perturbation over the symplectic basis is:

$$\begin{aligned} W_x[u] &= \frac{1}{2\pi} \int_0^\infty \frac{dk}{\beta(k)} (\mathcal{P}_x(x, k)\phi_W(k) - \mathcal{Q}_x(x, k)\rho_W(k)) \\ &\quad - \sum_{n=1}^N (P_{n,x}(x)\phi_{n,W} - Q_{n,x}(x)\rho_{n,W}). \end{aligned} \quad (29)$$

The substitution of the above expansion (29) in (28) together with (21) and (22) leads to a modification of the time evolution (27) of the scattering data as follows:

$$\phi_t = 4i\beta(k)\Omega(k^2) + \phi_W(k, t; \rho(k, t), \phi(k, t), \rho_n(t), \phi_n(t)), \quad (30)$$

$$\rho_t(k) = \rho_W(k, t; \rho(k, t), \phi(k, t), \rho_n(t), \phi_n(t)), \quad (31)$$

$$\phi_{n,t} = 4ik_n\Omega(k_n^2) + \phi_{n,W}(k, t; \rho(k, t), \phi(k, t), \rho_n(t), \phi_n(t)), \quad (32)$$

$$\rho_{n,t} = \rho_{n,W}(k, t; \rho(k, t), \phi(k, t), \rho_n(t), \phi_n(t)). \quad (33)$$

Since $W = W[u]$ and u depend on the scattering data, we observe that the expansion coefficients of the perturbation ($\phi_W(k) = \llbracket \mathcal{Q}(y, k), W(y) \rrbracket$ etc.) also depend on the

scattering data. Thus for generic W the new dynamical system (30) – (33) for the scattering data can be extremely complicated and non-integrable in general. This reflects the obvious fact that the perturbed integrable equations are, in general, not integrable.

4. KdV Hierarchy with Self-consistent Sources (SCS). Let us investigate the integrability of the following equation:

$$\Lambda^*(u_t + \partial_x \Omega(\Lambda)u(x, t)) = 0, \quad (34)$$

where the star is a notation for a Hermitian conjugation. KdV6 in (4) is a particular case of this equation with $\Omega(\Lambda) = -4\Lambda$. In order to simplify our further analysis, instead of the equation (34) we study the following one:

$$(\Lambda^* - \lambda_1)(u_t + \partial_x \Omega(\Lambda)u(x, t)) = 0, \quad (35)$$

where λ_1 is a constant. The corresponding analogue for KdV6 is

$$v_{6x} + v_{txxx} - 2v_t v_{xx} - 4v_x v_{xt} - 10v_x v_{4x} - 20v_{xx} v_{xxx} + 30v_x^2 v_{xx} + 4\lambda_1(v_{xt} + v_{xxxx} - 6v_x v_{xx}) = 0. \quad (36)$$

Since the operator ∂ does not have a kernel when u is Schwartz class, (34) is equivalent to

$$u_t + \partial_x \Omega(\Lambda)u(x, t) = \begin{cases} (c_1 P_1(x, t) + c_2 Q_1(x, t))_x & \text{for } \lambda_1 = k_1^2 < 0, \\ (c_1 \mathcal{P}(x, k_1, t) + c_2 \mathcal{Q}(x, k_1, t))_x & \text{for } \lambda_1 = k_1^2 > 0, \end{cases} \quad (37)$$

where $c_{1,2} = c_{1,2}(t, k_1; \rho(k_1, t), \phi(k_1, t), \rho_n(t), \phi_n(t))$ are x -independent functions, but the important observation is that the time-dependence could be implicit through the scattering data of the potential $u(x, t)$. Equation (37) is a perturbed equation from the KdV hierarchy. The perturbation in the right-hand side of (37) is in the eigenspace of the recursion operator corresponding to the eigenvalue λ_1 , i.e. it is given by 'squared' eigenfunctions of the spectral problem (7) at λ_1 . Such a special perturbation is often called 'self-consistent sources' perturbation. For simplicity we use the symplectic basis, see the precise definitions (11) – (13). Typically the SCS in the literature is taken with $c_2 = 0$; such perturbations do not violate integrability. For example, if $\lambda_1 > 0$ is a continuous spectrum eigenvalue, the dynamical system (30) – (33) has the form

$$\phi_t = 4i\beta(k)\Omega(k^2) + 2\pi\beta(k)c_1(t, k_1; \rho(k_1, t), \phi(k_1, t), \rho_n(t), \phi_n(t))\delta(k - k_1), \quad (38)$$

$$\rho_t(k) = -2\pi\beta(k)c_2(t, k_1; \rho(k_1, t), \phi(k_1, t), \rho_n(t), \phi_n(t))\delta(k - k_1), \quad (39)$$

$$\phi_{n,t} = 4ik_n\Omega(k_n^2), \quad (40)$$

$$\rho_{n,t} = 0. \quad (41)$$

Similar equations can be written for the time evolution of the action-angle variables on the discrete spectrum of the Lax operator L .

It is clear, that dynamical systems like (38) – (41) can not be integrable for a general functional dependence of $c_{1,2}$ on the scattering data. Thus the equations (34), including KdV6, are not *completely* integrable. In other words, there are solutions, which can not be obtained via the Inverse Scattering Method, since the aforementioned dynamical systems for the scattering data are not always integrable.

5. Conclusions and Outlook Here we have used the expansion over the eigenfunctions of the recursion operator for the KdV hierarchy for studying nonholonomic deformations of the corresponding NLEE from the hierarchy. We have shown, that in the case of self-consistent sources, the corresponding perturbed NLEE is integrable, but not completely integrable.

The approach presented in this article can be applied also to the study of inhomogeneous versions of NLEE, related to other linear spectral problems, e.g. the Camassa-Holm equation, various difference and matrix generalizations of KdV-like and Zakharov - Shabat spectral problems, various non-Hamiltonian systems, etc.

Acknowledgements This material is based upon works supported by the Science Foundation of Ireland (SFI), under Grant No. 09/RFP/MTH2144.

References

- [1] V. A. Arkad'ev, A. K. Pogrebkov and M. K. Polivanov, *Theor. Math. Phys.* **72** (1987) No. 3, 909–920; *Theor. Math. Phys.* **75** (1988) No. 2, 448–460.
- [2] V. S. Gerdjikov and E. Kh. Khristov, *Bulgarian J. Phys.* **7** No.1, 28–41, (1980); *Bulgarian J. Phys.* **7** No.2, 119–133, (1980) (In Russian).
- [3] V.S. Gerdjikov, G. Vilasi and A.B. Yanovski, *Integrable Hamiltonian hierarchies. Spectral and geometric methods*. Lecture Notes in Physics, **748**. Springer-Verlag, Berlin, 2008.
- [4] G. G. Grahovski, R. I. Ivanov, *Discr. Cont. Dyn. Syst. B* **12** (2009), no. 3, 579 – 595.
- [5] I. Iliev, E. Khristov and K. Kirchev, *Spectral Methods in Soliton Equations*, Pitman Monographs and Surveys in Pure and Appl. Math. vol. **73**, Pitman, London, 1994.
- [6] A. Karasu-Kalkantli, A. Karasu, A. Sakovich, S. Sakovich, R. Turhan, *J. Math. Phys.* **49**, 073516, 2008.
- [7] B. A. Kupershmidt, *Phys. Lett. A* **372**, 2634–2639, 2008.
- [8] S.P. Novikov, S.V. Manakov, L.P. Pitaevskii and V.E. Zakharov, *Theory of solitons: the inverse scattering method*, Plenum, New York, 1984.
- [9] Y. Q. Yao, Y. B. Zeng, *J. Phys. A: Math. Theor.* **41**, 295205, 2008; *Lett. Math. Phys.* **86**, 193–208, 2008.
- [10] V. Zakharov and L. Faddeev, *Func. Anal. Appl.* **5** (1971), 280-287.

Fluxon States in Linear Josephson Stacks

Ivan Hristov

Introduction

In recent years, stacked Josephson junctions (JJs) have been considered as a source of THz radiation. Fluxons moving coherently (bunched fluxons) in such junctions are a possible source of radiation. Bunching of fluxons due to coupling between junctions was numerically investigated in [2] in the case of three stacked JJs of annular geometry. Bunching due to boundary conditions (external microwave source, external cavity) is discussed in [3]. Good agreement between theoretical predictions and experimental measurements is established there. In this paper we investigate numerically bunching of fluxons due to coupling between junctions of linear geometry. In particular we consider the case, when 3 or 5 stacked inductively coupled junctions are placed in zero magnetic field.

Mathematical model

In the case of symmetric N -stacked inductively coupled JJ, considered here, the dynamics of the Josephson phases $\varphi(x, t) = (\varphi_1(x, t), \dots, \varphi_N(x, t))^T$ is described by the following system of perturbed sine-Gordon equations [1]:

$$\varphi_{tt} + \alpha\varphi_t + J + \Gamma = L^{-1}\varphi_{xx}, \quad -l \leq x \leq l, \quad 0 \leq t \leq T. \quad (1)$$

Here $2l$ is the length of the stack, α is the dissipation coefficient, $\Gamma = \gamma(1, \dots, 1)^T$ is the vector of the external currents, $J = (\sin \varphi_1, \dots, \sin \varphi_N)^T$ is the vector of the Josephson currents. The symmetric matrix $L = \text{tridiag}(1, S, 1)$ represents the inductive interaction between junctions. In this work we consider stacks of linear geometry placed in external magnetic field h_e , therefore the system (1) should be solved together with the boundary conditions:

$$\varphi_x(-l, t) = \varphi_x(l, t) = H, \quad (2)$$

where H is the vector $H = h_e(1, \dots, 1)^T$. To close the differential problem appropriate initial conditions must be posed:

$$\varphi(x, 0) - \text{given}, \quad \varphi_t(x, 0) - \text{given}. \quad (3)$$

The important for us solution of the unperturbed one-dimensional sine-Gordon equation ($S = \alpha = \gamma = 0$)

$$\varphi_{tt} - \varphi_{xx} + \sin \varphi = 0$$

is given by:

$$\varphi(x, t) = 4 \arctan\left[\exp\left(\sigma \frac{x - ut - x_0}{\sqrt{1 - u^2}}\right)\right].$$

It is called a fluxon ($\sigma = -1$) or an antifluxon ($\sigma = 1$), u is the wave velocity. The location of the fluxon at $t = 0$ is x_0 . The maximum velocity for one single equation is the velocity of the plasma waves $|u| = 1$ [3]. The so called Swihart velocities [1] c_m , $m = 1, 2, \dots, N$,

$$c_m = \frac{1}{\sqrt{1 - 2S \cos(\frac{m\pi}{N+1})}},$$

appear in the analysis of the bunched fluxon states in N-staked JJ. Bunching of fluxons may take place in the interval $[c_1, c_N]$.

Josephson currents J generates a specific magnetic flux. An important fact is that when the external current γ is less than some critical value, all the junctions are in some static state, i.e., we have a time independent solution of (1), (2), (3):

$$J + \Gamma = L^{-1}\varphi_{xx}, \quad -l \leq x \leq l, \quad (4)$$

$$\varphi_x(-l) = \varphi_x(l) = H, \quad (5)$$

The external current γ plays role as a force which pushes fluxons (antifluxons) in some direction. For example positive γ means fluxon moving to left, and antifluxons moving to right. In order to obtain appropriate initial values for problem (1), (2), (3) we solve additionally the static problem. Then we obtain the desired state by increasing the external current γ . This procedure corresponds to the procedure in real experiments with JJs.

Let us mention, the boundary conditions (2) lead to reflections of fluxons from stack edges, but this does not destroy the bunched states.

Numerical method and numerical results

To solve the dynamic problem (1), (2), (3), we use the finite difference method. Let h and τ be the steps in space and time respectively, $\delta = (\tau/h)^2$, n - the number of points in space, $x_k = -l + kh$, $h = 2l/n$, $k = 0, \dots, n$, $t_j = j\tau$, $j = 0, 1, \dots$. We use the standard notations: $y_k^l = \varphi_l(x_k, t_j)$, $\hat{y}_k^l = \varphi_l(x_k, t_{j+1})$, $\check{y}_k^l = \varphi_l(x_k, t_{j-1})$, $l = 1, \dots, N$. The main equation is approximated by second order centered finite differences for both space and time:

$$\hat{y}_k^l = (1 + 0.5\alpha\tau)^{-1} [2y_k^l + (0.5\alpha\tau - 1)\check{y}_k^l - \tau^2(\sin y_k^l + \gamma) + \sum_{m=1}^N \delta a_{lm} y_{\bar{x},k}^m],$$

where $k = 1, \dots, n-1$, $L^{-1} = (a_{l,m})_{l,m=1}^N$, $l = 1, \dots, N$, $m = 1 \dots N$

The boundary conditions are approximated by second order one-sided finite differences:

$$\hat{y}_0^l = (4\hat{y}_1^l - \hat{y}_2^l - 2hh_e)/3, \quad \hat{y}_n^l = (4\hat{y}_{n-1}^l - \hat{y}_{n-2}^l + 2hh_e)/3.$$

The step τ in time and step h in space are taken under the condition $c_N\tau \leq h$. To check the numerical stability and accuracy we compare the wave profiles for different τ and h . In addition we verify the integral identity [4], [5], given here for the case of N stacked JJs:

$$Q(t) = \frac{d}{dt}E + \alpha \int_{-l}^l \sum_{i=1}^N \varphi_{i,t}^2 dx = 0,$$

$$E(t) = \int_{-l}^l \left[\frac{1}{2} \langle \varphi_x, L^{-1} \varphi_x \rangle + \sum_{i=1}^N \left(\frac{1}{2} \varphi_{i,t}^2 + 1 - \cos \varphi_i - \gamma \varphi_i \right) \right] dx.$$

To solve numerically the static problem (4),(5), we use an iterative algorithm, based on the continuous analog of Newton's method (CAMN) [6].

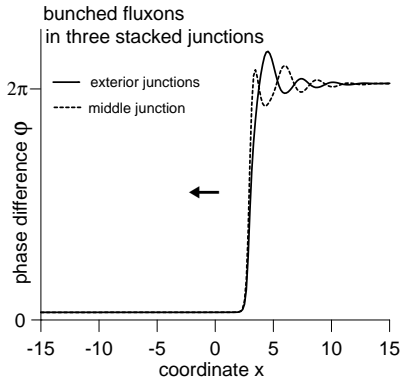


Figure 1: Bunched fluxons in 3-JJs stack. The arrow shows the direction of moving.

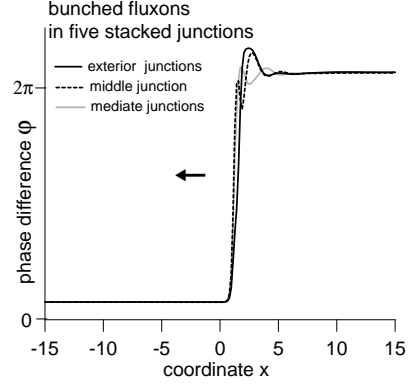


Figure 2: Bunched fluxons in 5-JJs stack. The arrow shows the direction of moving.

We first briefly discuss the case of three stacked JJs.

When the external current γ is above a threshold value, the fluxons in the adjacent (exterior and middle) junctions have oscillating tails of opposite polarity, which cause the fluxon's attraction, i.e., their bunching. The fluxons in the exterior junctions are the same, because of the symmetry of the stack. On Figure 1. the bunched state of one moving fluxon in each junction of the stack for parameters $S = -0.05$, $h_e = 0$, $\gamma = 0.75$, $2l = 30$, $\alpha = 0.1$ is shown

The unbunched and bunched states of one and two moving fluxons in each junction are described in terms of the current-voltage and current-velocity characteristics in [5]. Different behavior of the moving fluxons is observed there for small and big in modulus values of the coupling parameter S .

The mechanism of fluxon's bunching in the common N -stacked case is not investigated by now. We made a step in this direction: in the numerical experiments for five-stacked symmetric JJ and parameters $S = -0.02$, $h_e = 0$, $\gamma = 0.9$, $2l = 30$, $\alpha = 0.1$ we found a bunched state of three different fluxons (Figure 2). Let us mention, the fluxons in the adjacent junctions have tails of opposite polarities; the tails of the fluxons in the nonadjacent junctions have the same polarity, but nevertheless they don't repel each other.

Conclusions

We show by numerical experiment that in the case of five stacked JJs of linear geometry and weak coupling ($S = -0.02$), placed in zero magnetic field ($h_e = 0$), the bunching of fluxons takes place.

Acknowledgment

This work is supported by Sofia University Scientific foundation under Grant No 196/2010.

References

- [1] S. Sakai, P. Bodin, N.F. Pedersen, Fluxons in thin-film superconductor-insulator superlattices, *J. Appl. Phys.*, v. **73**, No. 5, 1993, pp. 2411 – 2418.
- [2] C. Gorria, P.L. Christiansen, Yu.B. Gaididei, V. Muto, N.F. Pedersen, M.P. Soerensen, *Phys. Rev. B* 66 (2002) 172503.
- [3] S.Madsen, N.F. Pedersen, P.L.Christiansen, Stacked Josephson junctions, *Physica C* 470(2010)822–826
- [4] Kazacha, G.S., Serdyukova, S.I.: Numerical Investigation of the Behaviour of Solutions of the Sine-Gordon Equation with a Singularity for Large t . *Comput. Maths. Math. Phys.* 33(3), 377–385 (1993)
- [5] I. Hristov, S. Dimova, Fluxon Dynamics in Stacked Josephson Junctions, LNCS, v.6046, 2011, pp. 428–436.
- [6] I. V. Puzynin *et al.*, Methods of computational physics for investigation of models of complex physical systems, *Particals & Nucley* **38**, 1 (2007), Dubna.

On the Computation with Approximate Numbers

Svetoslav Markov

Approximate numbers are ordered pairs comprising a real “exact” number and an error bound, briefly *error*. Errors are real non-negative numbers considered together with certain operations and relations that are typically used in numerical computations. To compute with approximate numbers one should know the algebraic properties of the arithmetic operations on errors. This work is devoted to the algebraic study of the arithmetic operations addition and multiplication by scalars for (vectors of) errors. Such a setting leads to so-called quasilinear spaces. We formulate and prove several new properties of such spaces, which are important from computational aspect. In particular, we focus our study on the operation “distance between two nonnegative numbers” $|A - B|$. We show that this operation plays an important role in the study of the concept of linear dependence; it is also important for the efficient computation with errors and approximate numbers.

1 Introduction

Narrow intervals are sometimes interpreted as approximate numbers; such are for example floating point numbers. An approximate number is an ordered pair consisting of a real number considered as exact and an error bound. In the case of floating-point numbers the “exact” real number is a machine number and an error bound is, e. g. the distance between the neighboring machine numbers. Error bounds, also called computational errors or just *errors*, are (real) non-negative numbers. To compute with approximate numbers one should know the arithmetic operations on errors and the properties of these operations. Computations with errors require suitable definitions and study of the arithmetic operations and order relations over the set of non-negative numbers. In this work we discuss the algebraic properties of non-negative numbers starting from familiar properties of real numbers. We restrict ourselves in the algebraic study of the arithmetic operations addition and multiplication by scalars for errors. Such a setting leads to so-called quasilinear spaces. In particular, we focus our study on the operation “+⁻” defined as the distance between two nonnegative real numbers: $A+^-B = |A-B|$ in combination with the familiar order relation. This operation plays an important role in the computation with errors and approximate numbers. We study the algebraic properties of this operation. Based on this study we formulate and prove some new algebraic properties of errors, which are important from computational aspect.

Specialists in algebra would ask why is it necessary to restrict ourselves in computing with non-negative numbers. Indeed, non-negative numbers are embeddable in the set of reals where computation is easy due to the nice algebraic properties of the latter, especially the presence of inverse elements. However, such an approach is not easily acceptable in certain application areas, such as error analysis, where the introduction of inverse improper elements requires special interpretation and leads to specific novel

theoretical formalisms, such as Kaucher/modal interval arithmetic. Besides, it is of theoretical interest to study abstractly the system of non-negative numbers. Parts of the material in this extended abstract is developed in some detail in [2].

Real numbers in signed-magnitude form. Denote by $\mathbf{R}^+ = \{a \in \mathbf{R} \mid a \geq 0\}$ the set of non-negative real numbers. In computational sciences non-negative real numbers are often related to computational errors (error bounds); thus instead of “nonnegative real numbers” we shall sometimes speak of “error numbers” or briefly “e-numbers”. A real number $a \in \mathbf{R}$ is usually presented in the form $\pm A$, that is as an ordered pair of the form $(A; \alpha)$, with $A = |a| \in \mathbf{R}^+$ and $\alpha = \sigma(a) \in \Lambda = \{+, -\}$, where

$$\sigma(a) = \begin{cases} + & \text{if } a \geq 0; \\ - & \text{if } a < 0. \end{cases}$$

We have

$$a = (A; \alpha) \in \{(X; \xi) \mid X \in \mathbf{R}^+, \xi \in \Lambda\} = \mathbf{R}^+ \otimes \Lambda.$$

The presentation $a = (A; \alpha)$ will be referred as signed-magnitude form, briefly *sm-form*.

A basic difference between \mathbf{R} and \mathbf{R}^+ with respect to addition is that \mathbf{R} is an additive group whereas \mathbf{R}^+ is a semigroup. There are no inverse elements in $(\mathbf{R}^+, +)$; consequently no operation subtraction and generally no solution to an equation of the form $a + x = b$. To underline this difference in the sequel we shall denote the elements of \mathbf{R} by lower-case letters a, b, c, \dots , whereas the elements of \mathbf{R}^+ by upper-case letters, A, B, C, \dots

The set of pairs $\mathbf{R}^+ \otimes \Lambda$ admits both elements $(0; +)$ and $(0; -)$, which both correspond to the element $0 \in \mathbf{R}$. Assuming $(0; +) = (0; -)$, we obtain a bijection between \mathbf{R} and $\mathbf{R}^+ \otimes \Lambda$. This allows us to identify a real number with its sm-form $a = (A; \alpha)$.

Addition of reals in sign form. Let us formulate addition of real numbers using the sm-form $a = (A; \alpha)$ minding the isomorphism $(\mathbf{R}, +, \leq) \cong (\mathbf{R}^+ \otimes \Lambda, +, \leq)$. Since addition of real numbers with the same sign and with a different sign are handled differently, to add $(A; \alpha)$ and $(B; \beta) \in \mathbf{R}^+ \otimes \Lambda$ we should consider separately the cases $\alpha = \beta$ and $\alpha \neq \beta$. In the case $\alpha = \beta$ we have $(A; \alpha) + (B; \alpha) = (A + B; \alpha)$. Here “ $A + B$ ” is the operation addition in \mathbf{R}^+ which is the restriction of addition in \mathbf{R} . To add $(A; \alpha)$, $(B; \beta) \in \mathbf{R}^+ \otimes \Lambda$ in the case $\alpha \neq \beta$ we need the operation $|A - B|$ in \mathbf{R}^+ . Since there is no subtraction in \mathbf{R}^+ we shall denote $A +^- B = |A - B|$ and define operation “ $+^-$ ” correctly as follows:

$$A +^- B = \begin{cases} Y|_{B+Y=A} & \text{if } B \leq A; \\ X|_{A+X=B} & \text{if } A \leq B. \end{cases} \quad (1)$$

Operation (1) is well defined in \mathbf{R}^+ ; we call it “c-addition” (here and in the sequel “c” stands for “conditional”).

Using mapping $\mu : \mathbf{R}^+ \otimes \Lambda^2 \longrightarrow \Lambda$ defined by:

$$\mu((A; \alpha), (B; \beta)) = \begin{cases} \alpha & \text{if } B \leq A, \\ \beta & \text{if } B > A. \end{cases}$$

we have

$$a + b = (A; \alpha) + (B; \beta) = \begin{cases} (A + B; \alpha) & \text{if } \alpha = \beta; \\ (A +^- B; \mu(a, b)) & \text{if } \alpha \neq \beta, \end{cases}$$

which can be compactly written as

$$(A; \alpha) + (B; \beta) = (A +^{\alpha\beta} B; \mu(a, b)). \quad (2)$$

In (2) we assume that for $\alpha, \beta \in \Lambda$ a binary boolean operation “ \cdot ” is defined by $\alpha \cdot \beta = \alpha\beta = \{+, \alpha = \beta; -, \alpha \neq \beta\}$. In addition we assume $+^+ = +$.

2 Properties of e-numbers relative to addition and order

It is easy to see that $(\mathbf{R}^+, +, \leq)$ is an ordered cancellative commutative monoid. The monoid $(\mathbf{R}^+, +, \leq)$ possesses the following properties:

- P1. For $A, B \in \mathbf{R}^+$, $A \neq B$, exactly one of the equations $A + X = B$, $B + Y = A$ is solvable.
- P2. For $A, B \in \mathbf{R}^+$ $A + B = 0$ implies $A = B = 0$.
- P3. For $A, B, C, D \in \mathbf{R}^+$ we have $A \leq B \iff A + C \leq B + C$, and $A \leq B$, $C \leq D \implies A + C \leq B + D$.

The following properties of c-addition “ $+^-$ ” follow from Definition (1):

- i) “ $+^-$ ” is a closed (total) operation;
- ii) “ $+^-$ ” is “c-associative”: $(A +^- B) +^- C = A +^- (B +^- C)$, if $B \geq A$ and $B \geq C$;
- iii) $A +^- 0 = A$ for all $A \in \mathbf{R}^+$;
- iv) there is an additive inverse; namely for all $A \in \mathbf{R}^+$ the element A is opposite to A itself, that is $A +^- A = 0$;
- v) “c-cancellation law”: $A +^- X = B +^- X \implies A = B$ or $X + X = A + B$;
- vi) “commutative law”: $A +^- B = B +^- A$, for all $A, B \in \mathbf{R}^+$.

The extended additive monoid $(\mathbf{R}^+, +, +^-, \leq)$. We have shown that the algebraic system $(\mathbf{R}^+, +, \leq)$ possesses null and c-addition; thus the system can be fully denoted as $(\mathbf{R}^+, +, +^-, \leq)$ or as $(\mathbf{R}^+, +, 0, +^-, \leq)$. To emphasize that system $(\mathbf{R}^+, +, \leq)$ includes c-addition we shall call it *extended additive error system*.

C-subtractability. i) For $A, B \in \mathbf{R}^+$, such that $A \leq B$, the unique solution of $A + X = B$ is $X = B +^- A$. ii) Equation $A +^- X = B$ has a solution $X = A + B$ for $A, B \in \mathbf{R}^+$. If $A, B \in \mathbf{R}^+$ are such that $A \geq B > 0$, then equation $A +^- X = B$ has one more solution $X = A +^- B$.

3 The quasilinear error space

Let \mathbf{R}^n be the set of real vectors $a = (a_1, a_2, \dots, a_n)$, and \mathbf{R}^{+n} be the set of n -tuples $A = (A_1, A_2, \dots, A_n)$, $A_i \geq 0$. Component-wise generalizations of previous definitions such as $a = (A; \alpha) \in \mathbf{R}^n$ with $A = (A_1, A_2, \dots, A_n) \in \mathbf{R}^{+n}$, $\alpha \in \Lambda^n$, etc. are obvious.

Definition 2. For $A = (A_1, A_2, \dots, A_n), B = (B_1, B_2, \dots, B_n) \in \mathbf{R}^{+n}$, we define $A+B$ and $A+^-B$ by means of:

$$\begin{aligned} A+B &= (A_1, A_2, \dots, A_n) + (B_1, B_2, \dots, B_n) = (A_1+B_1, \dots, A_n+B_n), \\ A+^-B &= (A_1, A_2, \dots, A_n) +^- (B_1, B_2, \dots, B_n) = (A_1+^-B_1, \dots, A_n+^-B_n). \end{aligned}$$

Multiplication by scalars. Introducing in \mathbf{R}^n multiplication by scalars from the real ordered field $\mathbf{R} = (\mathbf{R}, +, \cdot, \leq)$, we arrive to the familiar vector space $(\mathbf{R}^n, +, \mathbf{R}, \cdot, \leq)$. Multiplication of a real vector $a = (A; \alpha) \in \mathbf{R}^n$ in sm-form by a scalar $c \in \mathbf{R}$ is given by

$$c \cdot (A; \alpha) = (|c| \cdot A; \sigma(c)\alpha). \quad (3)$$

In (3) $\sigma(c)$ is the sign of the scalar c , resp. $\sigma(c)\alpha$ is equal to either α or $-\alpha$ depending on the sign of c . Relation (3) shows that multiplication of a real vector by scalars induces a new “quasivector” multiplication by scalars “*” in the “error space” $(\mathbf{R}^{+n}, +, \mathbf{R}, *, \leq)$ to be defined as follows

Definition 3. Quasivector multiplication by scalars “*” is defined as

$$c * A = |c| \cdot A, \quad c \in \mathbf{R}, \quad A \in \mathbf{R}^{+n}. \quad (4)$$

Componentwise, (4) reads:

$$\begin{aligned} c * A &= |c| \cdot A = |c| \cdot (A_1, A_2, \dots, A_n) \\ &= (|c|A_1, |c|A_2, \dots, |c|A_n). \end{aligned}$$

Proposition 1 (For a proof see [3]). For $A, B \in \mathbf{R}^{+n}$, all $s, t \in \mathbf{R}$ and $\lambda \in \Lambda$:

$$s * (t * A) = (st) * A, \quad (5)$$

$$1 * A = A, \quad (6)$$

$$s * (A +^\lambda B) = s * A +^\lambda s * B, \quad (7)$$

$$(s+t) * A = s * A +^{\sigma(s)\sigma(t)} t * A, \quad (8)$$

$$A \leq B \implies \gamma * A \leq \gamma * B, \quad (9)$$

$$(-1) * A = A, \quad (10)$$

Linear combinations and linear dependency. Recall that k real vectors $c_1, c_2, \dots, c_k \in \mathbf{R}^n$ are linearly dependent if there exist k real numbers $\alpha_1, \alpha_2, \dots, \alpha_k \in \mathbf{R}$, not all equal to zero, such that

$$\sum_{i=1}^k \alpha_i c_i = \alpha_1 c_1 + \alpha_2 c_2 + \dots + \alpha_k c_k = 0.$$

W. l. g. we shall assume that $\alpha_1 \geq 0$. Our next aim is to suitably modify this definition for e-vectors. To this end let us represent in sm-form the linear combination of k real vectors that appears in the above definition, namely:

$$c = \sum_{i=1}^k \alpha_i c_i = \alpha_1 c_1 + \alpha_2 c_2 + \dots + \alpha_k c_k, \quad (11)$$

wherein $c_i = (c_i^{(1)}, c_i^{(2)}, \dots, c_i^{(n)}) \in \mathbf{R}^n$, $\alpha_i \in \mathbf{R}$, $i = 1, \dots, k$. We substitute each component of c_i by its sm-form: $c_i = (C_i; \gamma_i)$, resp. $c_i^{(j)} = (C_i^{(j)}; \gamma_i^{(j)})$, $j = 1, \dots, n$, $i = 1, \dots, k$. As we are interested in the linear combination of e-vectors, we assume that $\gamma_i^{(j)} = +$, $j = 1, \dots, n$, $i = 1, \dots, k$, so that $c_i^{(j)} = (C_i^{(j)}; +)$, $j = 1, \dots, n$, $i = 1, \dots, k$. In vector notation the latter reads: $c_i = (C_i; +)$, $i = 1, \dots, k$.

Definition. The e-vectors $C_1, C_2, \dots, C_k \in \mathbf{R}^{+n}$ are “linearly dependent” if there exists a nonzero vector $(\alpha_1, \alpha_2, \dots, \alpha_k) \neq 0$, $\alpha_1, \alpha_2, \dots, \alpha_k \in \mathbf{R}$, and signs $\lambda_i \in \Lambda$, $i = 1, 2, \dots, k - 1$, such that

$$\alpha_1 * C_1 +^{\lambda_1} \alpha_2 * C_2 +^{\lambda_2} \dots +^{\lambda_{k-1}} \alpha_k * C_k = 0, \quad (12)$$

with order of executions of the operations “ $+^{\lambda_i}$ ” in (12) from left to right.

Conclusions. In the present work we show that:

- i) addition of real numbers naturally induces the operation c-addition of non-negative numbers (distance, modulus of the difference);
- ii) the operation c-addition of non-negative numbers enriches the additive monoidal system of non-negative numbers up to a structure close to a group where many typically group operations can be performed under somewhat sophisticated conditions;
- iii) the operation c-addition of non-negative numbers is fundamental in real analysis, in interval analysis, and resp. in error analysis;
- iv) error arithmetic involves naturally an operation “multiplication by scalars” which leads to a special algebraic structure “quasilinear space”, close but yet different from linear spaces.
- v) it is possible to introduce “linear dependence” remaining in the set of non-negative numbers.

The idea of the present paper appeared while the author worked on a motion paper presented at the IEEE P1788 Working Group on Standardization of interval arithmetic [1]. The results in this work have been partially reported at the Mathematics in Industry Conference <http://www.math.bas.bg/MathInIndustry/index.php> and at the SCAN-2010 Symposium <http://scan2010.ens-lyon.fr/>.

Acknowledgment. The work is partially supported by the Bulgarian NSF Project DO 02-359/2008.

References

- [1] Edmonson, W., G. Melquiond, IEEE Interval Standard Working Group - P1788: Current Status, Proc. 19th IEEE Symposium on Computer Arithmetic, 2009. ARITH 2009, 231–234.
- [2] Markov, S., N. Hayes, On the Arithmetic of Errors, *Serdica Journal of Computing* 4 (4), 2010, 447–462.
- [3] Markov, S., Computation with Errors: Algebraic Properties, *Mathematica Balkanica*, submitted.

PDE Arising in Fluid Mechanics: Singularities, Creation and Propagation

Petar Popivanov

This book deals with several equations of Mathematical Physics as Korteweg-de Vries (KdV) equation and its different modifications (shortly mKdV), the Camassa-Holm equation and its generalizations, the nonlinear hyperbolic equation describing the vibrations of a chain of particles interconnected by springs, the viscoelastic generalization of Burger's equation, the sin-Gordon equation, the Hunter-Saxton equation and others. They originate from Physics - for example Camassa-Holm equation is modeling the propagation of unidirectional irrotational shallow water waves over a flat bed. The corresponding solutions (geometrically their profiles) may have different kind of singularities - peaks, cusps, compactly supported and are called peakons, cuspons, compactons. Certainly, solitons, kinks and periodic solutions can appear and we have found the asymptotic behavior of the solutions near the singular points. We list below several equations to be discussed further. They are the Camassa-Holm equation:

$$u_t - u_{xxt} + 3uu_x = 2u_x u_{xx} + uu_{xxx}, t > 0, x \in \mathbf{R} \quad (1)$$

the γ -Camassa-Holm equation:

$$u_t + c_0 u_x + 3uu_x - \alpha^2(u_{xxt} + uu_{xxx} + 2u_x u_{xx}) + \gamma u_{xxx} = 0, \quad (2)$$

where α^2 , c_0 and γ are real-valued parameters.

Another generalization of Camassa-Holm equation given in [] is:

$$u_t + K(u^m)_x - (u^n)_{xxt} = \left[\frac{((u^n)_x)^2}{2} + u^n (u^n)_{xx} \right]_x, \quad (3)$$

where $K = const > 0$ and $m, n \in \mathbf{N}$.

The PDE describing the vibrations of a chain of particles interconnected by springs is the following:

$$u_{tt} + \Phi'(u) = (T(u_x))_x, \quad (4)$$

where $T(p) = p + p^\alpha$, $\alpha > 1$.

Finally, we consider the Boussinesq type equation:

$$u_{tt} = u_{xx} + \lambda(u^n)_{xx} + \mu(u^m)_{xxx} + \sum_{j=1}^{N-1} u_{y_j} u_{y_j}. \quad (5)$$

The classical Boussinesq equation describes the formation of patterns in liquid drops. After some technical moments the finding of travelling wave solutions of those equations (i.e. $u = \varphi(x - ct)$, $c = const$, $\xi = x - ct$) is reduced to the solvability of the following Cauchy problem:

$$\begin{cases} Q(y)(y')^2 = P(y), y = y(x) \\ y(x_0) = y_0, \end{cases} \quad (6)$$

where $P(y)$, $Q(y)$ are polynomials of y , $Q(y)P(y) > 0$, $\forall y \in (\alpha, \beta)$ and without loss of generality $P(y) > 0$, $Q(y) > 0$ for each $y \in (\alpha, \beta)$, $\alpha < \beta$; $\alpha, \beta \in \mathbf{R}^1$. Eventually $P(\alpha)Q(\alpha) = 0$, $P(\beta)Q(\beta) = 0$.

We suppose that:

$$\left| \begin{array}{l} P(y) = c_1(y - \alpha)^{m_1}(1 + o(1)), m_1 \geq 0, c_1 > 0, y > \alpha, y \rightarrow \alpha \\ Q(y) = c_2(y - \alpha)^{m_2}(1 + o(1)), m_2 \geq 0, c_2 > 0, y > \alpha, y \rightarrow \alpha \end{array} \right. \quad (7)$$

$$\left| \begin{array}{l} P(y) = c_3(\beta - y)^{n_1}(1 + o(1)), n_1 \geq 0, c_3 > 0, y < \beta, y \rightarrow \beta \\ Q(y) = c_4(\beta - y)^{n_2}(1 + o(1)), n_2 \geq 0, c_4 > 0, y < \beta, y \rightarrow \beta \end{array} \right. \quad (8)$$

Then there are four different cases to be considered, namely:

$$\begin{aligned} (A) \quad 1) \quad \lim_{y \rightarrow \alpha} F(y) = \tilde{c} < 0 &\iff \frac{m_2 - m_1}{2} + 1 > 0 \\ (A) \quad 2) \quad \lim_{y \rightarrow \alpha} F(y) = -\infty &\iff \frac{m_2 - m_1}{2} + 1 \leq 0 \\ (A) \quad 3) \quad \lim_{y \rightarrow \beta} F(y) = d > 0 &\iff \frac{n_2 - n_1}{2} + 1 > 0 \\ (A) \quad 4) \quad \lim_{y \rightarrow \beta} F(y) = \infty &\iff \frac{n_2 - n_1}{2} + 1 \leq 0. \end{aligned}$$

We are ready now to formulate our Theorem 1:

Theorem 1. (i) Suppose that (A) 1), (A) 3) hold and denote by $\frac{T}{2} = \int_{\alpha}^{\beta} \sqrt{\frac{Q(\lambda)}{P(\lambda)}} d\lambda > 0$. Then (6) possesses a strictly monotonically increasing solution for $x \in [0, \frac{T}{2}]$.

Moreover, in the case (A) 1) $y \approx \alpha + [(\frac{m_2 - m_1}{2} + 1)\sqrt{\frac{c_1}{c_2}}x]^{1 + \frac{1}{\frac{m_2 - m_1}{2}}}$, $x \approx 0$, $x > 0$,

while in the case (A) 3) $y \approx \beta - [(\frac{T}{2} - x)\sqrt{\frac{c_3}{c_4}}(\frac{n_2 - n_1}{2} + 1)]^{1 + \frac{1}{\frac{n_2 - n_1}{2}}}$, $x \approx \frac{T}{2}$, $x < \frac{T}{2}$.

(ii) Suppose that (A) 2) and (A) 3) hold.

Then (6) possesses a strictly monotonically increasing solution on the half line $(-\infty, 0]$.

Moreover, the solution has a horizontal asymptote at $y = \alpha$, while $y \approx \beta - [(1 + \frac{n_2 - n_1}{2})\sqrt{\frac{c_3}{c_4}}x]^{1 + \frac{1}{\frac{n_2 - n_1}{2}}}$, $x \approx 0$, $x < 0$.

(iii) Assume that (A) 2), (A) 4) hold. Then (6) has a kink type solution, i.e. strictly monotonically increasing solution with two horizontal asymptotes at $y = \alpha$ and $y = \beta$.

(iv) Assume that (A) 1), (A) 4) hold. Then (6) has a monotonically increasing solution in the interval $[0, +\infty)$. Moreover, its behavior for $x \rightarrow 0$ is given in (i), while it has a horizontal asymptote at $y = \beta$.

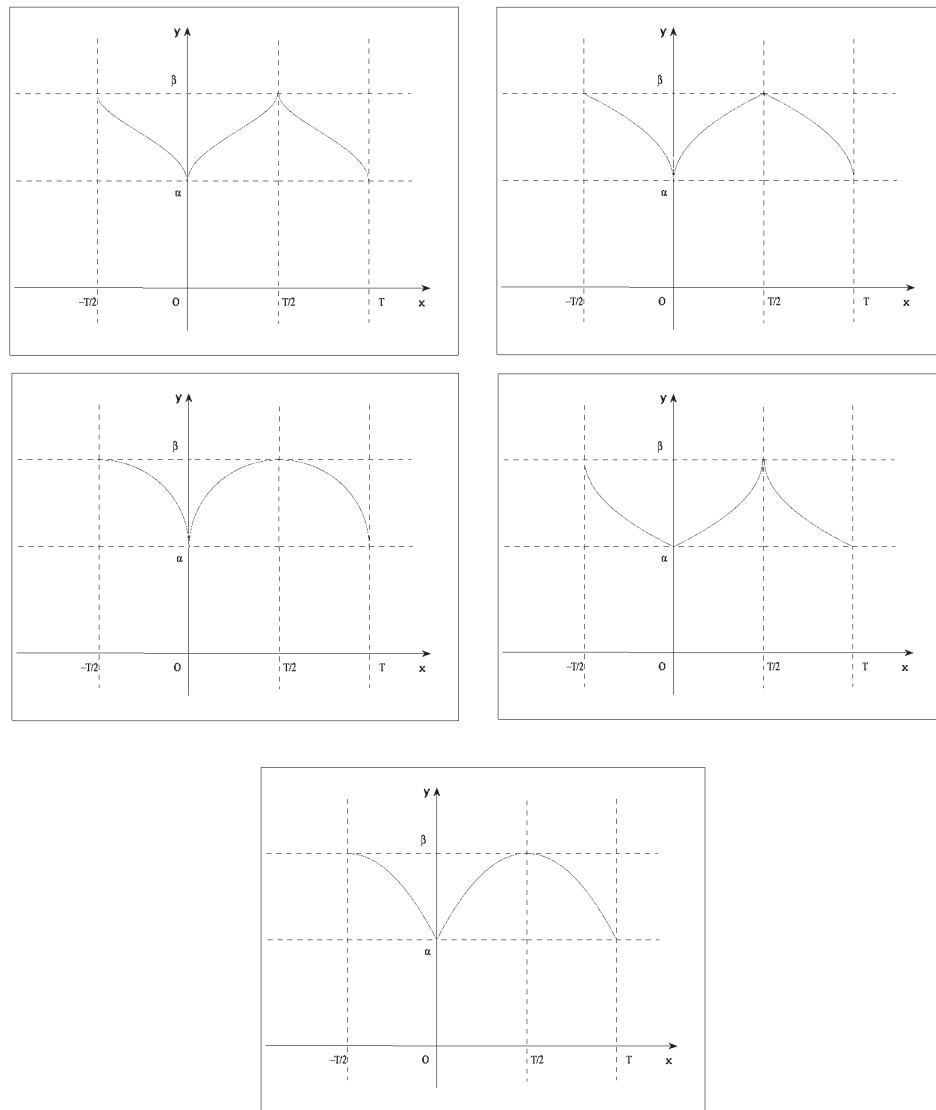


Fig.1.

Solitons having a peak (cusp) type singularity are called solitons-peakons (solitons-cuspons). Certainly, periodic traveling waves with peaks (cusps) could exist too. They are called periodic peak (cusp) type traveling wave solutions.

Acknowledgments. This work is supported by NATO Grant NRCLR.9837 16.

References

- [1] Bressan, A. and Constantin, A. (2007). Global conservative solutions of the Camassa-Holm equation, *Arch. Rational Mech. Anal.*, vol. 183, pp. 215–239.
- [2] Camassa, R., Holm, D. and Hyman, J. (1994). A new integrable shallow water equation, *Adv. Appl. Mech.*, vol. 31, pp. 1–33.
- [3] Constantin, A. and Escher, J. (1998). Global existence and blow up for a shallow water equation, *Ann. Sc. Norm. Sup. Pisa*, IV Ser., vol. 26, pp. 303–328.
- [4] Dullin, H., Gottwald, G. and Holm, D. (2001). An integrable shallow water equation with linear and non-linear dispersion, *Phys. Rev. Lett.*, vol. 87:19, 194501-1-4.
- [5] Fokas, A. and Fuchssteiner, B. (1981) Symplectic structures, their Backlund transformation and hereditary symmetries, *Physica D*, vol. 4, pp. 47–66.
- [6] Lin, Z. and Qian, T. (2002). Peakons of the Camassa-Holm equation, *Appl. Math. Modeling*, vol. 26, pp. 473–480.
- [7] Popivanov, P., Slavova, A., *Nonlinear waves. Introduction*, World Scientific, Singapore, 2010.
- [8] Tang, M. and Zhang, W. (2007). Four types of bounded solutions of CH- γ equation, *Science in China Series A: Mathematics*, vol. 50:1, pp. 132–152

Dynamic crack problems in functionally graded magnetoelectroelastic solids

Tsviatko Rangelov, Yonko Stoyanov, Petia Dineva

An exponentially inhomogeneous transversely isotropic magnetoelectroelastic (MME) medium with a finite crack is studied. The crack is impermeable and subjected to anti-plane mechanical and in-plane electric and magnetic dynamic loads. The problem is solved by a non-hypersingular traction boundary integral equation method (BIEM) based on the usage of the analytically derived fundamental solution. A numerical scheme based on the collocation method and on the parabolic type of approximation of the field variables is proposed.

Program codes in Mathematica and Fortran are developed and validated by comparison tests for anisotropic elastic and piezoelectric materials. Illustrative examples reveal the dependence of the stress, electric and magnetic concentration fields near the crack-tips on the frequency and direction of the external load and on the magnitude and direction of the material gradient.

1 Introduction

The MEE composites are brittle and highly sensitive to the presence of defects like cracks, holes, impurities, etc. that can reach a critical size during service and thus compromise the structure safety, see Chue and Hsu [1].

The concept for functionally graded materials (FGM) was proposed in the last years, see Ma and Lee [2]. To enhance the promising applications, it is necessary to better understand this new class of multifunctional intelligent composite materials in the context of their fracture state evaluation.

The solution of general boundary value problems for continuously inhomogeneous magneto-electric-elastic solids requires advanced numerical tool due to the high mathematical complexity arising from the electro-magneto-elastic coupling plus smooth variation of material characteristics.

The aim of this note is to propose nonhypersingular traction BIEM for the solution of the problem for wave propagation in a smooth exponentially inhomogeneous MEE plane with a finite crack subjected to an incident SH-wave. The BIEM technique is based on a frequency dependent fundamental solution derived analytically by the usage of an appropriate algebraic transformation for the displacement vector and the Radon transform.

2 Statement of the problem

In a Cartesian coordinate system consider a linear MEE medium poled in Ox_3 direction and subjected to a time-harmonic anti-plane mechanical load on Ox_3 axis and in-plane electrical and magnetic loads in the plane Ox_1x_2 . The only non-vanishing

fields are the anti-plane mechanical displacement u_3 , the in-plane electrical displacement D_i , the in-plane magnetic induction B_i , the electric field $E_i = -\varphi_{,i}$ and the magnetic field $H_i = -\psi_{,i}$, where φ, ψ are electric and magnetic potentials correspondingly. The constitutive relations in the plane Ox_1x_2 are, see Soh and Liu [3]

$$\sigma_{iK} = C_{iKJl}u_{J,l}, \quad x \in R^2 \setminus \Gamma, \quad (1)$$

where $x = (x_1, x_2)$, $\Gamma = \Gamma^+ \cup \Gamma^-$ is a finite crack - an open arc. Here coma denotes partial differentiation, small indexes $i, l = 1, 2$, capital indexes $K, J = 3, 4, 5$ and it is assumed summation in repeating indexes. The generalized displacement is $u_J = (u_3, \phi, \varphi)$, and the generalized stress tensor is $\sigma_{iJ} = (\sigma_{i3}, D_i, B_i)$, where σ_{i3} is the stress. Generalized elasticity tensor C_{iJKl} is defined as: $C_{iJKl} = 0$ for $i \neq l$ and $C_{i33i} = c_{44}$; $C_{i34i} = C_{i43i} = e_{15}$; $C_{i35l} = C_{i53l} = q_{15}$; $C_{i44l} = -\varepsilon_{11}$; $C_{i45l} = C_{i54l} = -d_{11}$; $C_{i55l} = -\mu_{11}$.

Functions $c_{44}(x)$, $e_{15}(x)$, $\varepsilon_{11}(x)$ are: elastic stiffness, piezoelectric coupled coefficient and dielectric permittivity, while $q_{15}(x)$, $d_{11}(x)$, $\mu_{11}(x)$ are piezomagnetic, magneto-electric coefficients and magnetic permeability correspondingly. It is assumed that $c_{44}(x)$, $\varepsilon_{11}(x)$ and $\mu_{11}(x)$ are positive that corresponds to a stable material, see [3]. Suppose that the material parameters C_{iJKl} and density ρ depend in the same manner exponentially on x

$$C_{iKJl}(x) = C_{iKJl}^0 e^{2\langle a, x \rangle}, \quad \rho(x) = \rho^0 e^{2\langle a, x \rangle}, \quad (2)$$

where \langle, \rangle means the scalar product in R^2 , $a = (a_1, a_2)$ and we use the notations $a_1 = r \cos \alpha$, $a_2 = r \sin \alpha$, $r = |a|$ is the magnitude and α is the direction of the material inhomogeneity.

Assuming the quasistatic approximation of MEE material in the absence of body forces, electric charges and magnetic current densities, the balance equation is

$$\sigma_{iK,i} + \rho_{KJ}\omega^2 u_J = 0. \quad (3)$$

where $\rho_{QJ} = \begin{cases} \rho, Q = J = 3 \\ 0, Q, J = 4 \text{ or } 5 \end{cases}$ and ω is the frequency of the applied time-harmonic load.

The boundary condition on the crack is

$$t_J|_{\Gamma} = 0. \quad (4)$$

where $t_J = \sigma_{iJ}n_i$ is the generalized traction and $n = (n_1, n_2)$ is the normal vector to Γ . That means the crack is impermeable, i.e. the crack line is free of mechanical traction, electric charge and magnetic current. In the following we will study the case $\omega > \omega_0$ when the dynamic behavior of the MEE material is characterized with a wave propagation phenomena. The total generalized displacement u_J and traction t_J field is a sum of an incident SH-wave and scattered by the crack wave, i.e. $u_J = u_J^{in} + u_J^{sc}$

and $t_J = t_J^{in} + t_J^{sc}$. Here $\omega_0 = \sqrt{\frac{\det M}{(\varepsilon_{11}^0 \mu_{11}^0 - d_{11}^0)^2} \rho^0} |a|$, where $M = \begin{pmatrix} c_{44}^0 & e_{15}^0 & q_{15}^0 \\ e_{15}^0 & -\varepsilon_{11}^0 & -d_{11}^0 \\ q_{15}^0 & -d_{11}^0 & -\mu_{11}^0 \end{pmatrix}$.

Suppose that $U_J(x, \omega) = e^{<a, x>} u_J(x, \omega)$ satisfies Sommerfeld–type condition at infinity, more specifically $U_3 = o(|x|^{-1})$, $U_4 = o(e^{-|a||x|})$, $U_5 = o(e^{-|a||x|})$ for $|x| \rightarrow \infty$. This condition ensures uniqueness of the scattering field u_J^{sc} for a given incident field u_J^{in} and it can be proved that the boundary value problem (BVP) (3), (4) admits continuous differentiable solutions.

The non-hypersingular traction BIE is derived following Wang and Zhang [4] for the homogeneous, Rangelov et al. [5] for the inhomogeneous piezoelectric case and Stoynov and Rangelov [6, 7] for the MEE case. The following system of BIE, that is equivalent to the BVP (3), (4) is obtained

$$\begin{aligned} -t_J^{in}(x, \omega) &= C_{iJKl}(x)n_i(x) \int_{\Gamma^+} [(\sigma_{\eta PK}^*(x, y, \omega) \Delta u_{P,\eta}(y, \omega) \\ &\quad - \rho_{QP}(y)\omega^2 u_{QK}^*(x, y, \omega) \Delta u_P(y, \omega)) \delta_{\lambda l} \\ &\quad - \sigma_{\lambda PK}^*(x, y, \omega) \Delta u_{P,l}(y, \omega)] n_\lambda(y) d\Gamma, \quad x \in \Gamma^+. \end{aligned} \quad (5)$$

where u_{JQ}^* is the fundamental solution of (3), obtained with Radon transform in Stoynov and Rangelov [7], $\sigma_{iJQ}^* = C_{iJMI} u_{MQ,l}^*$ is its stress, $\Delta u_J = u_J|_{\Gamma^+} - u_J|_{\Gamma^-}$ is the generalized crack opening displacement, x, y denote the field and the source point respectively. Equation (5) is traction non-hypersingular BIE on the crack line Γ for the unknown Δu_J . Once having a solution or the generalized crack opening displacement, the generalized displacement u_J can be obtained at every point in $R^2 \setminus \Gamma$ by using the corresponding representation formulae, see Stoynov and Rangelov [7].

3 Numerical realization

The numerical procedure for the solution of the BVP follows the numerical algorithm developed and validated in Rangelov et al. [5] for the inhomogeneous piezoelectric material and in Stoynov and Rangelov [7] for the homogeneous MEE case. The crack Γ is discretized by quadratic boundary elements (BE) away from the crack-tips and special crack-tip quarter-point BE near the crack-tips to model the asymptotic behavior of the displacement and the traction. Applying the shifted point scheme, the singular integrals converge in Cauchy principal value (CPV) sense, since the smoothness requirements $\Delta u_J \in C^{1+\alpha}(\Gamma)$ of the approximation are fulfilled.

In the numerical examples the crack Γ with a half-length $c = 5mm$, occupying an interval $(-c, c)$ on Ox_1 axis is considered. The crack is divided into 7 BE with lengths correspondingly: $l_1 = l_7 = 0.15c$, $l_2 = \dots = l_6 = 0.34c$, 1st BE is a left quarter point BE, 7th BE is a right quarter point BE and the rest BE are ordinary BEs.

The material is magneto-electroelastic composite $BaTiO_3/CoFe_2O_4$ with reference material constants C_{iJKl}^0 given in Song and Sih [8].

The described numerical scheme is validated by benchmark examples describing fracture behaviour of a line finite crack in an infinite plane subjected to a normal incident time-harmonic SH-wave in three different kinds of material, more specifically: (a) graded elastic anisotropic, see Daros [9]; (b) graded piezoelectric, see Rangelov et al. [5]; (c) homogeneous MEE composite, see Stoynov and Rangelov [7].

The dynamic fracture state of MEE is characterized by the leading term of the asymptotic of the generalized displacement and the generalized traction near the crack-tips

presented by the generalized intensity factor (GIF). For the considered MEE media GIFs are stress intensity factor K_{III} , electric field intensity factor K_E and magnetic field intensity factor K_H . For the straight crack on Ox_1 , $\Gamma = (-c, c)$ they are defined as

$$\begin{aligned} K_{III} &= \lim_{x_1 \rightarrow \pm c} t_3 \sqrt{2\pi(x_1 \mp c)}, \\ K_E &= \lim_{x_1 \rightarrow \pm c} E_2 \sqrt{2\pi(x_1 \mp c)}, \\ K_H &= \lim_{x_1 \rightarrow \pm c} H_2 \sqrt{2\pi(x_1 \mp c)} \end{aligned} \quad (6)$$

where t_3 and E_2, H_2 are calculated at the point $(x_1, 0)$ close to the crack-tip. In the figures the normalized frequency is $\Omega = ck^0, k^0 = \sqrt{\rho^0/c_{44}^0} \omega$ and normalized GIFs mechanical stress intensity factor $K_{III}^* = \frac{K_{III}}{t_3^n \sqrt{\pi c}}$, electric field intensity factor $K_E^* = \frac{10K_E}{t_3^n \sqrt{\pi c}}$ and magnetic field intensity factor $K_H^* = \frac{10^4 K_H}{t_3^n \sqrt{\pi c}}$, are plotted.

Fig. 1 shows the frequency dependence of the GIF K_{III}^*, K_E^* and K_H^* for the left crack tip, at different magnitudes of the material gradient $\beta = 2rc$ for $\beta = 0.0; 0.2; 0.4; 0.6$, at direction of material inhomogeneity along the crack, i.e. $\alpha = 0$ and in the case of a normal incident wave, i.e. $\theta = \pi/2$. Analysis of these results leads to the following observations: (a) there is a frequency $\Omega = 1.1$ where dynamic overshoot occurs and this frequency is not shifted when the material inhomogeneity is involved; (b) the magnitude of the material gradient has influence on all stress, electric field and magnetic induction concentration near the crack. A comparison between the results for the homogeneous material and for the inhomogeneous one with magnitude $rc = 0.3$ shows K_{III}^*, K_E^* and K_H^* increase with about 19%, 24% and 22% respectively when the observer point is near the left crack-tip.

The sensitivity of the generalized stress concentration with respect to the direction of the material gradient $\alpha = k\pi/2, k = 0.0, 0.1 \dots 1$ is demonstrated on Fig. 2, where case (a) is for the right crack tip and case (b) is for the left crack tip correspondingly. The fixed parameters are: $\Omega = 1.0, \theta = \pi/2$ and $\beta = 0.2, 0.4, 0.6$. The obtained results show that stress concentration fields are different at both crack-tips and even they have quite different behaviour: (a) the right crack-tip shows the maximal values for GIF in the case when the direction of material gradient is $\alpha = \pi/2$, while in contrast, the left crack-tip has its maximal values of GIF at $\alpha = 0.0$. These presented results show that in functional graded MEE material the local stress fields depend on the magnitude and direction of material gradient r, α .

4 Conclusion

A dynamic fracture analysis of an exponentially inhomogeneous MEE cracked plane subjected to time-harmonic anti-plane mechanical and in-plane electromagnetic loads is presented in this study. The results show the sensitivity of the GSIFs to the type of the material inhomogeneity characteristics, to the coupled nature of MEE continua and to the properties of the applied dynamic electro-magneto mechanical load. The presented method can be successfully used for the more complex problems of crack interactions, cracks with arbitrary shapes and composites with different combinations of piezoelectric and piezomagnetic constituents.

Acknowledgement. The authors acknowledge the support of the BNSF under the Grant No. DID 02/15 and the support of TU Sofia under the Grant No. 102 NI 218-11.

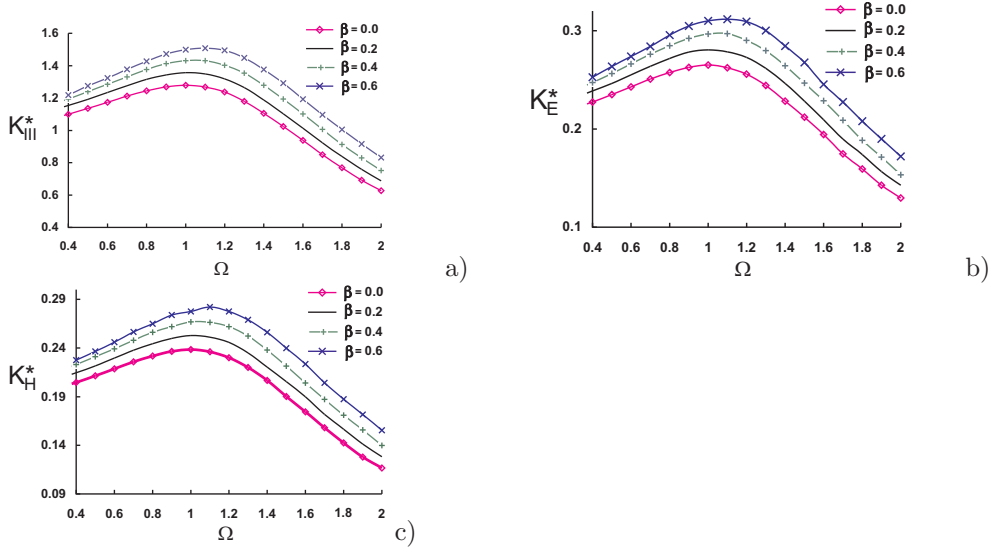


Figure 1: GIF versus normalized frequency Ω at the left crack-tip for different values of the magnitude β at a direction of material inhomogeneity $\alpha = 0.0$ and a wave incident angle $\theta = \pi/2$: (a) K_{III}^* ; (b) K_E^* ; (c) K_H^* .

Acknowledgement. The authors acknowledge the support of the BNSF under the Grant No. DID 02/15 and the support of TU Sofia under the Grant No. 102 NI 218-11.

References

- [1] C. H. Chue and W. H. Hsu. Antiplane internal crack normal to the edge of a functionally graded piezoelectric/piezomagnetic half plane. *Meccanica*, 43:307–325, 2008.
- [2] C. C. Ma and J. M. Lee. Theoretical analysis of in-plane problem in functionally graded nonhomogeneous magneto-electroelastic bimaterials. *Int. J. Solids Struct.*, 46:4208–4220, 2009.
- [3] A. K. Soh and J. X. Liu. On the constitutive equations of magnitoelectroelastic solids. *J. Intell. Mater. Syst. Struct.*, 16:597–602, 2005.
- [4] C. Y. Wang and C. Zhang. 2D and 3D dynamic Green’s functions and time-domain BIE formulations for piezoelectric solids. *Engng. Anal. BE*, 29:454–465, 2005.

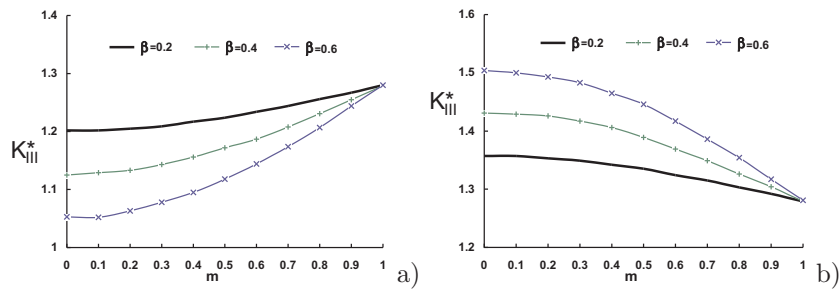


Figure 2: K_{III}^* versus the direction of material inhomogeneity $\alpha = m\pi/2$, $m = 0.0, 0.1 \dots 1.0$ at a wave propagation direction $\theta = \pi/2$ for different values of the magnitude β and normalized frequency $\Omega = 1.0$: (a) right crack-tip; (b) left crack-tip.

- [5] T. Rangelov, P. Dineva, and D. Gross. Effect of material inhomogeneity on the dynamic behavior of cracked piezoelectric solids: a BIEM approach. *ZAMM-Z. Angew. Math. Mech.*, 88:86–99, 2008.
- [6] Y. Stoyanov and T. Rangelov. Time-harmonic behaviour of anti-plane cracks in inhomogeneous magnetoelastic solid. *Compt. Rend. Acad. Bulg. Sci.*, 62 (2):175–186, 2008.
- [7] Y. Stoyanov and T. Rangelov. Time-harmonic crack problems in magnetoelastic plane by BIEM. *J. Theor. Appl. Mech.*, 39(4):73–92, 2009.
- [8] Z. F. Song and G. C. Sih. Crack initiation behavior in magneto - electro - elastic composite under in - plane deformation. *Theor. Appl. Fract. Mech.*, 39:189–207, 2003.
- [9] C. H. Daros. On modelling SH-waves in a class of inhomogeneous anisotropic media via the Boundary Element Method. *ZAMM-Z. Angew. Math. Mech.*, 90: 113–121, 2010.

Modeling tsunami waves via Cellular Nonlinear Networks

Angela Slavova, Maya Markova, Pietro Zecca

The study of propagation of tsunami from their small disturbance at the sea level to the size they reach approaching the coast has involved the interest of several scientists. It is clear that in order to predict accurately the appearance of a tsunami it is fundamental to built up a good model. From this point of view the most important tool in the context of water waves is soliton theory [6]. Frequently in the literature it is stated that a tsunami is produced by a large enough soliton. Solitons arise as special solutions of a widespread class weakly nonlinear dispersive PDEs modeling water waves, such as the KdV or Camassa-Holm equation [1,5], representing to various degrees of accuracy approximations to the governing equations for water waves in the shallow water regime. How the tsunami is initiated? The thrust of a mathematical approach is to examine how a wave, once initiated, moves, evolves and eventually becomes such a destructive force of nature.

In Constantin and Johnson [4] the model of the motion of the water before arrival of a tsunami wave is proposed. They require that a flat free surface for the background state excludes linear vorticity functions, unless the flow is trivial. So, nonlinear vorticity distributions are introduced in order to admit nontrivial flows with a flat free surface. Consider the following dynamical system

$$\varphi_{tt} + \varphi_{xx} = -f(\varphi), \tag{1}$$

$$f(\varphi) = \begin{cases} \varphi - \varphi|\varphi|^{-1/2} & \text{if } \varphi \neq 0 \\ 0 & \text{if } \varphi = 0. \end{cases} \tag{2}$$

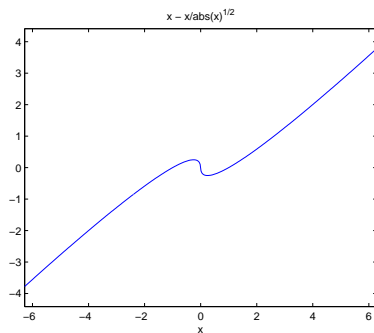


Fig.1. Bifurcation diagram of the nonlinear vorticity distribution.

By applying Cellular Neural Networks (CNN) approach [2,3,8] we shall study the wave propagation of the model (1), (2).

CNN model of our system (1), (2) will be the following:

$$\begin{aligned}\frac{dv_j}{dt} &= A_1 * u_j + f(u_j), \\ \frac{du_j}{dt} &= v_j, 1 \leq j \leq N\end{aligned}\tag{3}$$

Our objective in this paper is to study the structure of the travelling wave solutions of the CNN model (3). There has been many studies on the travelling wave solutions of spatially discrete or both spatially and time discrete systems [7,9]. The study of travelling wave solutions can proceed as follows. Consider solutions of (3) of the form:

$$z_j = \Phi(j - ct),$$

$z_j = \text{col}(u_j, v_j)$ for some continuous functions $\Phi : \mathbf{R}^1 \rightarrow \mathbf{R}^1$ and for some unknown real number c . Denote $s = j - ct$. Let us substitute (4) in our CNN model (3). Then $\Phi(s)$ and c satisfies the system of the form:

$$\begin{aligned}-c\Phi'(s) &= G(\Phi(s + r_0), \Phi(s + r_1), \dots, \Phi(s + r_n)) + \\ &+ F(\Phi(s + r_0)) = 0,\end{aligned}\tag{4}$$

here $r_0 = 0$, r_i are real numbers for $i = 1$ to n . Equation (5) is called bistable because it has three spatially homogeneous solutions $\Phi(s) \equiv z^-, z^0, z^+$ satisfying $z^- < z^0 < z^+$, and

$$\begin{aligned}G(z, z, \dots, z) &> 0 \text{ for } z \in (-\infty, z^-) \cup (z^0, z^+), \\ G(z, z, \dots, z) &< 0 \text{ for } z \in (z^-, z^0) \cup (z^+, \infty),\end{aligned}$$

Recently, Mallet-Paret [7] showed that (5) has a unique monotone solutions satisfying the boundary conditions:

$$\lim_{s \rightarrow -\infty} \Phi(s) = z^- \quad \text{and} \quad \lim_{s \rightarrow \infty} \Phi(s) = z^+.\tag{5}$$

More precisely, it is proved that under some assumptions, there is a unique c^* such that (5) has a monotone solutions satisfying (6) iff $c = c^*$, and such solution is also unique up to a phase shift if $c = c^* \neq 0$. Indeed, the solution $\Phi(s)$ of (5) and $\lim_{s \rightarrow \infty} \Phi(s) = z^+$ can be represented as

$$\Phi(s) = z^+ - \gamma e^{\sigma s} - \tilde{\Phi}(s) e^{2\sigma s},$$

for $s \gg 1$, $\sigma^+ < 0$, $\gamma > 0$, $\tilde{\Phi}(s)$ is a bounded and C^1 -function.

Suppose that our CNN model (3) is a finite circular array of $L = N.N$ cells. For this case we have finite set of frequencies [2,3]:

$$\Omega = \frac{2\pi k}{L}, \quad 0 \leq k \leq L - 1.\tag{6}$$

The following proposition then hold:

Proposition 1. Suppose that $z_j(t) = \Phi(j - ct)$ is a travelling wave solutions of the CNN model (3) with $\Phi \in C^1(\mathbf{R}^1, \mathbf{R}^1)$ and $\Omega = \frac{2\pi k}{L}$, $0 \leq k \leq L - 1$. Then there exist constants $c_* < c^* < 0$ such that

(i) if $c \leq c_*$ then $\Phi(s; c)$ is nondecreasing and satisfies

$$\lim_{s \rightarrow -\infty} \Phi(s) = z^0 \quad \text{and} \quad \lim_{s \rightarrow \infty} \Phi(s) = z^+; \quad (7)$$

(ii) if $c = c^* > c_*$, then $\Phi(s; c)$ is nondecreasing and satisfy (6);

(iii) if $c^* < c < 0$, then $\Phi(s; c)$ is nondecreasing and unbounded.

Let us introduce the following energy function for our CNN model (3):

$$E(u_j, v_j) = \frac{1}{2}u_j^2 + \frac{1}{2}v_j^2 - \frac{2}{3}|v_j|^{3/2}. \quad (8)$$

We obtain the following simulation results in the plane (u, v) which present two closed curves representing the solution set of the equation $u_j^2 = \frac{4}{3}|v_j|^{3/2} - v_j^2$:

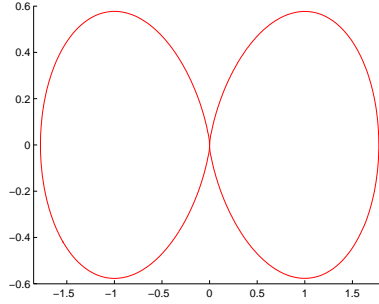


Fig.2.

The stationary points of (3) are $(\pm 1, 0)$, or $(0, 0)$. If the energy function $E < 0$ the set of solutions consists of the interiors of the two closed curves given on Fig.2. By virtue of (12), once a solution of (1) intersects the boundary of these two closed curves at a point other than $(0, 0)$, it will remain in that set having the asymptotic limit $(-1, 0)$, or, correspondingly $(1, 0)$. Notice that on the boundary of the two closed curves (Fig.2) we have $E = 0$, while within these sets $E < 0$, with the minimum attained at $(\pm 1, 0)$ where $E = -\frac{1}{6}$.

Let us consider the following initial conditions for our CNN model (3):

$$\begin{cases} u_j(0) = a \\ v_j(0) = 0. \end{cases} \quad (9)$$

If $z^+ \rightarrow a$, for $s \rightarrow \infty$, the number of intersections approaches infinity. Denote by Ω_+ , Ω_- the sets of points $(a, 0)$, where $a \in (-\infty, 0) \cup (0, \infty)$ and suppose that the corresponding solution of (3) has asymptotic limit $(1, 0)$, $(-1, 0)$ respectively. It is easy to prove that all intersections being transversal to the horizontal axis are

stable under small perturbations [5]. Therefore, for any integer $M \geq 1$ by continuous dependence on the initial data it might be proved that as $a \rightarrow \infty$ the number M of intersections approaches infinity.

In our case $\Phi : [0, \infty) \rightarrow [0, \infty)$ is defined implicitly by

$$r = \int_{\Phi}^{1/4} \frac{dt}{\sqrt{\frac{4}{3}|t|^{3/2} - t^2}}, r \in [0, I]$$

where

$$I = \int_0^{1/4} \frac{dt}{\sqrt{\frac{4}{3}|t|^{3/2} - t^2}}$$

and extend to $s \geq 1$ by setting Φ equal to zero here. Simulations of the implicit solution Φ are given below:

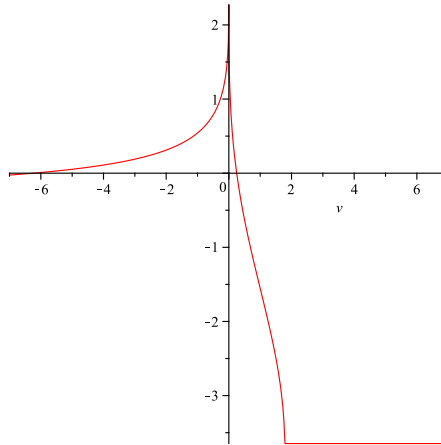


Fig.3. Real part of the solution Φ .

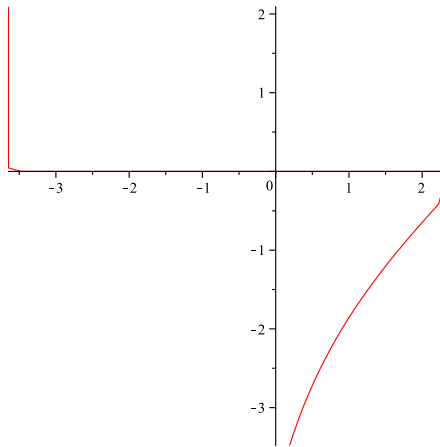


Fig.4. Implicitly solution Φ .

Remark 1. Notice that

$$\Phi_+'' + \Phi_+ - \Phi_+ |\Phi_+|^{-1/2} = 0,$$

with

$$\Phi_+(0) = \frac{1}{4}, \Phi_+'(0) = -\frac{1}{4}\sqrt{\frac{5}{3}}, \Phi_+(I) = \Phi_+'(I) = 0.$$

Since $\lim_{s \rightarrow \infty} \Phi_0(s) = 0$, there exists some $s_0 > 0$ such that $|\Phi_0(s)| < \frac{1}{4}$ for $s \geq s_0$. So we claim

$$-\Phi_+(s - s_0) \leq \Phi_0(s) \leq \Phi_+(s - s_0), s \geq s_0.$$

Acknowledgments. This work is supported by NATO Grant NRCLR.9837 16 and by the Bulgarian National Science Fund under grant DID 02/15.

References

- [1] R.Camassa, D. Holm, An integrable shallow water equation with peaked solutions, *Phys. Rev. Letters*, vol. 71, pp. 1661–1664, 1993
- [2] L.O.Chua, L.Yang, Cellular Neural Network: Theory and Applications, *IEEE Trans. CAS*, vol. 35, pp. 1257-1290, Oct. 1988.
- [3] L.O.Chua, M.Hasler, G.S.Moschytz, J.Neirynsk, Autonomous cellular neural networks: a unified paradigm for pattern formation and active wave propagation, *IEEE Trans. CAS-I*, vol. 42, N 10, pp. 559-577, Oct. 1995.
- [4] A.Constantin, R.S.Johnson, Propagation of very long water waves, with vorticity, over variable depth, with applications to tsunamis, *Fluid Dyn.Res.*, 40, pp. 175-211, 2008.

- [5] A.Constantin, W.Strauss, Stability of the Camassa-Holm solitons, *J.Nonlinear Sci.*, 12, pp.415-422, 2002.
- [6] P.G.Drazin, R.S.Johnson, *Solitons:An Introduction*, Cambridge University Press, Cambridge, 1989.
- [7] J. Mallet-Paret, Spatial patterns, spatial chaos and travelling waves in lattice of differential equations, in: *Stochastic and Spatial Structure of Dynamical Systems*, editors van Strien, S. and Verduyn Lunel, S., North-Holland, pp. 105–129, 1996.
- [8] T.Roska, L.O.Chua, D.Wolf, T.Kozek, R.Tetzlaff, F.Puffer, Simulating nonlinear waves and partial differential equations via CNN- Part I: Basic techniques, *IEEE Trans. CAS-I*, vol. 42, N 10, pp. 807-815, Oct. 1995.
- [9] A.Slavova, *Cellular Neural Networks: Dynamics and Modelling*, Kluwer Academic Publishers, 2003.

Cellular Nonlinear Network Model for Image Denoising

Angela Slavova, Victoria Rashkova

1 Introduction

Recently many mathematical models for image processing have been widely applied in computer visualization. The nonlinear diffusion partial differential equation have been broadly applied in image processing since the first model was introduced in 1987 [3]. Through the time evolution, the diffusion can effectively remove the noise as well as having edge enhancement simultaneously. Since then various nonlinear diffusion filters have been widely proposed in implementing the image denoising / enhancement, edge detection and flow field visualization . The common feature for nonlinear diffusion model is that the diffusion coefficient is small as the gradient of image is large. However the diffusion coefficient is a function of the convolution of the Gaussian kernel and solution such that this requires an extra cost in computing the nonlinear diffusion coefficient. In the numerical experiments we find that when using the nonlinear diffusion model in denoising the noise is not quite good [6]. Hence we propose a convection- diffusion filter by adding a convection term in the modified diffusion equation as a physical interpretation for removing the noise. The aim of this paper is to focus on the noise removal algorithm for extracting the target information (image) precisely. The main idea of our model algorithm is to diffuse the noise by following the convection direction during time evolution. To prevent the numerical layer in the discontinuities on the relative coarse grids we use the Cellular Nonlinear Network (CNN) approach [1,2,4].

2 Perona- Malik type nonlinear diffusion equation and its CNN model

Dynamic properties of Perona-Malik based filters are summarized in [3]. It is well known that it converges toward a constant steady state solution, representing the average value of the initial image. In order to obtain a non trivial output image, the system evolution has to be stopped after a finite time (usually called scale). In the most general case, the scale depends on the object and on the characteristics of the input image, and hence is no *a priori* known time for stopping the image processing. Let the noisy image be a given scaled intensity map $u_0(x) : \Omega \rightarrow [0, 255]$ for the image domain $\Omega \in \mathbb{R}^2$. The nonlinear diffusion equation was first proposed by Perona and Malik in filtering the noise. They built a sequence of continuous images $u(x, t)$ on the abstract scale t and through the nonlinear diffusion equation to remove the noise during the scaling ($i_{\frac{1}{2}} \text{time} i_{\frac{1}{2}}$) revolution. Many of such nonlinear diffusion filtering

models have been implemented. We briefly review this model as follows. The Perona-Malik type nonlinear isotropic diffusion equation (ND) is:

$$\begin{cases} u_t(x, t) - \operatorname{div}(g(|\nabla G_\sigma * u|)\nabla u(x, t)) = 0 & \text{in } \Omega \times I \\ \frac{\partial u}{\partial n}(x, t) = 0 & \text{on } \partial\Omega \times I \\ u(x, 0) = u_0(x) & \text{on } \Omega \end{cases} \quad (1)$$

where the initial value $u_0(x)$ is the given noisy image in the gray level, $I = [0, T]$ is the scaling (time) interval for some $T > 0$, Ω is a simply bounded rectangular domain with boundary $\partial\Omega$ and n is the outward unit normal vector to $\partial\Omega$; g is a given non-increasing function. There are several choices for $g(s)$. Select a monotonic decreasing function

$$g(s) = \frac{1}{1 + s^2}$$

and in [3] it is introduced the Gaussian kernel, $G_\sigma * u$, for the existence and uniqueness of (1). Thus, the diffusion coefficient $g(|\nabla G_\sigma * u|)$ is inhibited as the gradient of image intensity is big i.e. the diffusion coefficient is small around the image edge. Hence ND preserves the edges of image and protects the brightness of the image simultaneously. Perona and Malik considered the Galerkin finite element method for the discretization of (1). We shall apply polynomial CNN in order to study its dynamics. The following diffusion functions were proposed by Perona and Malik:

$$g(\|\nabla u\|^2) = e^{-\left(\frac{\|\nabla u\|}{k}\right)^2}, g(\|\nabla u\|^2) = [1 + \left(\frac{\|\nabla u\|}{k}\right)^2]^{-1} \quad (2)$$

Let us suppose that the continuous space domain is composed by $M \times M$ points arranged on a regular grid, u_{ij} represents the pixel value.

In order to implement a general polynomial CNN architecture, let us consider the following basis function:

$$f(z) = 1 - \frac{1}{2} \left(\left| \frac{z}{m} + 1 \right| - \left| \frac{z}{m} - 1 \right| \right)$$

and let approximate the $g(\cdot)$ functions (2) with the following expression:

$$\gamma(z) = \sum_{p=1}^Q C_p f^p(z)$$

We obtain a general nonlinear PDE based polynomial CNN model:

$$\frac{du_{ij}(t)}{dt} = \sum_{(kl) \in N_{ij}} \Gamma_{kl}(u_{kl} - u_{ij}) \quad (3)$$

$$\Gamma_{kl} = \sum_{p=1}^Q \frac{C_p}{2h^2} [f^p(\|\tilde{\nabla}u_{k,l}\|^2) + f^p(\|\tilde{\nabla}u_{i,j}\|^2)]$$

The polynomial CNN model (PCNN) (3) approximate the functions $g(\cdot)$ with the expression $\gamma(\cdot)$ that turns out to be different from zero only for $|z| = \|\tilde{\nabla}u_{i,j}\|^2 < m$. This practical approximation presents the advantage of stopping the evolution of the image when the approximated gradient magnitude $\|\tilde{\nabla}u_{i,j}\|^2$ is greater than the threshold m . Hence, the output image exhibits a segmented structure. The above behavior is possible because the PCNN system (3) presents ore than one equilibrium point and for each initial image, the output corresponds to one of these equilibria.

Conclusion 1 *The PCNN model (3) exhibit the coexistence of the constant average value equilibrium point (that is only admissible for the Perona-Malik discretized models) and of an infinite set of equilibrium points. As a consequence, the correct output is obtained without stopping the evolution of the system. This represents a significant advantage from the algorithmic point of view.*

We obtain the following simulation results for different values of the cell parameters:

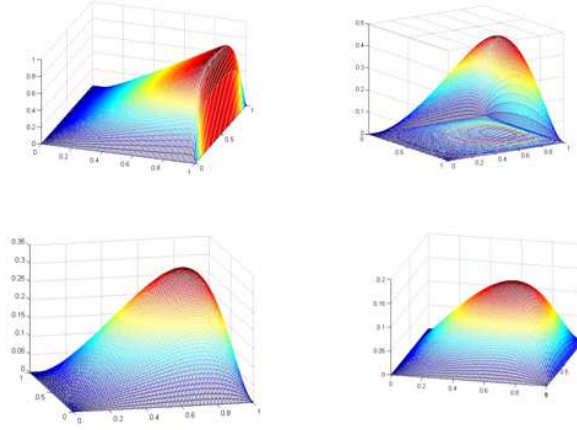


Fig.1. Simulations of the CNN algorithm for the problem (1).

Example 1. Consider the following singularly perturbed boundary value problem

$$\begin{aligned} -\varepsilon\Delta u + bu_x + cu &= 0, \quad \text{in } \Omega \equiv (0,1)^2 \\ u &= 0, \quad \text{on } \partial\Omega. \end{aligned} \quad (4)$$

In order to construct a robust numerical method for the considered problem, it is of key interest to have information on a behavior of the solution. The state equation of the CNN model of (4) is:

$$-\varepsilon A_1 * u_i + b * A_1 * u_i + c * u_i = 0 \quad (5)$$

Applying CNN algorithm we obtain the following simulation results:

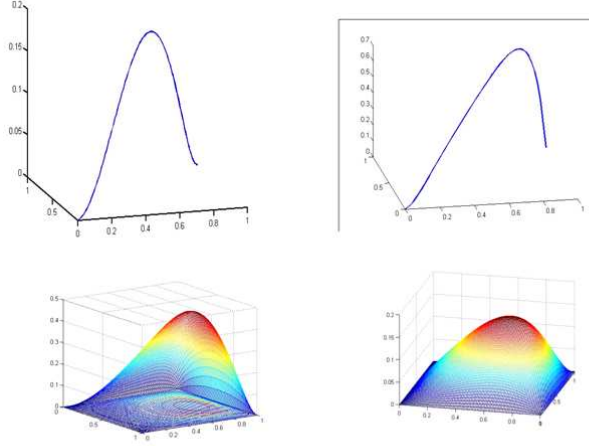


Fig.2. Simulation of the CNN algorithm of (4).

Example 2. We consider the following example on the layer-adapted mesh:

$$-\varepsilon \Delta u + (1 + x^3)u_x + (1 + xy)u = 0, \text{ in } \Omega \quad (6)$$

$$u = 0, \text{ on } \partial\Omega$$

CNN model of the above system is:

$$-\varepsilon A_1 * u_i + (1 + x^3)A_1 * u_i + (1 + xy)u_i = 0 \quad (7)$$

$$1 \leq i \leq N$$

We obtain simulation results of (6) on Fig.3.

Remark 1. We consider a CNN programmable realization allowing the calculation of all necessary processing steps in real time. The network parameter values of CNN models are determined in a supervised optimization process. During the optimization process the mean square error is minimized using Powell method and Simulated Annealing [5]. The results are obtained by the CNN simulation system MATCNN applying 4th order Runge-Kutta integration.

Acknowledgments. This work is supported by the Bulgarian National Science Fund under grant DID 02/15.

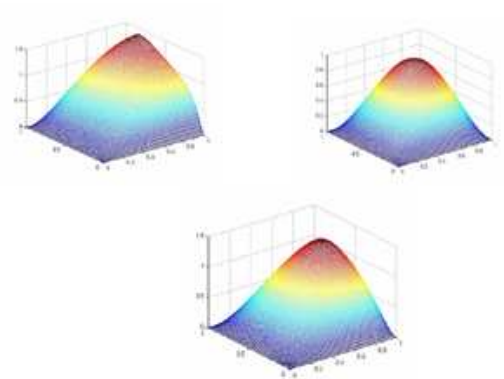


Fig.3. Simulation of the CNN algorithm of (6).

References

- [1] Chua L.O., Yang L., Cellular Neural Network: Theory and Applications, *IEEE Trans. CAS*, vol. 35, pp. 1257-1290, Oct. 1988.
- [2] Chua L.O., Hasler M., Moschytz G.S., Neirynsk J., Autonomous cellular neural networks: a unified paradigm for pattern formation and active wave propagation, *IEEE Trans. CAS-I*, vol. 42, N 10, pp. 559-577, Oct. 1995.
- [3] P. Perona, J. Malik, Scale space and edge detection using anisotropic diffusion. In: Proceedings of IEEE Computer Soc. Workshop and Computer Vision, 1987, pp. 16-22.
- [4] A.Slavova, Cellular Neural Networks: Dynamics and Modelling, Kluwer Academic Publishers, 2003.
- [5] R. Tetzlaff, F. Gollas, Modeling complex systems by reaction-diffusion Cellular Nonlinear Networks with polynomial Weight-Functions, Proc. IEEE CNNA2005, 2005.

Vibrational Recursive Geometry

Antoaneta Tsokova

Pythagoras first in the whole history of mathematics has found an isomorphism between geometry and music. The ancient philosopher uncovered numerical proportions in music, using algebraic proofs - each sound is a numeral. Geometrical patterns are used to visualize proportions, symmetry in music. Modern science has proven that such a relationship between both really exists; moreover: sounds have invisible geometrical patterns [2, 4, 6]. These patterns are the well known forms of Plato. In the late 1980-s Prof. Buckminster Fuller carried out an experiment with a balloon. A white balloon (filled with air) was put in a bathtub, filled with ink. The ink vibrated in perfect diatonic intervals. As expected, the ink concentrated in the points, where all surface motions annulled each other - the so called "sub-zero area". These "nodes" were absolutely straight lines and formed the well known forms of Plato: octahedron, icosahedron, dodecahedron, sidereal tetrahedron and cube (Fig. 1); all of them are simple 3D figures. This experiment proves the 3D-nature of sound. The forms of Plato represent vibrations of sound. All of these figures can be perfectly inscribed in a sphere. Because sphere is the most harmonic, ideal form; it is the base of all the other forms, it contains them in itself potentially.

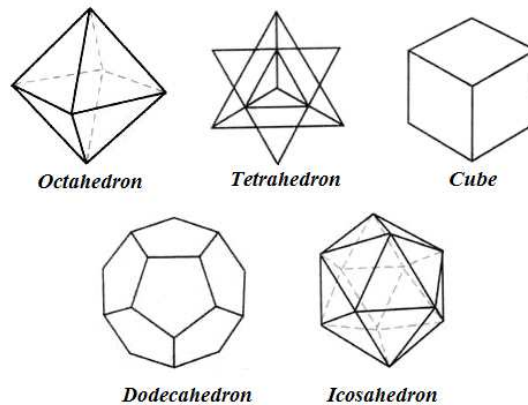


Figure 1:

Hans Jenny was inspired by Fuller's experiment. In his scientific research "Cymatics" Jenny used thin containers, filled with colloidal liquid. While the liquid was still, the colloids inside stayed in like manner, equally divided. Prof. Jenny has called this state "hydro-dynamic dispersion". But when the containers have been tuned

in perfect diatonic intervals, the particles inside gained together in well-arranged, isolated, visible geometric patterns, which were two and/or three-dimensional. They looked two-dimensional when only being observed from one point of view, but in fact they were volumetric; it was possible for one to see the depth inside the pattern. In Fig. 2 the five forms of Plato could be seen. Looking at them, our eyes "hear" music. Jenny called this picture "a hologram of sound".

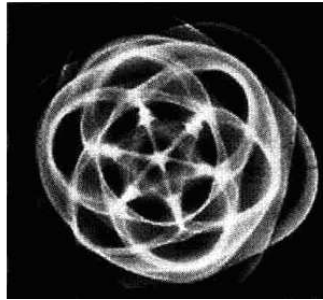


Figure 2: Hans Jenny: Sound vibrations in colloidal liquid

When the frequency of musical vibration in the bathtub full of ink increased, the old geometric forms disappeared and new, more complicated ones appeared in place. When the old frequency had been called out, the old forms appeared again. The size and complexity of forms depended on the vibration frequency: the higher the frequency, the bigger and more tangled the forms. In changing the frequency, the new, bigger forms comprised the old ones; they "embraced", contained them. The smaller figures were "nested" in the bigger ones; the progression of size was obvious. It was geometry of "sphere inside sphere". Strange and yet true nobody called this case by its proper name - recursion process. Recursion appears in nesting of the forms in each other. The musical process is a recursion, carried out in time - every musical event in the new key contains the idea of previous events in other keys.

In sonata movement first theme of the exposition is in tonic (triad of the first tone of the key), and the second - in dominant (triad of the fifth tone of the key). The correspondence between the two is recursive - dominant contains tonic in itself, because dominant arises out of tonic. The same is true about all the keys we are going through in the development. Returning in tonic and reconciliation of first and second themes marks the end of spiral development of musical recursion - we are in the starting key again, but the reprise is a summary of the whole musical material. According to harmony (science of chords) reprise is more complicated than exposition. The final level of recursion contains all its predecessors.

As musical (vibrational) recursion is a process, it is difficult to follow it. The experiments of Jenny and Fuller show the nesting of levels. Pythagoras himself preferred geometrical to arithmetical proofs, because geometry is more convincing; it is closer

to real musical development. Since progressions in mathematics are perfect examples of recursion (the following numbers contain their predecessors) and vibrational geometric forms increased by increasing the frequency, inscribing their predecessors, the conclusion is that we observe sound recursion.

The early Pythagoreans introduce in musical theory the scientific approach, in which musical intervals are expressed as numerical proportions, as well as develop also the more specific idea of harmonic "means". At an early date they discovered empirically that the basic intervals of Greek music include the elements of the golden section, since they have the proportions 1:1 (unison), 3:4 (fourth), 2:3 (fifth), 1:2 (octave), and relate them to geometrical primitives (polygons and polyhedra) [2, 3].

One of the aims of this work is to propose a relation, which serves as a link between the basic Pythagorean intervals and the regular polygons. Indeed, it is not difficult to calculate, that the values of the function $f(n) = \sqrt{\sin \frac{\pi}{n}}$ at the points $n = 2; 5; 7; 12$ approximate the ratios, corresponding to unison, fourth, fifth, octave, respectively [1]. On behalf of the angle $\frac{\pi}{n}$, it appears in the regular polygon with $2n$ vertices - the central angle around the center of the circumscribed circle consists of $2n$ angles equal to it (Fig. 3) [5].

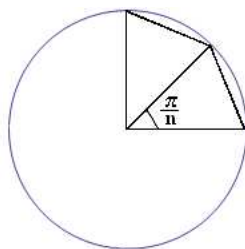


Figure 3:

Moreover, for other intervals and their ratios we come to the conclusion, that the proposed function gives a sufficiently good correspondence between the intervals and the regular polygons with even number of vertices [1, 4, 5]. The results are given in Table 1.

There are some interesting musical conclusions. It was mentioned that Fuller's bathtub vibrated in perfect diatonic intervals. Pythagoras' diatonic proportions will now be used to illustrate the isomorphism between music and geometry. Each figure which could be inscribed in a circle has its own musical interval. These intervals are diatonic - the perfect musical mode according to Pythagoras. We use two-dimensional forms; they are basic for three-dimensional ones. In the table above there are numerical proportions of the forms (the number of vertices is used - $2n$). These are the well-known

n	number of vertices	$\sqrt{\text{Sin}[\frac{\pi}{n}]}$	ratio	interval
2	4	1	1 : 1 = 1	Perfect Unison
3	6	0.931	15 : 16 = 0.937	Minor Second
4	8	0.841	5 : 6 = 0.8	Minor Third
5	10	0.767	3 : 4 = 0.75	Perfect Fourth
6	12	0.707	5 : 7 = 0.714	Minor Fifth
7	14	0.659	2 : 3 = 0.667	Perfect Fifth
8	16	0.619	5 : 8 = 0.625	Minor Sixth
9	18	0.585	3 : 5 = 0.6	Major Sixth
10	20	0.556	5 : 9 = 0.563	Minor Seventh
11	22	0.531	8 : 15 = 0.533	Major Seventh
12	24	0.509	1 : 2 = 0.5	Perfect Octave

Figure 4: Table 1

ancient diatonic proportions of Pythagoras and Plato. In the table there is neither major second, nor major third, there are two fifths - minor and perfect, because these intervals are intemperate, natural. The difference between major second and minor third cannot be fixed sharply; the same is true of major third and perfect fourth; in nature scale this differences are not so considerable to be able to give two or even one perfect Pythagoras' geometric pattern. These intervals have intentionally been called "imperfect". The tempered scale has nullified the difference between minor and perfect fifth: in the piano keyboard fifth is bigger than minor fifth, but smaller than perfect, Pythagoras' fifth.

In conclusion, the table above confirms Pythagoras' statement: "*When Noise married Mathematics, Music was born.*"

References

- [1] <http://functions.wolfram.com/>
- [2] West M.L.: Ancient Greek Music, Clarendon Press, Oxford, 1992.
- [3] Bloch E.: Essays on the Philosophy of Music, Cambridge, Cambridge University Press, 1985.
- [4] Kelevedjiev E., Dzhenkova Z.: Computer Science, Mathematics and Music, Proc. of the Sixth Spring Conf. of the Union of Bulgarian Mathematicians, 2007, 92-101 (in Bulgarian).
- [5] <http://mathworld.wolfram.com/RegularPolygon.html>
- [6] Fauvel J., Flood R., Wilson R.: Music and mathematics: from Pythagoras to fractals, Oxford University Press, 2006.

Part B

List of participants

Andrey Andreev
Technical University of Gabrovo
Hadji Dimitar str. 4
5300 Gabrovo, Bulgaria
andreev@tugab.bg

Roumen Anguelov
Department of Mathematics and
Applied Mathematics
University of Pretoria
Pretoria 0002, South Africa
roumen.anguelov@up.ac.za

Emanouil Atanassov
Institute of Information and
Communication Technologies
Bulgarian Academy of Sciences
Acad. G. Bontchev str., bl. 25A
1113 Sofia, Bulgaria
emanouil@parallel.bas.bg

Gergana Bencheva
Institute of Information and
Communication Technologies
Bulgarian Academy of Sciences
Acad. G. Bonchev Str., bl. 25A
1113 Sofia, Bulgaria
gery@parallel.bas.bg

Christo I. Christov
Dept. of Mathematics,
University of Louisiana at Lafayette
P.O.Box 41010
Lafayette, LA, 70504-1010, USA
christov@louisiana.edu

Ivan Dimov
Department of Parallel Algorithms
Institute of Information and
Communication Technologies
Bulgarian Academy of Sciences
Acad. G. Bonchev Str. Bl. 25A,
1113 Sofia, Bulgaria
ivdimov@bas.bg

Milena Dimova
Institute of Mathematics and Informatics
Bulgarian Academy of Sciences

Acad. G. Bontchev str., bl. 8
1113 Sofia, Bulgaria
mkoleva@math.bas.bg

Stefka Dimova
Faculty of Mathematics and Informatics
Sofia University
5, James Bourchier Blvd.
1164 Sofia, Bulgaria
dimova@fmi.uni-sofia.bg

Petia Dineva
Institute of Mechanics
Bulgarian Academy of Sciences
Acad. G. Bontchev str., bl. 4
Sofia 1113, Bulgaria
petia@imbm.bas.bg

Mariya Durchova
Institute of Information and
Communication Technologies
Acad. G. Bonchev Str., bl. 25A
1113 Sofia, Bulgaria
mabs@parallel.bas.bg

Stefka Fidanova
Institute of Information and
Communication Technologies
Bulgarian Academy of Sciences
Acad. G. Bonchev str. bl.25A
1113 Sofia, Bulgaria
stefka@parallel.bas.bg

Ivan Georgiev
Institute of Mathematics and Informatics
Bulgarian Academy of Sciences
Acad. G. Bonchev str., bl. 8
1113 Sofia, Bulgaria
john@parallel.bas.bg

Krassimir Georgiev
Institute of Informatrion and
Communication Technologies,
Bulgarian Academy of Science
Acad. G. Bontchev str., bl. 25-A
1113 Sofia, Bulgaria
georgiev@parallel.bas.bg

Rayna Georgieva

Institute of Information and
Communication Technologies
Bulgarian Academy of Sciences
Acad. G. Bontchev str., bl. 25A
1113 Sofia, Bulgaria
rayna@parallel.bas.bg

Vladimir Gerdjikov

Institute for Nuclear Research and
Nuclear Energy,
Bulgarian Academy of Sciences,
72 Tsarigradsko chaussee,
1784 Sofia, BULGARIA
gerdjikov@inrne.bas.bg

Georgi Grahovski

School of Mathematical Sciences,
Dublin Institute of Technology,
Kevin Street, Dublin 8, IRELAND and
Institute for Nuclear Research and
Nuclear Energy,
Bulgarian Academy of Sciences,
72 Tsarigradsko chaussee,
1784 Sofia, BULGARIA
georgi.grahovski@dit.ie

Ivan Hristov

Sofia University "St. Kl. Ohridski", FMI
5 James Bourchier Blvd.
1164 Sofia, Bulgaria
ivanh@fmi.uni-sofia.bg

Todor Gurov

Institute of Information and
Communication Technologies
Bulgarian Academy of Sciences
Acad. G. Bontchev str., bl. 25A
1113 Sofia, Bulgaria
gurov@parallel.bas.bg

Rossen Ivanov

School of Mathematical Sciences,
Dublin Institute of Technology,
Kevin Street, Dublin 8, IRELAND
rivanov@dit.ie

Sofia Ivanovska

Institute of Information and
Communication Technologies
Bulgarian Academy of Sciences
Acad. G. Bontchev str., bl. 25A
1113 Sofia, Bulgaria
sofia@parallel.bas.bg

Aneta Karaivanova

Institute of Information and
Communication Technologies
Bulgarian Academy of Sciences
Acad. G. Bontchev str., bl. 25A
1113 Sofia, Bulgaria
anet@parallel.bas.bg

Miglena Koleva

FNSE,
University of Rousse,
8 Studentska Str.,
7017 Rousse, Bulgaria
mkoleva@ru.acad.bg

Natalia Kolkovska

Institute of Mathematics and Informatics,
Bulgarian Academy of Sciences
Acad. G. Bonchev str., bl.8
1113 Sofia, Bulgaria
natali@math.bas.bg

Johannes Kraus

Johann Radon Institute for
Computational and Applied Mathemat-
ics,
Austrian Academy of Sciences
Altenberger Str. 69,
A-4040 Linz, Austria
johannes.kraus@oeaw.ac.at

Ivan Lirkov

Institute of Information and
Communication Technologies
Bulgarian Academy of Sciences
Acad. G. Bontchev str., bl. 25A
1113 Sofia, Bulgaria
ivan@parallel.bas.bg

Maria Lymbery

Institute of Information and

Communication Technologies
Bulgarian Academy of Sciences
Acad. G. Bontchev str., bl. 25A
1113 Sofia, Bulgaria
mariq@parallel.bas.bg

Svetozar Margenov
Institute of Informatrion and
Communication Technologies
Bulgarian Academy of Sciences
Acad. G. Bontchev str., bl. 25A
1113 Sofia, Bulgaria
marginov@parallel.bas.bg

Pencho Marinov
Institute of Information and
Communication Technologies
Bulgarian Academy of Sciences
Acad. G. Bonchev str. bl.25A
1113 Sofia, Bulgaria
pencho@parallel.bas.bg

Svetoslav Markov
Institute of Mathematics and Informatics
Bulgarian Academy of Sciences
Acad. G. Bontchev str., bl. 8
1113 Sofia, Bulgaria
smarkov@bio.bas.bg

Maya Markova
Department of Informatics,
University of Russe,
Studentska Str. 8,
7017 Russe, Bulgaria
maya.markova@gmail.com

Geno Nikolov
Faculty of Mathematics and Informatics
Sofia University
5, James Bourchier Blvd.
1164 Sofia, Bulgaria
geno@fmi.uni-sofia.bg

Tsvetan Ostromski
Institute of Information and
Communication Technologies
Bulgarian Academy of Sciences
Acad. G. Bonchev str. bl.25A

1113 Sofia, Bulgaria
ceco@parallel.bas.bg

Petar Popivanov
Institute of Mathematics and Informatics
Bulgarian Academy of Sciences
Acad. G. Bontchev str., bl. 8
1113 Sofia, Bulgaria
popivano@math.bas.bg

Georgi Popov
Laboratoire de mathématiques
Jean Leray,
Université de Nantes,
2, rue de la Houssinière,
BP 92208, 44072 Nantes
Cedex 03, France
georgi.popov@univ-nantes.fr

Milena Racheva
Technical University of Gabrovo
Hadji Dimitar str. 4
5300 Gabrovo, Bulgaria
milena@tugab.bg

Tsviatko Rangelov
Institute of Mathematics and Informatics
Bulgarian Academy of Sciences
Acad. G. Bontchev str., bl. 8
Sofia 1113, Bulgaria
rangelov@math.bas.bg

Victoria Rashkova
Department of Informatics,
University of Russe, Russe 7000,
viktoriqi_78@abv.bg

Angela Slavova
Institute of Mathematics and Informatics
Bulgarian Academy of Sciences
Acad. G. Bontchev str., bl. 8
1113 Sofia, Bulgaria
slavova@math.bas.bg

Stanislava Stoilova
Institute of Mathematics and Informatics
Bulgarian Academy of Sciences
Acad. G. Bontchev str., bl. 8

1113 Sofia, Bulgaria
stoilova @math.bas.bg

Yonko Stoynov

Faculty of Applied Mathematics and In-
formatics,
Technical University of Sofia,
Kl. Ohridski blv. 8
Sofia 1000, Bulgaria
ids@tu-sofia.bg

Antoaneta Tsokova

National Academy of Music
"Pantcho Vladigerov"
Evlogi Georgiev str. 94
1505 Sofia, Bulgaria
atsokova@yahoo.com

Daniela Vasileva

Institute of Mathematics and Informatics,
Bulgarian Academy of Sciences
Acad. G. Bonchev str., bl.8
1113 Sofia, Bulgaria
vasileva@math.bas.bg

Vladimir Veliov

Vienna University of Technology
Argentinierstr. 8/119
1040 Vienna, Austria
veliov@tuwien.ac.at

Pietro Zecca

Dipartimento di Energetica,
Universita di Firenze,
via S.Marta 3, Firenze, Italy,
zecca@unifi.it

Ludmil Zikatanov

Penn State
Department of Mathematics
16802 University Park, PA, USA
ludmil@psu.edu

Zahari Zlatev,

National Environmental
Research Institute
Aarhus University
Frederiksborgvej 399

P. O. Box 358
DK-4000 Roskilde, Denmark
zz@dmu.dk